A technical review on the energy yield estimation of offshore floating photovoltaic systems

Shanka Vasuki, Sathya; Levell, Jack; Santbergen, Rudi; Isabella, Olindo

DOI
10.1016/j.rser.2025.115596

Publication date
2025

Document Version
Final published version

Published in
Renewable and Sustainable Energy Reviews

Citation (APA)
Shanka Vasuki, S., Levell, J., Santbergen, R., & Isabella, O. (2025). A technical review on the energy yield estimation of offshore floating photovoltaic systems. *Renewable and Sustainable Energy Reviews*, *216*, Article 115596. https://doi.org/10.1016/j.rser.2025.115596

Renewable and Sustainable Energy Reviews 216 (2025) 115596

Contents lists available at ScienceDirect

Renewable and Sustainable Energy Reviews

journal homepage: www.elsevier.com/locate/rser

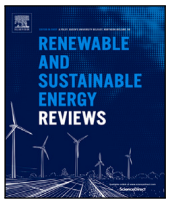

Review Article

A technical review on the energy yield estimation of offshore floating photovoltaic systems

Sathya Shanka Vasuki [a],*, Jack Levell [b], Rudi Santbergen [a], Olindo Isabella [a]

[a] Photovoltaic Materials and Devices, Delft University of Technology, Mekelweg 4, Delft, 2628 CD, South Holland, The Netherlands
[b] Shell Global Solutions International B.V., Grasweg 31, 1031, Amsterdam, The Netherlands

ARTICLE INFO

Keywords:
Offshore floating solar photovoltaics
Energy yield
Hydrodynamics
Cooling effect
Ocean surface albedo
Soiling
Degradation

ABSTRACT

The uncertainty surrounding land availability for renewable energy deployment is a growing concern, creating a strong need for alternative solutions. In recent years, offshore floating photovoltaic (OFPV) systems have shown great promise in meeting global energy demands without competing for land resources. With ambitious targets like 3 GW in The Netherlands by 2030 and global projections exceeding 20 GW, OFPVs are emerging as a key solution at this critical juncture in energy transition. The significance of this technology is also reflected in the 95% increase in research outputs over the past five years. Despite this growth, insights remain scattered, with limited understanding of both the technology and performance. This review fills this gap by providing a comprehensive overview of OFPV systems, addressing both technical and performance aspects. Specifically, the objectives are to: provide detailed information about technology readiness levels, real-world deployments, and a new classification matrix to categorize different OFPV designs; identify key processes like dynamic motion, cooling, optical changes, and long-term degradation that impact energy yield (EY); and quantify the impact of each process on EY based on reported data. The findings reveal that dynamic motion (-0.4% to -15%) and long-term degradation (-2% to -20%) generally reduce EY, while cooling (-4% to +20%) and optical effects (-40% to +5%) can enhance or reduce EY depending on operating conditions. While these insights are crucial, several challenges remain, with the most pressing being the need to standardize measurement and modeling techniques for EY prediction to propel OFPVs towards large-scale commercialization.

Contents

1. Introduction ... 3
1.1. Types of floating photovoltaic systems ... 5
1.1.1. Inland floating photovoltaics ... 5
1.1.2. Offshore floating photovoltaics ... 5
2. Purpose and contribution of this review ... 7
3. Technological overview of FPV systems ... 8
3.1. Classification of FPV archetypes ... 8
3.2. Technology readiness levels (TRL) ... 11
4. Performance overview of OFPV systems ... 11
4.1. Impact of dynamic motion ... 12
4.1.1. Hydrodynamic response of different FPV archetypes ... 13
4.1.2. EY quantification of different FPV archetypes due to the effect of motion ... 15
4.2. Impact of cooling effect ... 15
4.2.1. Thermal analysis and EY quantification of different FPV archetypes ... 16
4.3. Impact of optical effects ... 19
4.3.1. Studies on understanding the effect of ocean surface albedo ... 20
4.3.2. EY quantification due to the effect of shading ... 22
4.3.3. EY quantification due to the effect of soiling ... 23
4.4. Impact of long-term degradation ... 23

* Corresponding author.
E-mail address: S.S.S.ShankaVasuki@tudelft.nl (S. Shanka Vasuki).

https://doi.org/10.1016/j.rser.2025.115596
Received 18 October 2024; Received in revised form 10 February 2025; Accepted 5 March 2025
Available online 10 April 2025

5. Conclusion 24
6. Outlook & future direction 25
Declaration of competing interest 30
Acknowledgment 30
Appendix A. Compilation of articles reviewed in this work 30
Appendix B. Supplementary data 30
Data availability 30
References 30

Abbreviations

AC	Alternating current
AF	Attached fins
AgriPV	Agricultural integrated PV systems
AOD	Aerosol optical depth
BIPV	Building integrated PV systems
CFD	Computational fluid dynamics
CIGS	Copper indium gallium selenide solar cell
DC	Direct current
DoF	Degree of freedom
DR	Degradation rate
EU	European Union
EY	Energy yield
FBW	Floating breakwater
FPV	Floating photovoltaics
GHI	Global horizontal irradiance
GPV	Ground mounted PV systems
GW	Gigawatt
HR	Hydrodynamic response
HT	Heat transfer
IEA	International Energy Agency
IFPV	Inland photovoltaics
IPCC	Intergovernmental Panel on Climate Change
IRENA	International Renewable Energy Agency
IWA	Irradiance-weighted wind speed average
MW	Megawatt
NOCT	Nominal Operating Cell Temperature
NZE	Net-zero emissions
OFPV	Offshore photovoltaics
OSA	Ocean surface albedo
POA	Plane of array irradiance
PV	Photovoltaic
RAO	Response amplitude operator [(m or deg)/m]
RES	Renewable energy source
RH	Relative humidity
RPV	Roof mounted PV systems
RQ	Review questions
TRL	Technology readiness levels
TSM	Total suspended matter
TW	Terawatt
UV	Ultraviolet rays
U-value	Heat loss coefficient
$\alpha_{diffuse}$	Diffuse component of OSA
α_{direct}	Direct component of OSA
α_{OSA}	Ocean surface albedo [%]
$\alpha_{diffuse}^{SR}$	Surface reflection component of diffuse albedo
α_{direct}^{SR}	Surface reflection component of direct albedo
$\alpha_{diffuse}^{WS}$	Water scattering component of diffuse albedo
α_{direct}^{WS}	Water scattering component of direct albedo
β_0	Frequency factor [sec^{-1}]
β_1	Activation energy [eV]
β_2	Effect of cyclic temperature
β_3	Effect of UV radiation
β_4	Effect of relative humidity
ΔRH_{daily}	Daily average relative humidity [%]
ΔT	Temperature difference (front/back) of PV module [C]
ΔT_{daily}	Daily cyclic temperature of the module [K]
ΔUV_{daily}	Daily daytime average UV irradiance [W/m^2]
η	Power conversion efficiency of PV modules [–]
η_{ref}	Efficiency of PV module at STC condition [%]
γ_{pow}	Temperature coefficient of power
λ	Wavelength [m]
ω	Wave frequency [rad/s]
ψ	Absorptance [–]
τ	Transmittance [–]
$\theta_{pretilt}$	Pretilt angle of the PV module [deg]
θ_t	Tilt angle [deg]
θ_{wd}	Wind direction [deg]
θ_{wv}	Wave direction [deg]
a, b, c, d	General equation coefficients [–]
A_N	Normalization constant of the physical entities [$year^{-2}$]
A_R	Submergence ratio [%]
a_z	Azimuth angle [deg]
B	Solar angle [deg]
C	Roughness coefficient [–]
c_1, c_2, c_3	Constants depending on PV module mounting structure
$E_{PV,1}$	Energy output of the PV module in the first year
E_{PV,N_year}	Cumulative energy output of the PV module
f_{dif}	Fraction of the diffused incident irradiation of a tilted surface
f_{dir}	Fraction of the direct incident irradiation of a tilted surface
f_R	Ross coefficient [–]
G_{avg}	Daily average irradiance [W/m^2]
G_{POA}	Plane of array irradiance [W/m^2]
G_{STC}	Solar irradiance at standard test conditions [W/m^2]
G_{NOCT}	Solar irradiance at NOCT conditions [W/m^2]
h_{c_b}	Convective HT coefficient for the back surface
h_{c_f}	Convective HT coefficient for the front surface

h_{c_w}	Convective HT coefficient for the water surface
h_{r_b}	Radiative HT coefficient from the back surface to the water
h_{r_f}	Radiative HT coefficient from the front surface to the sky
I	Intercept of the trend line
k_H, k_P, k_{T_m}	Degradation rates due to different processes
k_{RT}, k_{UV}, k_{TC}	Aging rates of PV modules
k_B	Boltzmann constant [eV/K]
kW_p	Kilowatt peak
$L_x x$	Length of a particular archetype [m]
n_i	Weight of coupled environmental stresses &
p	Color coefficient [–]
P_e	Absorbed solar irradiance
Q_g	Absorbed radiation by glass
r_f	Angle of refraction [deg]
S	Slope
t	Time [hours]
T_{amb}	Ambient temperature [C]
T_{app}	Apparent temperature [C]
T_{BS}	Back surface PV module temperature [C]
T_{max}	Daily maximum temperature of the module [K]
T_{mod}	PV module temperature [C]
T_{mod_0}	Initial PV module temperature [C]
T_{wat}	Water temperature [C]
T_p	Wave period [s]
U_∞	Ambient wind speed [m/s]
U_{avg}	Average wind speed [m/s]
U_c	Constant heat loss coefficient [W/m^{2}K]
U_v	Convective heat loss coefficient [W/m^{3}sK]
U_{L_1}	Convective and radiative HT between module and air (front) [W/m^{2}K]
U_{L_2}	Convective and radiative HT between module and air (rear) [W/m^{2}K]
x, y	Cloudiness constants
z	Solar zenith angle [deg]

1. Introduction

In 2023, at the COP28 conference,[1] the International Energy Agency (IEA), International Renewable Energy Agency (IRENA), and Intergovernmental Panel on Climate Change (IPCC) proposed a target for all member countries to triple their global renewable energy capacity to reach net zero emissions (NZE) by 2030 [1–4]. To achieve the NZE goal by 2030, the capacity of renewable energy sources (RES) must increase from 4.7 TW in 2024 to approximately 11 TW by 2030 [2–4]. Therefore, the next 4–5 years are critical for determining the world's progress towards achieving NZE. Currently, several RES are being utilized for clean energy generation and to understand the importance of each source, certain key trends have been projected by [1–4]: (1) Wind and solar electricity generation combined will surpass hydropower in 2024 [1–4], (2) wind and solar energy will each exceed nuclear electricity generation by 2026 [1], and (3) solar energy will overtake wind and nuclear energy in electricity production by 2028 [1].

With these trends, wind and solar energy are expected to be the leading RES in the coming years. Amongst these, solar energy is set to be the main driver towards energy transition, making it the 'need of the hour' RES [1–4,6]. With the importance of solar energy now established, it is essential to recognize that solar energy can be generated through various application modes. Currently, the most common application modes of generating solar energy are shown and explained in Fig. 1 (a–d). In recent years, a new application mode has emerged known as floating photovoltaics (FPV) as shown in Fig. 1 (e). This application mode was first pioneered by two Japanese companies, Mitsui Engineering & Shipbuilding Co. Ltd. and Mitsui Zosen KK, which filed a patent positioning Japan as one of the early leaders in the field [7,8]. The first FPV system was also installed in Aichi, Japan, in 2007, developed by the National Institute of Advanced Industrial Science and Technology, demonstrating its potential in energy generation while highlighting initial advantages such as land conservation and enhanced performance, as well as challenges related to operation and maintenance [9,10]. Following this, FPV adoption expanded to

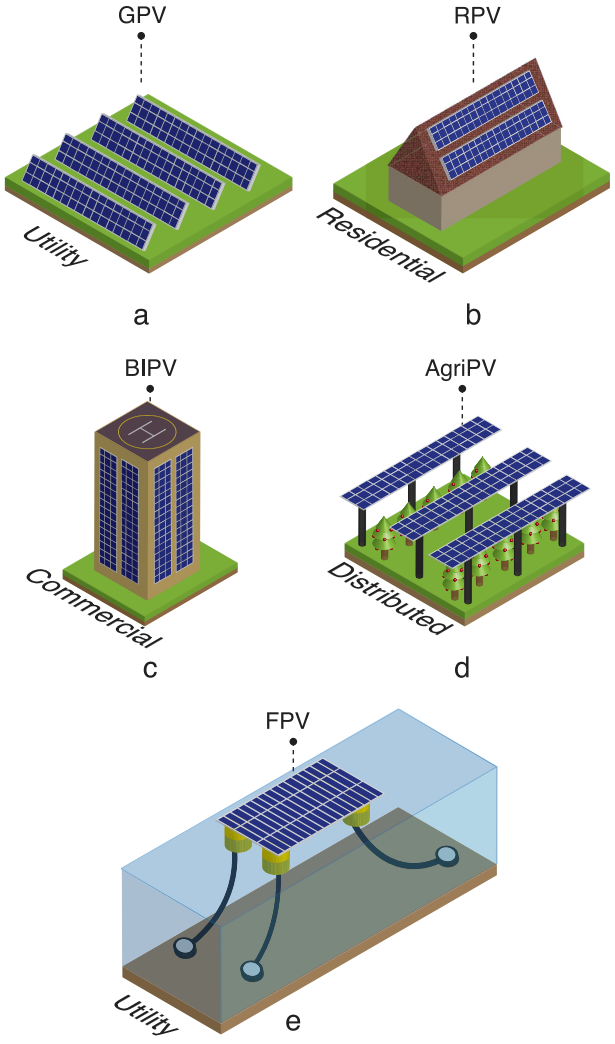

Fig. 1. Different modes of producing solar energy. (a) ground-mounted PV systems (GPV), where large areas of land are covered with PV modules, (b) rooftop PV systems (RPV), where PV systems are installed on the roofs of residential houses, (c) building-integrated PV (BIPV) systems, where PV modules are integrated onto the walls of large buildings, (d) Agriculture PV systems (AgriPV), where PV modules are placed on agricultural farmland amidst different crops, (e) Floating PV systems (FPV). Utility-Scale solar: This refers to the large scale PV production which are directly fed into the grid, Distributed solar: This refers to PV systems that are connected to the grid but distribute the energy to various sectors (such as schools, universities, residential homes etc.), Commercial solar: This refers to PV systems that provide energy to commercial properties, Residential solar: This refers to PV systems that provide energy to residential properties [5].

[1] United Nations Climate Change Conference held in Dubai, UAE in 2023.

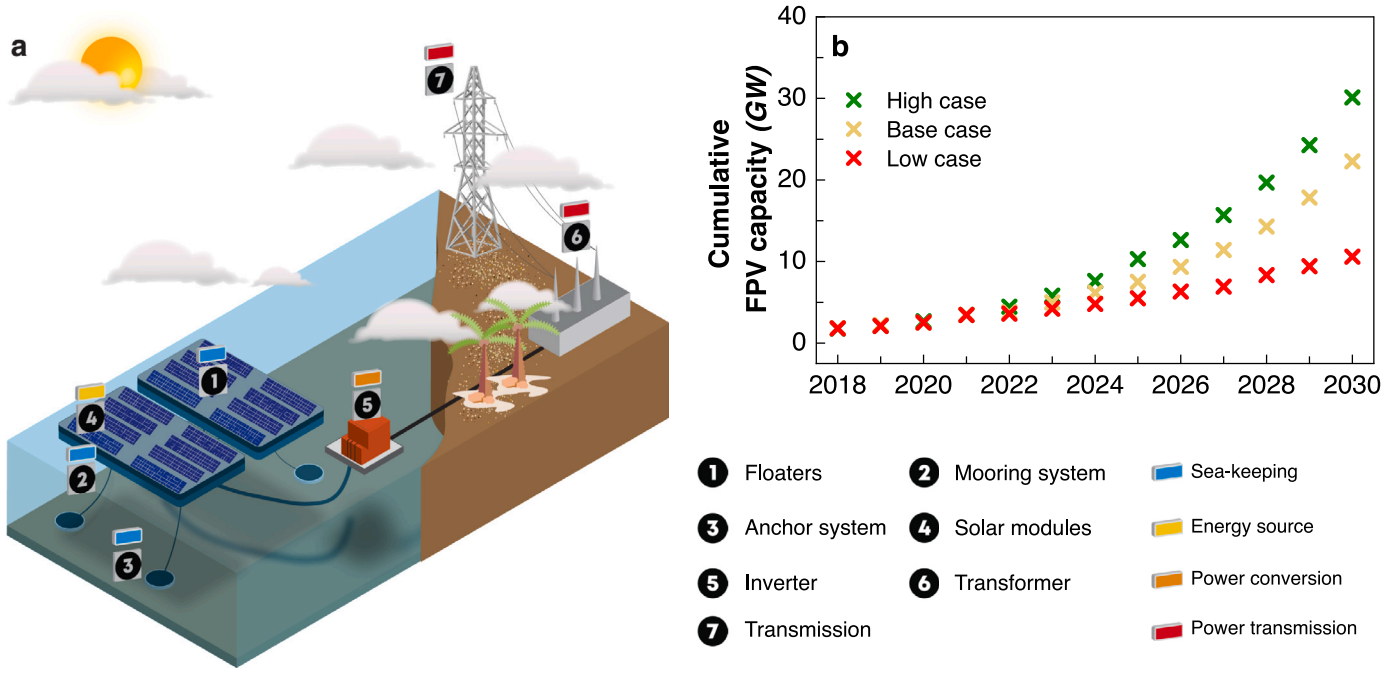

Fig. 2. (a) Key Components of an FPV system: The flotation system, mooring lines, and anchors are crucial sea-keeping components. They provide buoyancy, stabilize the system against environmental loads, and secure the system in place by connecting it to the waterbed [19]. PV modules are essential for generating DC power, while inverters convert this DC power into AC power. The transformed AC power is then transmitted to its intended destination through transformers and transmission towers, collectively known as the power transmission system, (b) Cumulative installed FPV capacity (high, base and low cases are projections based on different rates of FPV deployments over the years. More information pertaining to this can be found in [11]). *Data retrieved from* [1,6,11,23–25].

different countries worldwide, with China currently leading in active installations [8,11–13].

A floating photovoltaic system can be defined as the placement of PV modules on a buoyant floating structure to produce solar energy [12,14]. An FPV system can be better visualized via Fig. 2 (a). This figure illustrates the components that make up an FPV system, which includes a flotation system, mooring line cables, anchors, PV modules, inverters, transformer, and transmission towers [15–22]. Each of these components are designed to serve a specific purpose as explained in Fig. 2. These components collectively form the backbone of an FPV system by ensuring mechanical stability, energy generation, conversion, and transmission. Given this understanding of FPV systems, one might wonder why is there a need for this new technology when GPVs and RPVs are already well established, hold a major market share and can potentially fulfill the NZE targets?

The answer to this question is that by the end of 2030, a total of 6.1 TW of solar and 2.7 TW of wind capacity is required to achieve NZE, making solar and wind energy two essential pillars in the road to energy transition [1–4]. However, both of these RES are land-intensive technologies, requiring large areas of land to produce substantial amounts of energy. Studies have shown that a typical utility-scale solar project (see Fig. 1 (a)), with a capacity of 100 MW requires a land area of 1–3 km^2 [26–30].

With this range of land occupation, a simple back-of-the-envelope calculation can be performed to evaluate the upper limit of the total land area required for inland solar deployments by 2030. The cumulative land area required by solar energy installations are calculated based on the capacity projections made in [1–4]. By using the maximum land occupation values for the year 2030, the total land area required by inland solar installations sums up to approximately 0.2 million km^2.[2] While this figure is very small relative to the Earth's total land area, which is about 149 million km^2 [31], it is important to understand that not all land areas on Earth are suitable for renewable energy applications.

IEA [25] and McKinsey & company [32] conducted studies to estimate the total land area available for RES applications. In the assessment by IEA [25], it was found that one-third of the global land area is unsuitable for RES deployment (not just solar), leaving a potential 80 million km^2 of available land for energy generation [25,32].[3] Even within this potential, solar would ideally occupy only 0.25% of the total available land area. To put it in perspective, this is equivalent to approximately 5 times the total land area of the Netherlands.

Although requiring about 0.25% of land for solar deployment may still seem small, it is however important to note that certain factors, such as population growth, societal aspects, ecological protection, agricultural use, existing human settlements, and land required for traditional energy-generating sources like oil and gas, were not considered in deriving the potential 80 million km^2 of available land. All these factors combined could drastically reduce the overall land area available for deploying solar energy on land. As a result, the exact availability of land for inland solar deployment remains highly uncertain, both now and likely in the future. This limitation is therefore concerning, given the critical need for energy transition. Therefore, a new technology such as floating photovoltaics could be an ideal solution to address this uncertainty. This reason has been a driving force for the growth of FPVs in the recent years, as shown in Fig. 2 (b). Over the next six years (2024–2030), FPV installations are expected to reach a maximum of 30 GW, accounting for 0.5% of the total required solar energy capacity (approximately 6 TW by 2030). While this represents a small percentage of the total solar energy capacity needed, it also reflects the nascent nature of this technology. For FPVs to hold a more substantial

[2] this is derived by assuming that the energy needs by solar are already fulfilled in 2024, and therefore only the additional land area required from 2025–2030 is considered

[3] artificial surfaces (including urban and associated areas), tree-covered areas, woody crops, mangroves, aquatic or regularly flooded areas, and permanent snow and glaciers were excluded in their assessment.

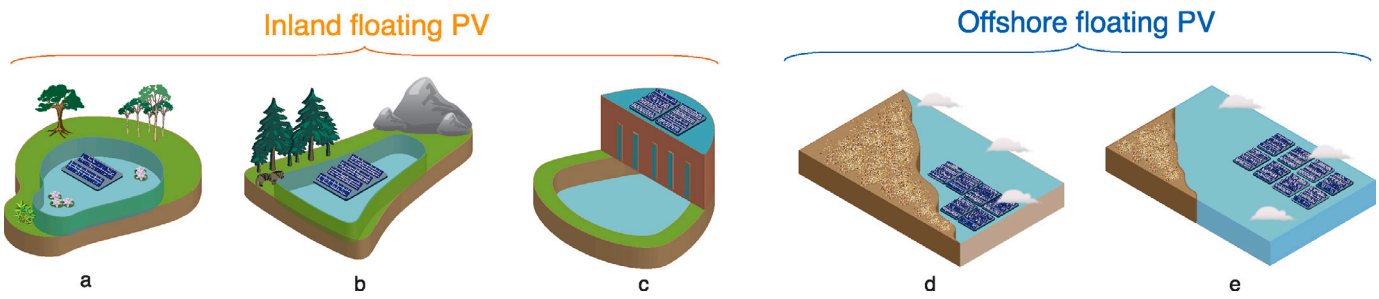

Fig. 3. Types of FPV systems based on location of placement. (a) Small freshwater bodies such as ponds and basins, where there are no waves and wind speeds are very limited [12], (b) Medium-sized inner waters such as lakes, with areas spanning from 1 to 3 km^2 and small waves reaching up to 1 m in height [12], (c) Large inner waters such as reservoirs, with areas exceeding 3 km^2 and medium waves greater than 1 m in height [12], (d) Nearshore regions, where FPV systems are positioned 5–10 km from the shore with sea depths ranging from 10–20 m [33], (e) Farshore regions, where FPV systems are deployed in deep water conditions, at distances greater than 30 km from the shore, with sea depths exceeding 40 m [33].

share of solar energy capacity by 2030, in line with trends established by GPVs and RPVs [11,24], a detailed understanding of this technology through dedicated research and development is necessary.

1.1. Types of floating photovoltaic systems

In the recent years, various types of FPV systems have been or are being developed depending on the type of waterbody on which they are installed [12], to facilitate commercial deployments. As depicted in Fig. 3, FPV systems can be categorized into two main types: inland floating PV and offshore floating PV. Further details about these systems are explained below.

1.1.1. Inland floating photovoltaics

Inland floating PV (IFPV) refers to the placement of photovoltaic systems on inland water bodies. There are three distinct types of inland water bodies, as illustrated and explained in Fig. 3 (a–c). Over the past 5–7 years, IFPVs have attracted significant attention from both technology developers and deployers, particularly for large-scale commercial projects.

Fig. 4 illustrates the total installed capacity of IFPV systems worldwide [11–13]. As shown in the figure, a total of 3.8 GW of installed capacity has been deployed on inland water bodies, which accounts for majority of the FPV installations occurred during 2022–2024, as shown in Fig. 2 (b). China is the leading deployer of this technology, followed by the EU. A country-wise breakdown of the installed capacity in the EU can be seen in the figure next to the map. The chart shows that out of the 451 MW installed in the EU, 275 MW of installed capacity is located in the Netherlands, followed by 81.2 MW in France, and 22.6 MW each in Austria and Germany.

According to a study conducted by SolarPower Europe [12], IFPVs are deemed to be a compelling option for the EU. This is because when IFPVs are combined with existing hydropower plants at a 10% coverage ratio, these systems have the potential to cover 6% of the EU's annual power consumption. This indicates that IFPVs hold a significant potential not only within the EU but also globally, highlighting the technology's progress towards full-scale commercialization.

1.1.2. Offshore floating photovoltaics

Offshore floating PV (OFPV) as the name suggests refers to the installation of photovoltaic systems on open sea waters. There are two distinct types of offshore water environments based on the distance from the shore and the depth of water as shown in Fig. 3 (d–e). OFPVs have gained significant attention over the past 2–3 years and this raises the question: why expand to OFPVs when IFPVs have already reached a substantial level of commercialization?

The rationale behind this expansion lies on several key factors. It is a fact that large-scale solar energy deployment demands substantial space, whether on land or water. Due to the uncertainty in the

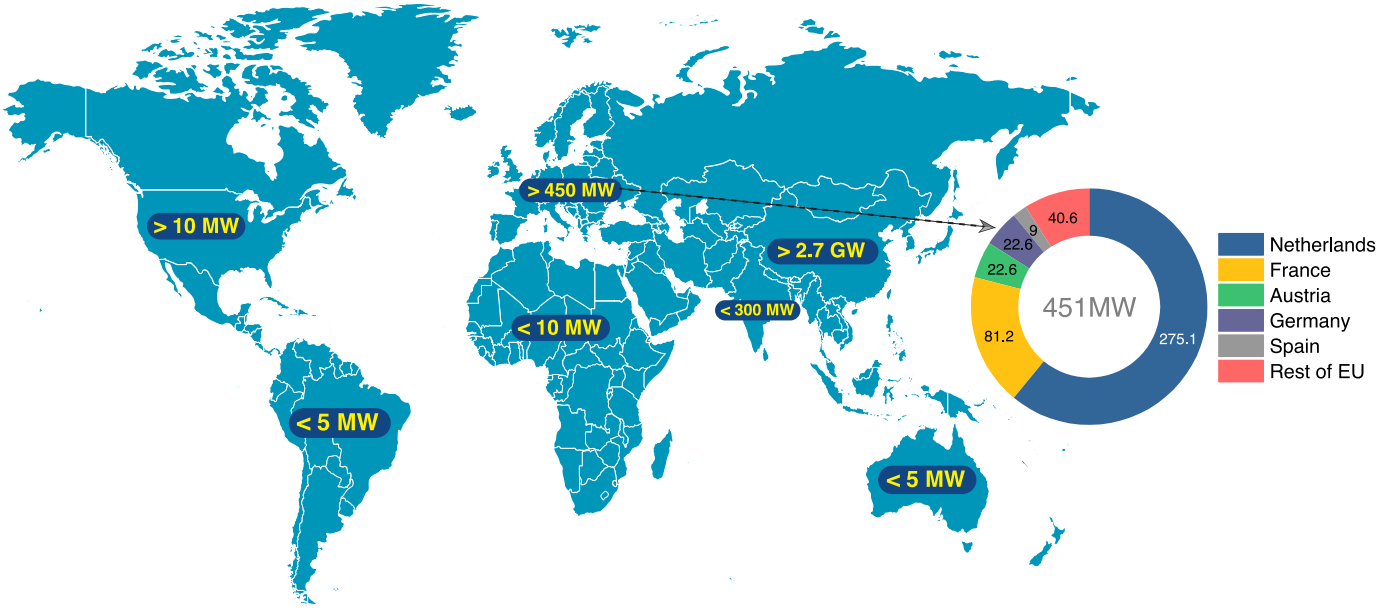

Fig. 4. Deployment status of IFPVs. *Data extracted from* [11–13].

Table 1
Deployment status of OFPVs as of 2024 [12,34]. (*Note: (a) The projects listed in this table are compiled based on publicly available information and may not represent all projects worldwide. (b) Most of the projects listed are pilot installations aimed at better understanding of OFPV systems, also indicated by their capacity. Therefore, their inclusion does not necessarily imply a high technology readiness level (TRL). More details on TRL can be found in Section 3.2.*)

Developer	Project[a]	Country	Location	Status[b]	Capacity (kWp)
Bluewater	Solar@Sea*		Oostvoornse lake	Con.	200
Fred. Olsen 1848	BRIZO		Norway	Oper.	150
HelioRec	Port of Ostend pilot		Ostend	Oper.	10
Moss Maritime	Moss Maritime pilot*		Frøya	Dev.	–
Oceans of Energy	North Sea 1		Dutch North Sea	Oper.	50
	North Sea 2		Dutch North Sea	Oper.	1000
	Hollandse Kust Noord*		Dutch North Sea	Dev.	500
	North Sea 3*		Ostend	Con.	3000
OceanSun	Kryholmen pilot		Kryholmen	Oper.	100
	Skaftå pilot		Skaftå	Oper.	6.6
	MP Quantum Greece		Greece Cyprus	Dev.	4000
	Haiyang		Shandong	Oper.	500
	Fish Farm 112		Johor Straits	Oper.	3.4
	Jurong Island pilot		Jurong Island	Dev.	1.5
	Singapore Strait pilot		Singapore Strait	Dev.	1200
	BOOST*		Gran Canaria	Dev.	250
SolarDuck	Merganser		Dutch North Sea	Con.	524
	Hollandse Kust West VII*		Dutch North Sea	Dev.	5000
	Malaysia pilot*		Tioman island	Dev.	780
	Tokyo Bay ESG Project*		Tokyo Bay	Dev.	200
	Tokyo Bay ESG Project*		Tokyo Bay	San.	5000
SolarinBlue	Sun'Sète		Sète	Con.	300
	Arabian Sea pilot*		Mangalore	Dev.	1000
Tractebel	SeaVolt*		Ostend	Oper.	–

[a] Projects marked with * indicate collaboration with other organizations along with the developer.
[b] Dev. — In development, Con. — Under construction, Oper. — Operational, San. — Project sanctioned.

availability of land, large-scale deployment of IFPVs emerged as an alternative solution. However, unlike the uncertain land availability, it is certain that there are only limited inland water bodies globally that are suitable for IFPV applications, which would ultimately not suffice to achieve NZE. Consequently, the solar industry is now moving towards ocean-based installations. The importance and necessity for offshore solar energy is increasingly evident in today's energy landscape mainly due to the following reasons:

- **Large-scale deployments opportunities:** Offshore renewables, oil & gas and aquaculture are set to occupy over $350,000\ km^2$ of ocean area by 2050 [11].
- **Potentially higher energy output:** The ocean provides 4%–8% higher irradiance compared to land, potentially leading to higher energy outputs [35].
- **Potential intermittency reduction:** The complementarity of offshore wind and solar energy offers significant synergies, enhancing energy throughput by reducing the overall intermittency [35,36].
- **Improved Reliability:** The simplicity of certain OFPV designs, combined with the absence of mechanically moving components, reduces the risks associated with mechanical failures, thereby enhancing the reliability of these systems [37].
- **Scalability:** Deploying an OFPV system requires less time compared to offshore wind installations, providing shorter time frames for scaling the technology [36].

These reasons show that the deployment of OFPVs is anticipated to grow substantially in the coming years, potentially capturing a larger share of the solar energy generation market. To gauge the growth of OFPVs, Table 1 presents examples of the latest offshore solar deployments that have been made public. The current installed capacity of OFPVs amounts to approximately 24 MW, which is about 10% of the total installed capacity of IFPVs in the Netherlands (see Fig. 4). Out of the 24 MW installed capacity, 14 MW is located in the EU, making it one of the active member state in developing this technology.

From Table 1, it is also clear that this technology is still in its early stages which indicates that there is a strong need to conduct detailed research and analysis to understand OFPVs comprehensively. This understanding will not only help in identifying the necessary actions required to promote OFPVs as a reliable technology but will also help in establishing OFPVs as a viable third pillar in the solar energy generation chain alongside GPVs and RPVs.

As with any new technology, there are associated advantages and risks that determines its rate of growth. Fig. 5 provides the reader with a detailed overview of the potential advantages, risks, and uncertainties currently associated with OFPVs to provide a bird's eye view of the current challenges associated with this technology.

Thus, the discussion so far has highlighted (1) importance of solar energy in energy transition, (2) introduction to FPVs, (3) a discussion of the various types of FPV systems, their significance, and current deployment status, and (4) an overview of the advantages, risks, and uncertainties currently associated with this technology. Going forward, this review focuses on providing readers with a comprehensive overview of the technological and performance-oriented aspects of OFPVs by addressing the potential risks and uncertainties associated with each aspect, as depicted in Fig. 5. While the risks and uncertainties associated

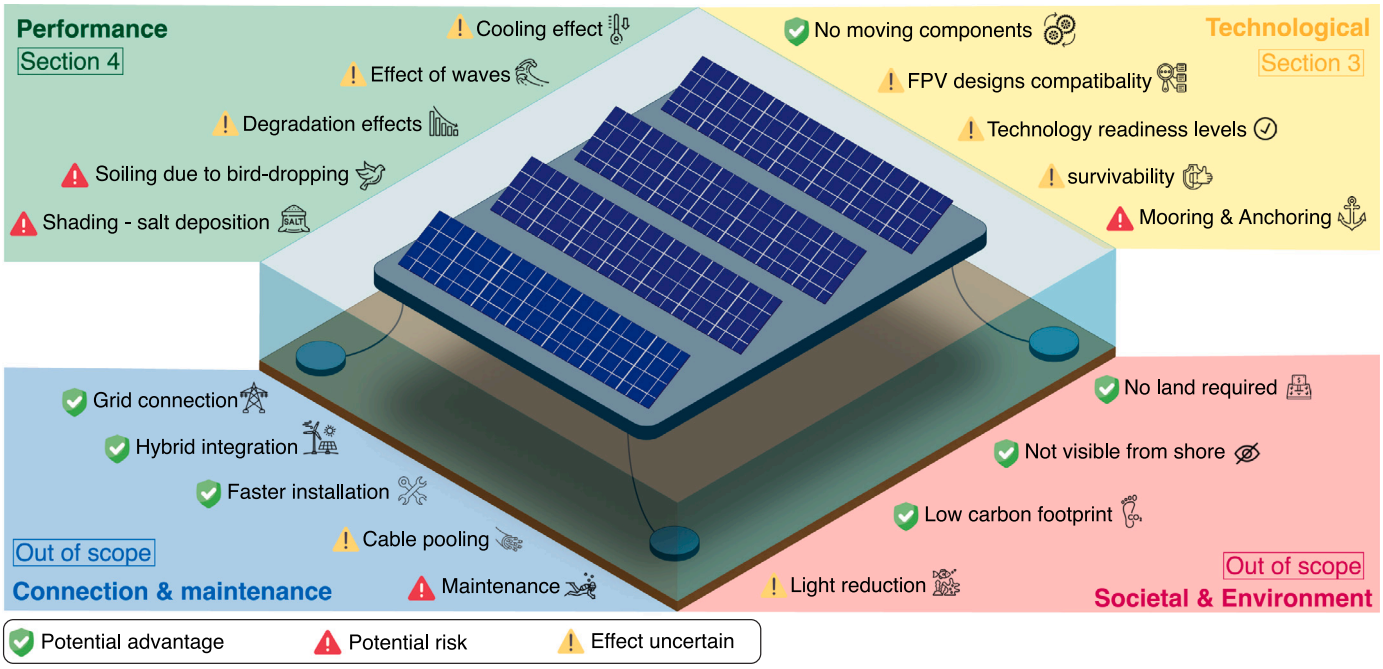

Fig. 5. Current understanding of OFPVs. *Potential advantages:* OFPVs do not require land space, allowing for energy generation without competing for terrestrial real estate; some studies suggest that OFPVs experience lower module temperatures offshore, leading to higher EY compared to GPVs; the carbon footprint of IFPVs is reported to be 3–4 times lower than GPVs, and this potentially could also apply to OFPVs [38]; OFPVs can optimize space and resource utilization by hybridizing with offshore wind turbines; societal restrictions are reduced as the system is not visible from the shore, minimizing public objections and aesthetic concerns [12,39]. *Potential risks:* The design and installation of mooring and anchoring systems pose challenges due to harsh offshore and deep water conditions, leading to increased operational and maintenance costs (more information on mooring and anchoring can be found in Appendix B); shading from salt deposition, water overflow, and soiling from bird droppings may reduce the overall energy output of the system [12,39] also increasing the frequency of regular maintenance; maintenance of OFPV systems presents several risks related to cleaning of PV modules, ensuring long term safe operation of electrical cable connections, and mechanical reliability of multiple floaters, connectors and mooring line connection to maintain the system's electrical and mechanical integrity [36,40]. *Uncertainties:* The specific FPV designs currently in use and their technology readiness levels are not well documented; the effects of waves, cooling, optical influences, and system degradation on the overall EY remain unclear; and the ecological impacts, survivability, and feasibility of cable pooling remain topics of uncertainty.

with connection, maintenance, societal, and environmental aspects are important, they fall outside the scope of this work.

2. Purpose and contribution of this review

Before delving into the core of this review, it is important to acknowledge the significance of existing review articles in this field, as this work aims to build upon them. This is achieved by performing a detailed survey of the existing review articles, as shown in Table 2, to provide readers with an overview of the most widely researched topics (T1 to T6) in the field of FPVs. To get a holistic understanding of the field, 37 review articles are compiled, published from 2014 to mid-2024.

This chart offers critical insights into the level of understanding within the field by assigning a color corresponding to each topic, indicating the level of depth covered in their review. As seen from Table 2, six topics have garnered significant interest over the last decade. These topics can be grouped into four clusters: (1) Technical Overview (encompassing topics T1, T2, T3), (2) Performance Overview (encompassing topic T4), (3) Environmental Impact (encompassing topic T5), and (4) System Application (encompassing topic T6). The table reveals that existing reviews generally provide a fundamental to intermediate perspective on clusters (1) and (2) compared to the latter, leading to ambiguities and knowledge gaps concerning the technology and its performance, which is one of the most critical aspect for any energy generating system. Additionally, with the increasing momentum of FPVs across both industry and academia, it becomes all the more important to understand these aspects comprehensively.

Hence, the aim of this review is to address this gap by providing a well-rounded comprehensive overview focused on these two clusters as highlighted in Table 2. To address these gaps, the following review questions (RQ) are formulated:

1. **Technological Overview of FPV (IFPV & OFPV) Systems**
   (a) *How can different FPV system designs be classified?*
   (b) *What are the technology readiness levels (TRLs) of different FPV technologies used by organizations working within the field?*
2. **Performance Overview of OFPV Systems**
   (a) *What processes influence the EY of OFPV systems?*
   (b) *What methods are currently used to quantify the effects of these processes?*
   (c) *Which environmental or geometrical parameters affect the EY of OFPV systems?*
   (d) *With the current state of research, how well is each process quantified in terms of the EY as a loss or gain?*

By answering these questions, this review contributes to the field in the following ways: (1) It provides a well-rounded and complete overview of the technological aspects of IFPV and OFPV systems, (2) It gives a perspective on OFPVs from both an industrial and academic outlook, which is currently not addressed in existing review articles, (3) To the best of the authors' knowledge, it is also the only review that provides an in-depth understanding of the performance aspects of OFPV systems, particularly focusing on quantifying the processes and factors that affect their EY, and (4) This work also contributes to reducing the overall ambiguity concerning the current status and understanding of OFPV systems. All in all, this review aims to be a valuable resource for researchers, technology developers, and any new reader who seeks to understand OFPVs.

Table 2
Review of existing review articles [8,9,15–20,41–70]. Color code explanation: Fundamental: Introduces key concepts and foundational ideas, establishing the basis for understanding the topic, Intermediate: Explores the topic in greater detail, building on foundational concepts and offering broader insights across key areas, Comprehensive: Provides an in-depth and expansive review, integrating a wide range of perspectives and analyses, offering a thorough exploration of the topic.

RA*	T1	T2	T3	T4	T5	T6	RA*	T1	T2	T3	T4	T5	T6
[15]	♦	×	■	■	♦	×	[18]	♦	■	♦	♦	♦	×
[57]	♦	×	×	■	★	■	[62]	×	×	×	♦	■	×
[20]	♦	×	×	×	■	×	[49]	■	×	×	×	♦	♦
[60]	■	×	×	♦	×	■	[8]	■	×	×	♦	♦	■
[61]	■	×	×	■	×	×	[58]	■	■	×	♦	■	×
[53]	■	■	×	■	■	★	[19]	■	♦	×	■	×	■
[42]	★	×	♦	■	×	×	[50]	■	♦	■	■	■	×
[65]	■	×	♦	■	■	×	[66]	×	×	×	×	★	×
[67]	×	■	×	■	×	×	[68]	×	×	■	■	×	×
[69]	×	×	×	♦	×	×	[70]	■	×	×	×	★	×
[63]	★	×	×	■	■	■	[44]	♦	×	♦	♦	♦	♦
[41]	★	■	♦	■	×	×	[46]	■	×	×	♦	♦	♦
[59]	♦	×	×	×	♦	♦	[51]	■	×	×	■	×	×
[55]	♦	×	×	×	×	×	[52]	■	×	×	×	×	×
[56]	♦	×	×	■	★	×	[45]	♦	♦	■	■	×	×
[16]	■	■	■	×	×	×	[48]	■	×	×	♦	■	■
[9]	■	×	♦	×	×	×	[43]	■	★	■	×	■	×
[17]	♦	■	×	■	×	■	[54]	×	×	×	×	★	×
[47]	■	■	■	■	■	×	This work	✓	✓	✓	✓	×	×

Topic addressed	
T1	IFPV outlook
T2	OFPV outlook
T3	FPV classification
T4	FPV performance
T5	Environmental mpact
T6	Hybrid system

Color code	
×	Not addressed
■	Fundamental
♦	Intermediate
★	Comprehensive
*	Review article

3. Technological overview of FPV systems

In this section, a technological overview of FPV (including both IFPV and OFPV) systems is provided by exploring the following aspects: (1) the classification of FPV archetypes, and (2) the technology readiness levels of the most widely used archetypes. This section addresses the first review question (RQ1).

3.1. Classification of FPV archetypes

As highlighted above, the objective of this subsection is to offer a classification of the various FPV designs, also referred to as FPV archetypes, presently employed by researchers and technology developers for commercial/research purposes. Firstly, a compilation of various classification methods published from 2014 to 2024 is illustrated in Fig. 6. This arrangement shows the evolution and updates encountered in FPV archetype design over the span of a decade. While this classification offers a broad understanding of the available designs, there are certain associated limitations.

For instance, S. Kim et al. [175] used the method of foothold installation as a criterion for classification. D. Friel et al. [41] and S. Gorijan et al. [44] based their classifications on tracking systems, mooring configurations, and materials used for the floaters. On the other hand, A. Ghosh et al. [15], M. Kumar et al. [18], C. Ma et al. [42], S. Oliveira et al. [19], R. Cazzaniga et al. [176], W. Soppe et al. [179], R. Claus et al. [180], W. Shi et al. [43], M. Tina et al. [177], A. Pringle et al. [21], and the World Bank Group [24] classified the FPV archetypes based on the combination of floater design and waterbody suitability. A compilation of all their classifications is shown in Fig. 6.

From this, it can be deduced that each researcher has used different criteria to classify FPV archetypes. This raises several questions such as: Which classification scheme is most useful under the broadest set of conditions? Which criteria should be used for classifying FPV archetypes? And do all FPV archetypes fit within the existing classification schemes? These are some of the questions that are important and needs to be addressed. This review aims to do so by proposing a more generalized classification scheme, as shown in Fig. 7, which includes majority of the publicly available FPV designs categorized based on a defined set of criteria, as explained in Appendix B. With these criteria, the publicly available FPV designs can be categorized in a 3 × 5 matrix as shown in Fig. 7. This classification aims to serve two purposes: (1) providing a simple and effective classification that

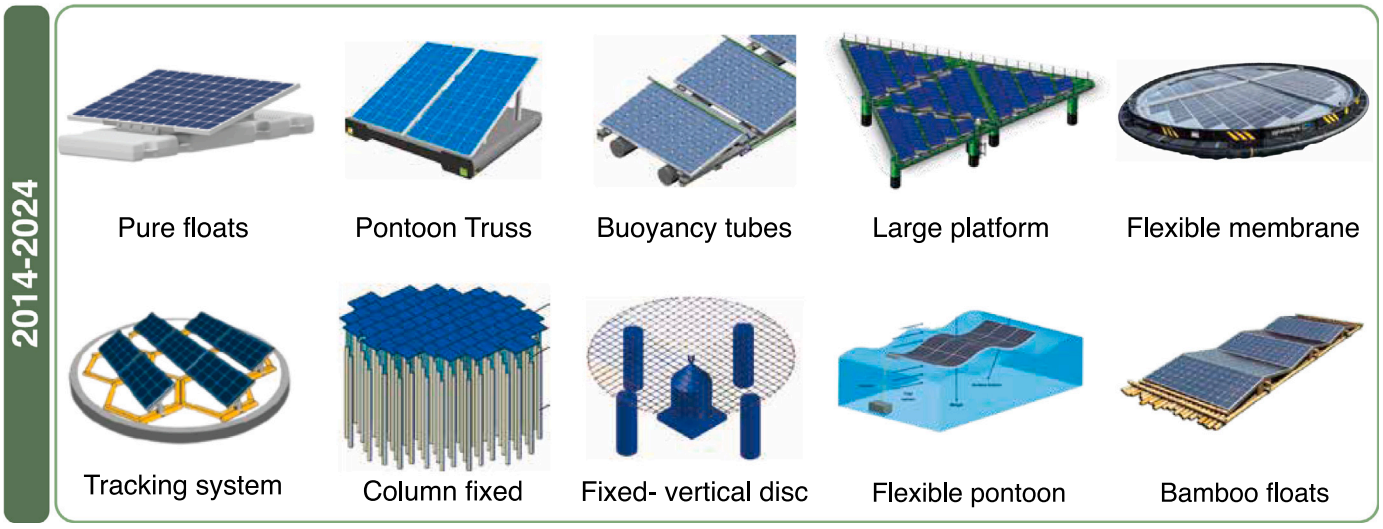

Fig. 6. Examples of the most commonly used classification schemes. *Compiled using* [8,9,15,18,19,24,41–44,46,47,50,54,55,175–181].

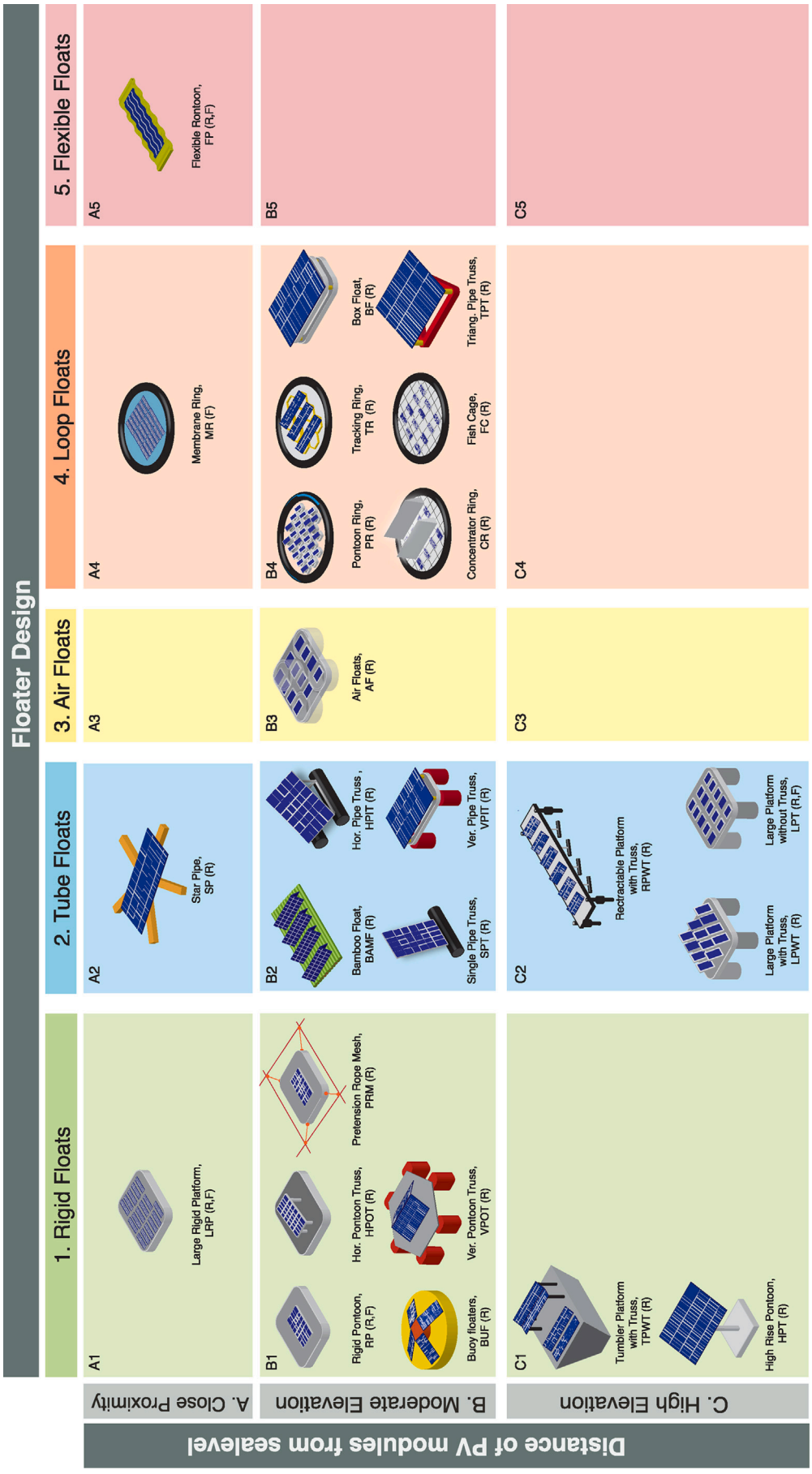

Fig. 7. Proposed classification framework. *FPV designs compiled and classified based on research publications and designs used by technology providers.*

Table 3
TRLs of different FPV archetypes hosted by different organizations. ‖ *This table shows the TRL of each provider based on the information available publicly and may subject to change.*

Archetype #	Organization	Country	Organization Type ⋆			Criteria ⋆⋆							TRL	
						Pub.	Pat.	Lab.	Pil.		Comm.		Inland	Offshore
			TP	RO	TD				I	NS/OS	I	NS/OS		
AF (R)	Technische Universität Wien [71]		×	✓	×	✓	×	➞	×	×	×	×	※	2–3
CR (R)	Infratech industries [72]		✓	×	✓	×	×	?	✓	×	×	×	3–5	※
FP (F)	Mirarco [9]		×	✓	×	✓	×	×	×	×	×	×	1–2	※
	Bluewater [73–75]		✓	×	×	×	✓	✓	×	➞	×	×	※	4–5
	DNV (SUNdy) [76]		✓	×	×	✓	×	×	×	×	×	×	※	1–2
HPIT (R)	Floating solar B.V. [77]		✓	×	✓	×	×	?	✓	×	✓	×	5–7	※
	Swimsol [78,79]		✓	×	✓	✓	✓	✓	×	✓	×	✓	※	4–6
HPOT (R)	Akuo Industries [80]		✓	×	✓	×	×	?	✓	×	✓	×	5–7	※
	BayWa r.e [81]		✓	×	✓	×	×	?	✓	×	✓	×	6–8	※
	Bouygues energies services [82]		×	×	✓	×	×	×	✓	×	×	×	5–7	※
	Bryo SpA [83]		×	×	✓	×	×	×	✓	×	×	×	4–5	※
	Celemin Energy [48]		✓	×	×	✓	×	×	×	×	×	×	1	※
	Chenya energy [84]		✓	×	✓	×	×	?	✓	✓	✓	✓	6–7	6–7
	Groenleven [85]		✓	×	✓	×	×	?	✓	×	✓	×	6–7	※
	HelioRec [86–88]		✓	×	?	✓	✓	✓	✓	✓	×	×	4–5	4–5
	Innosea [89]		×	×	✓	✓	×	✓	✓	?	✓	×	6–8	※
	Intech clean energy [90]		✓	×	✓	✓	➞	?	✓	×	➞	×	4–6	※
	Kyoraku Co. [91–93]		✓	×	✓	✓	✓	?	✓	×	✓	×	6–8	※
	LS industrial systems Co. [94,95]		✓	×	✓	✓	✓	?	✓	×	×	×	6–7	※
	Masdar [96]		?	×	✓	✓	×	×	×	×	✓	×	4–6	※
	Isigenere [97–99]		✓	×	?	✓	✓	✓	✓	×	✓	×	7–8	※
	Mibet energy [100]		✓	×	✓	✓	✓	✓	✓	×	✓	×	7–8	※
	Narime Qihua [101]		×	✓	×	✓	×	?	✓	×	×	×	4–5	※
	NEMO Eng [102]		✓	×	×	✓	✓	✓	✓	×	✓	×	5–6	※
	Nova innovation [103]		✓	×	✓	✓	×	×	×	➞	×	×	※	3–4
	NP Solar [104,105]		✓	×	✓	✓	×	×	×	×	✓	×	4–7	※
	NRG energia [106–109]		✓	×	✓	✓	✓	?	✓	×	✓	×	5–7	※
	Profloating [110–114]		✓	×	✓	✓	✓	✓	✓	×	✓	×	7–8	※
	Solinoor B.V. [115]		✓	×	?	✓	×	✓	✓	×	✓	×	7–8	※
	PV-floating Zimmermann [116]		✓	×	✓	✓	×	?	✓	×	✓	×	7–8	※
	Sumitomo Mitsui [117–119]		✓	×	✓	✓	✓	✓	✓	×	✓	×	7–8	※
	SCG Chemicals [120–124]		✓	×	✓	✓	×	?	✓	×	✓	×	6–7	※
	Sungrow [125]		✓	×	✓	✓	?	✓	✓	✓	✓	×	7–8	3–5
	Vikram solar Ltd [126]		×	×	✓	✓	×	×	✓	×	×	×	5–6	※
LPWT (R)	SeaVolt [127]		✓	×	✓	✓	➞	✓	×	✓	×	×	※	4–5
	Solarduck [128–134]		✓	×	✓	✓	✓	✓	×	➞	×	×	※	5–6
LRP (R)	Oceans of energy [135–138]		✓	×	✓	✓	✓	✓	×	➞	×	×	※	4–5
MR (F)	4C solar [139]		✓	×	×	×	✓	?	➞	×	×	×	2–5	※
	OceanSun [140–144]		✓	×	✓	✓	✓	✓	✓	➞	✓	×	6–7	4–6
PR (R)	Solaris float [145–148]		✓	×	✓	✓	✓	✓	✓	×	×	×	5–6	※
PRM (R)	FredOlsen 848 [149]		✓	×	✓	×	?	?	×	✓	×	×	※	4–5
RP (R)	Sunlit Sea [150,151]		✓	×	✓	✓	✓	✓	✓	×	×	×	4–5	※
SPT (R)	Sunfloat B.V. [152]		✓	×	?	✓	×	?	✓	×	×	×	4–5	※
TPWT (R)	Scotra [153]		✓	×	✓	✓	×	?	✓	×	✓	×	7–8	※
VPOT (R)	Moss maritime [154,155]		✓	×	✓	✓	✓	➞	×	➞	×	×	※	3–4
	Novar [156]		✓	×	✓	✓	×	?	➞	×	×	×	3–4	※
	SolarinBlue [157–159]		✓	×	✓	✓	✓	✓	×	✓	×	×	※	5–6
BF (R) HPOT (R), RPWT (R), SPT (R)	SINN power [160]		✓	×	✓	✓	×	?	✓	×	×	×	4–5	※
HPIT (R) FC (R)	Sunrise [161]		✓	×	✓	✓	?	?	×	?	×	×	※	3–4
HPIT (R), CR (R)	Upsolar [162,163]		✓	×	✓	✓	✓	?	✓	×	×	×	5–6	※
HPOT (R) TPT (R)	Ciel et Terre [164–168]		✓	×	✓	×	✓	✓	✓	✓	✓	×	6–9	3–5
VPOT (R) VPIT (R) BF (R)	CIMC raffles [169–174]		✓	×	✓	×	✓	✓	×	✓	×	×	※	4–6

‖ Symbol definitions: ✓— Yes, ×— No, ?— Not certain, ➞ - In process, ※— Not the intended application.
The FPV archetype abbreviations can be referred to Fig. 7
⋆ TP — Technology provider, RO — Research organization, TD — Technology deployer
⋆⋆ Pub. — Publication showing the concept, Pat. — Patent granted/applied, Lab. — Performed lab-scale testing, Pil. — Installed a pilot project, Comm. — have commercial installations on operating site, I — Inland conditions, NS — Near-shore conditions, OS — Offshore conditions.

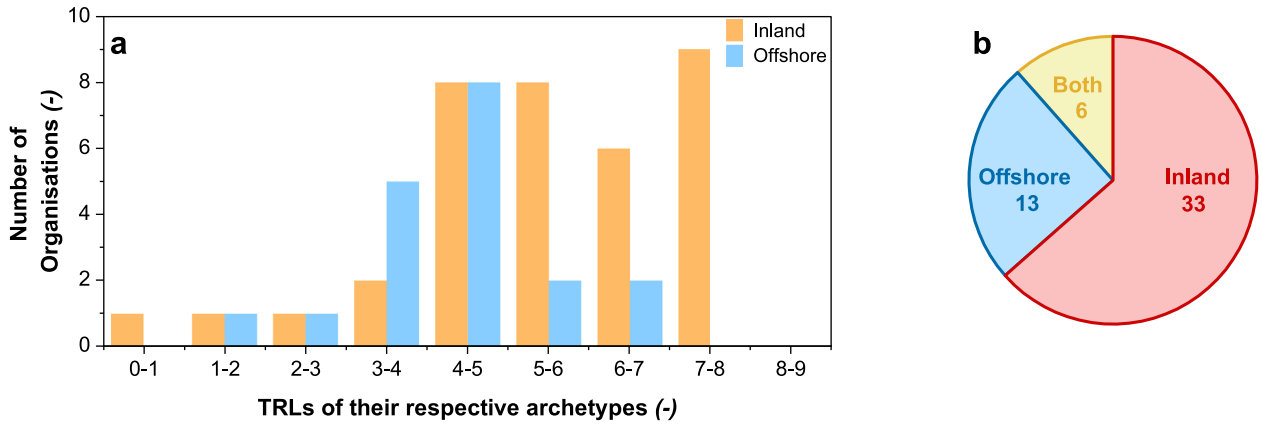

Fig. 8. Current technology readiness landscape. (a) The trend of TRLs for inland and offshore solar deployments, (b) number of organizations working on inland and offshore solar deployment. *Data derived from Table 3.*

incorporates majority of the publicly available FPV designs up to 2024, and (2) providing a template for the addition of any new or innovative concepts that might become relevant in future years.

3.2. Technology readiness levels (TRL)

With the classification introduced above, it is essential to understand the current technological status of each archetype. This subsection addresses this need by evaluating the Technology Readiness Level (TRL) of different FPV archetypes used by various organizations working within this field. It is important to note that assigning a singular TRL value to each archetype may not be practical or timely within the scope of this review. Therefore, this work provides a range of TRLs based on certain criteria derived from publicly available information, while still keeping the standard TRL definitions as Ref. [182] (see Appendix B for more details on the TRL definitions used in this work).

With these criterion's, Table 3 has been formulated that presents the TRL ranges of 17 different FPV archetypes widely used by 52 organizations working within this field. In this review, the TRLs are given for both inland and offshore applications, offering a comprehensive view of the current technological status of the field, also shown in Fig. 8 (a, b). From this table and figure, three important observations can be made, which are as follows:

- The TRLs for inland installations are higher compared to offshore installations as shown in Fig. 8 (a) which is expected due to the nascent nature of OFPVs.
- Majority of the archetypes in the offshore sector have a TRL of 4–5 indicating a need for further research and development as shown Fig. 8 (a).
- The most commonly used archetype is the horizontal pontoon truss (HPOT), followed by the vertical pontoon truss (VPOT) as shown in Table 3.
- Out of the 52 organizations reported in Table 3, 33 are focused solely on the inland FPV space, 13 are dedicated exclusively to the offshore space, and 6 are engaged in both areas, as shown in Fig. 8 (b).

4. Performance overview of OFPV systems

Up until this point, the technological overview of FPV systems were discussed. In this section, the second review question (RQ2) pertaining to the performance evaluation of OFPV systems will be addressed. At the end of this section, the reader will have a clear understanding of the following: (1) processes that needs to be considered when evaluating the EY of OFPV systems, (2) the current state of research on understanding these processes, (3) environmental and geometrical factors that affect these processes, and (4) the current state of quantification of these processes in terms of loss or gain in the EY.

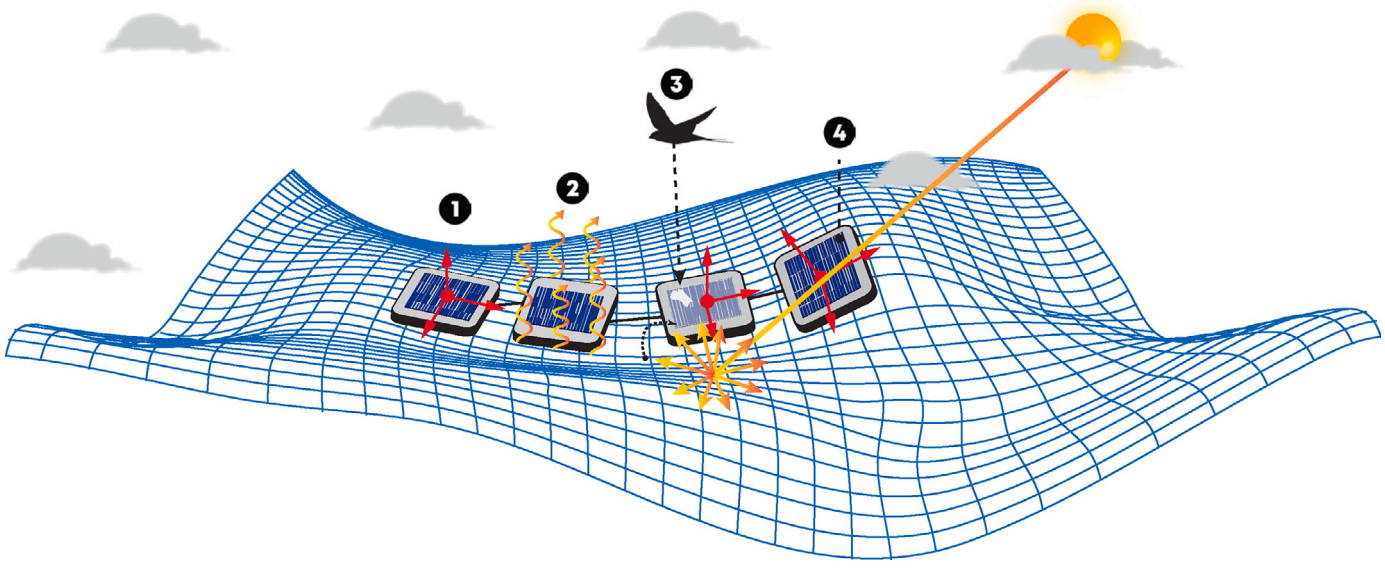

Fig. 9. Factors that can potentially influence the energy output of OFPV systems.

Offshore environments introduce a distinct set of conditions and challenges compared to inland environments. These conditions carry a degree of uncertainty when assessing their impact on the overall performance of OFPV systems. This section therefore aims to provide readers with a detailed overview on the effect of offshore conditions on the EY to help reduce the current ambiguity on this topic. Fig. 9 outlines all the potential processes encountered in offshore environments that could affect the EY of OFPV systems. A brief description of each process is provided below:

1. **Dynamic motion**: The first process is due to the combined effect of wind, waves, and current that lead to dynamic movement of the OFPV system, resulting in differences in irradiance falling on each module which affects the overall EY of the system.
2. **Cooling effect**: The second process is the effect of cooling, where the heat transfer process due to the combined action of wind and water changes the temperature of the PV modules, thereby affecting the EY.
3. **Optical effect**: The third process is due to various changes in the optical aspects such as dynamic albedo (sea-surface reflection), shading (salt deposition), and soiling (bird droppings), all of which influence the optical performance of PV modules, hence affecting the EY of the system.
4. **Degradation**: The fourth process affects the long-term performance of PV modules. The offshore environment presents a set of harsh conditions such as salinity, humidity, mechanical stresses etc. which degrade the PV module over time, thereby affecting the long-term EY of the system.

With the above explanation, it is important to explore these processes in greater detail and assess our current understanding on how they impact the EY. The upcoming subsections will therefore provide an in-depth examination of each of the processes mentioned above, along with a comprehensive summary of the existing research on quantifying their impact on the EY.

4.1. Impact of dynamic motion

This subsection deals with understanding the effect of dynamic motion (also known as hydrodynamic response, HR) on the EY. Four important objectives will be covered in this subsection: (1) understanding why and how dynamic motion affects the EY, (2) reviewing the current state of research focusing on HR characteristics of different archetypes, (3) identifying key factors that influence the hydrodynamic behavior, and (4) quantifying the HR in terms of loss/gain in the EY.

Fig. 10 shows the methodology in which the dynamic motion of OFPV systems can affect their EY. To understand this process, two types of analysis needs to be performed: hydrodynamic and EY. Under the hydrodynamic analysis, the loads acting on the system are first determined followed by the response of the structure when subjected to the above-mentioned loads. Ideally, a floating structure can have a response in six degrees of freedom (DoF), as shown in Fig. 10 (b). In the maritime field, the response of any floating structure is commonly demonstrated through a parameter called the response amplitude operator (RAO) [185] (see Appendix B).

With the HR of the system, the EY analysis can be understood. Normally, for GPVs, two angles are crucial—tilt and azimuth, as shown in Fig. 10 (b) which can be correlated to the rotational DoFs of the OFPV system. The tilt (θ_t) and azimuth (a_z) angles dictate the plane of array irradiance (see Appendix B) on the modules [186]. For example, if two series-connected modules in the case of an OFPV system have different rotational orientations (in terms of θ_t, a_z) over time t, then the irradiance falling on each module at every time instant will be different, as shown in Fig. 10 (c) leading to a situation where the irradiation on one module will be higher than the other. In this case, the module producing the lowest current limits the energy output of the entire system, as shown in Fig. 10 (d). This effect is termed as response induced mismatch losses.

Therefore, it is critical to determine and incorporate the mismatch losses caused due to the motion of an OFPV farm in the EY estimation of such systems. The lower the mismatch losses, the better is the energy output from the system. Hence, in this section, a literature overview is provided focusing on: the HR studies pertaining to different FPV

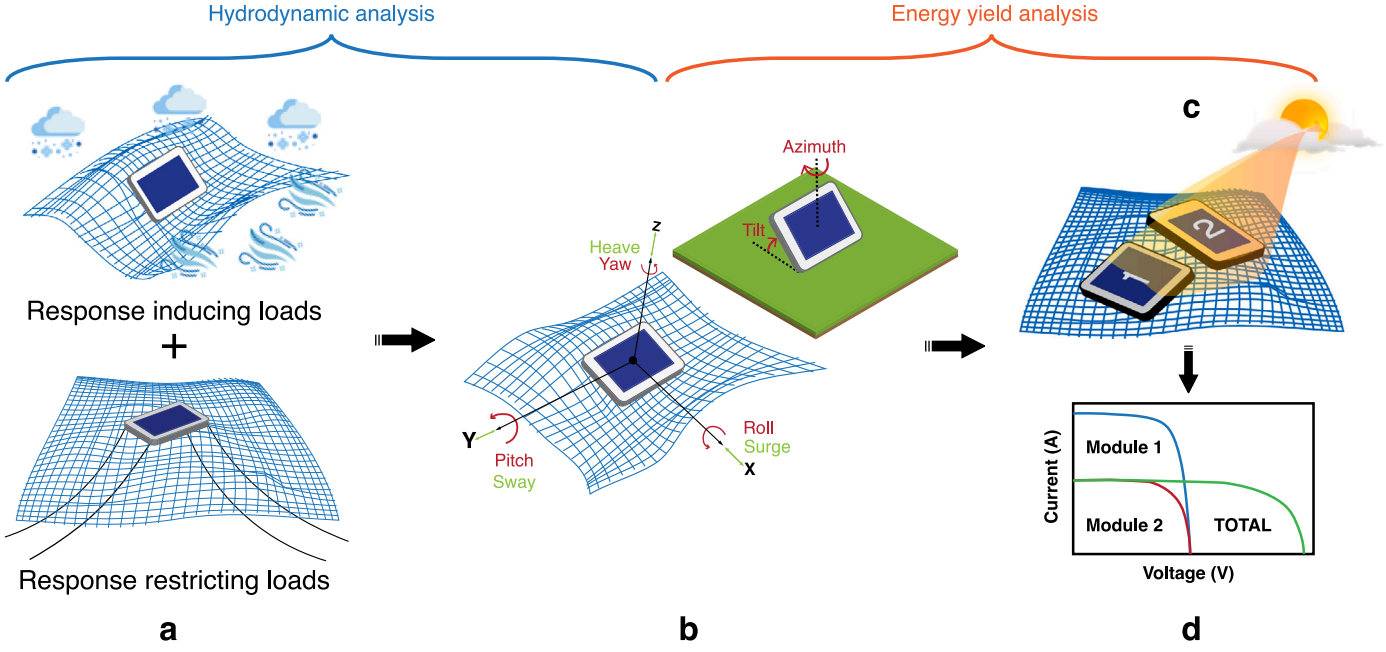

Fig. 10. Method in which the dynamic motion of FPV systems affect the EY. (a) Types of loads acting on the system: response-inducing loads (such as wind, wave, current, and snow loads), which tend to alter the equilibrium of the system, and response-restricting loads (such as mooring and anchoring loads), which tend to stabilize the system and restore equilibrium [11,15,19,42,183,184]. (b) 6 DoF motion (three translational motions (surge, sway, heave) and three rotational motions (roll, pitch, yaw)) of a FPV system compared to the tilt and azimuth angles of GPV system, (c) difference in irradiation levels due to constant variation in the orientation, (d) energy mismatch due to non-uniform irradiance.

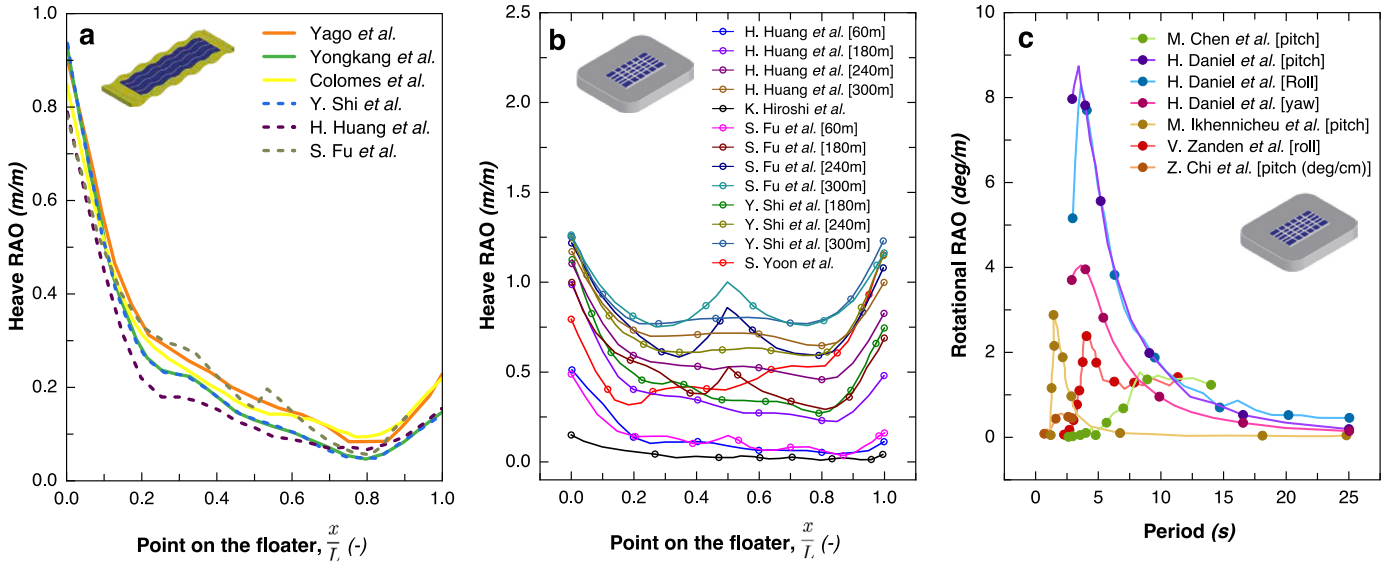

Fig. 11. Case studies on the hydrodynamic responses of flexible (FP) and rigid pontoons (RP). (a) comparison of heave RAO of FP and MC-RP archetypes at $\lambda = 120$ m, (b) Heave response of MC-RP archetype at $\lambda = 60$ m, 240 m, 300 m, (c) Rotational RAOs for the RP archetype from different studies. *Data extracted using matlab digiplotter package [187].*

archetypes (as outlined in Fig. 7), factors that influence the response, and the effects these response have on the EY.

To facilitate easy readability, the literature review has been structured according to the types of analysis, as shown in Fig. 10. Under each type of analysis, further subheadings are provided categorized based on the FPV archetypes, further allowing readers to navigate and read each section independently. This structure is consistently followed throughout the work. Additionally, Table B.5 has been constructed (see Appendix A) which categorizes all the research articles based on the type of processes they study (list of processes shown in Fig. 9). This table serves as a quick reference to identify the focus of each article along with certain specific information, such as the type of study, archetype information, environmental conditions used, and the observations made in terms of EY. Hence, in the summary of the literature, only the most important takeaways from each study is highlighted.

4.1.1. Hydrodynamic response of different FPV archetypes

This part of the review focuses on providing a summary on the methods used to determine the HR of different FPV archetypes. The important figures of merit that influence the HR are also discussed in detail.

Flexible pontoon

Y. Shi et al. [188], M. Ohkusu et al. [189], Y.Cheng et al. [190], H. Maeda et al. [191], O. Colomés et al. [192], Z. Li et al. [193] and K. Yago et al. [194,195] have worked on evaluating the hydroelastic response of a flexible pontoon (FP) archetype. Each study performed is different with respect to the dimensions of the archetype, wave conditions, and wave directions, as seen in Table B.5. Vertical displacement, also known as the heave RAO, was measured/simulated by [188–192, 194,195] at different points (x) on the pontoon at varying wavelengths (results observed at $\lambda = 0.4L$ is shown by the solid lines in Fig. 11 (a)). It was noted that the heave RAO attains the highest value at the first point of contact between the wave and pontoon and then gradually dampens towards the end of the pontoon due the attenuation of wave energy, see Fig. 11 (a). Studies by [188–192,194,195] highlighted that FPs are prone fail when $\frac{\lambda}{L} \in [0.2, 0.8]$, due to observed peaks in stability that are mainly influenced by the direction of the incident wave : stable for $\theta_{wv} < 40°$ and unstable for $\theta_{wv} > 60°$.

Z. Li et al. [193] considered a multi-directional hinge connected arrangement (see Table B.5) of the FP archetype and performed a sensitivity analysis by varying parameters such as module size, number of modules, wave direction, and connection stiffness. It was observed that systems with smaller module sizes exhibited larger translational responses and lower rotational responses compared to medium and large-sized PV modules. Increasing the number of PV modules beyond a threshold did not show any changes in the motion response. However, oblique waves and higher connector stiffness resulted in more pronounced responses of the system. All the mentioned effects showed less effectiveness in the long-wavelength regime.

The works of H. Kagemoto et al. [196], J. Yoon et al. [197], Y. Shi et al. [198], S. Fu et al. [199], H. Heng et al. [200,201], P. Xu et al. [202], Y. Wei et al. [203], D. Zhang et al. [204], Z. Deqing et al. [205], and H. Daniel et al. [206] have compared the hydroelastic response of the FP archetype to the HR of a multi-connected rigid pontoon (MC-RP) archetype. The results obtained by [198–201] are shown by the dotted lines in Fig. 11 (a), estimated at $\lambda = 0.4L$, which shows a good match between both approaches. The heave RAOs at other wavelengths are also shown in Fig. 11 (b), allowing for further comparison of the results.

Rigid pontoon

Certain case studies pertaining to the multi-connected rigid pontoon (MC-RP) have been performed by [196–203,207]. P. Xu et al. [202] studied the action of freak waves on the response of the MC-RP archetype. It was noted that the surge response was deemed the dominant motion of the entire farm. On the other hand, studies by [196–201,203] evaluated the effect of connectors between the floaters and indicated that hinge connections significantly influence the system's response based on their stiffness values. Z. Deqing et al. [205] observed stronger pitch responses with hinged connectors, noting that the floater adjacent to the end of the array experiences a larger pitch response. However, the hinge connectors did not show uniformity in their effect on the heave response.

J. Zanden et al. [207] conducted an experiment using an external floating breakwater (FBW) with MC-RP archetype. It was observed that FBWs are less effective when the wave frequency, $\omega \in [1, 1.6]$ rad/s. In this configuration, the PV modules tend to move independently in the heave, pitch, and roll motions, whereas the entire farm moves as a whole in the surge response. However, this response characteristic is dependent on the relative spacing between the PV modules, which needs to be optimized. Similarly, Y. Wei et al. [203] performed a simulation of a pontoon ring (PR) archetype with a hexagonal breakwater and noticed that breakwaters can be beneficial for this archetype to reduce response and structural damage in rough sea state condition.

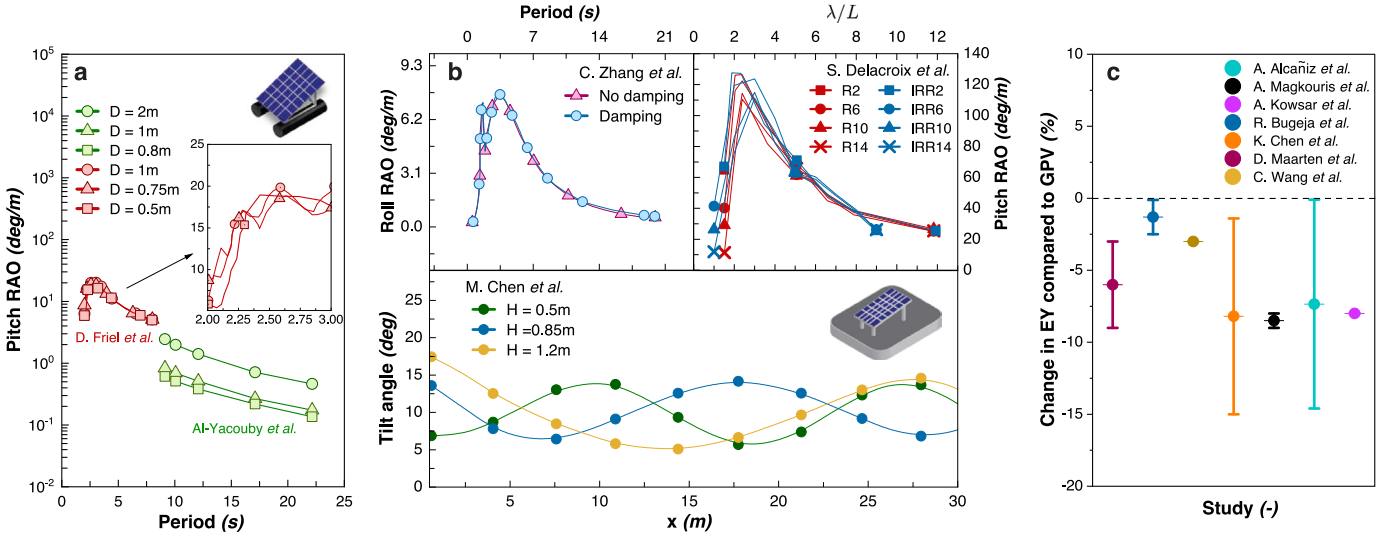

Fig. 12. Case studies on the hydrodynamic response of HPIT and HPOT archetypes with EY quantification. (a) pitch RAO of HPIT archetype showing the effect of cylinder diameter, (b) compilation of different studies on rotational response of the HPOT archetype, (c) examples of studies that have estimated the change in EY with respect to a GPV system due to the effect of motion. *Data extracted using matlab digiplotter package [187].*

M. Ikhennicheu et al. [208], C. Zhang et al. [209], and M. Chen et al. [210] have compared different methodologies to evaluate the HR of a MC-RP archetype as shown in Fig. 11 (c). M. Ikhennicheu et al. [208] studied three scenarios: (1) when no hydrodynamic interactions exist between the floats, (2) when no transfer of dynamic motion occurs between the floats, and (3) when both hydrodynamic and dynamic motion interactions exist between all the floaters. A 16% difference in the motion response was observed between scenarios (1) and (3) and a 19% difference between scenarios (2) and (3). Scenario (3) was deemed to be the most accurate with the downside of having high computational time. C. Zhang et al. [209] studied three other methods: empirical, two-step, and hydroelastic mode method. It was noted that these three methods show similar results in the long wave regime, while the empirical and the two-step methods over-predict the responses in short wave conditions (when $T_p < 2s$ and $\lambda \approx L_{RP}$). M. Chen et al. [210] developed the constant-parameter hydrodynamic–structural time-domain model (CPHSTDM) to simulate the response of the RP archetypes with complex connector configurations. It was found that the bending stiffness of the connectors have a significant influence on the HR of the system. The main takeaway from [208–210] is that for a MC-RP system, a complete hydrodynamic simulation (with the relevant wave effects) has to be performed including appropriate values for the connector stiffness to predict a realistic response of the system.

Horizontal pipe truss

A. Al-Yacouby et al. [211], G. Baruah et al. [212], D. Friel et al. [213,214], R. Claus et al. [215], and A. Abbasnia et al. [216] have performed hydrodynamic analyses for the horizontal pipe truss archetype (HPIT). A. Al-Yacouby et al. [211] and D. Friel et al. [213,214] have focused on evaluating the effect of cylinder diameter on the HR. A. Al-Yacouby et al. [211] reports that wave height, wave period, and increasing cylinder diameters have a major influence on the response of the system. On the other hand, D. Friel et al. [213,214] reports that increasing the diameter of the cylinder has a minor effect on the response. The comparison of their results of their study can be seen in Fig. 12 (a). The difference in observations can be attributed to multiple factors such as the number of cylinders, range of diameter variation, and wave conditions. From the plot, it can be visualized that the wave period influences the extent to which the cylinder diameter affects the pitch RAO of this archetype.

The studies of G. Baruah et al. [212], R. Claus et al. [215], and A. Abbasnia et al. [216] have focused on understanding the HR behavior of HPIT archetype when subjected to real-sea conditions with mooring lines (see Table B.5). G. Baruah et al. [212] noted that wind forces primarily affect the translational motions, while wave loads majorly influence the rotational motions. R. Claus et al. [215] observed a 32% to 76% reduction in yaw motion (equivalent to a_z) depending on the cross-section of the mooring line. A. Abbasnia et al. [216] studied the effect of gaps between the cylinders and concluded that when $\frac{\lambda}{gap} \in [1.6, 2.51]$, the response in heave and surge increased, while it decreased in pitch.

Horizontal pontoon truss

H. Joo et al. [217], R. Yang et al. [218], F. Zhang et al. [209], S. Delacroix et al. [219], C. Bi et al. [220], and K. Chen et al. [221] have worked on evaluating the HR of the horizontal pontoon truss archetype (HPOT). H. Joo et al. [217] and R. Yang et al. [218] studied the effect of wind loads and observed that the largest loads due to wind are usually experienced by the first and last arrays of the modules when the wind direction is $\theta_{wd} = 0°, 180°$. Wind loads caused large drift motion of the floating platform by generating a vortex area between each floater that can lead to damage of the PV modules. With their test conditions (see Table B.5), the archetype experienced a ±6° change in the pitch response (affecting θ_t) without overturning.

The works of F. Zhang et al. [209] and S. Delacroix et al. [219] focused on understanding the difference between unit archetype (UA) dynamics and multi-connected horizontal pontoon truss (MC-HPOT) dynamics. F. Zhang et al. [209] observed that even medium wave conditions (see Table B.5) could cause large motion responses for a unit archetype, which would not be the case with MC-HPOT due to the presence of gaps between each floater, affecting the wave-floater interaction. Zhang et al. [209] suggests including appropriate surface gap damping coefficients in numerical models to avoid discrepancies in the responses, as shown in Fig. 12 (b). S. Delacroix et al. [219] highlighted that the RAO of the pitch motion of all rows of floaters exhibited a peak when $\lambda = 2L$, corresponding to the resonance of the system, as shown in Fig. 12 (b). It was also observed that the first row experienced larger pitch motions compared to the last row, indicating a shadowing effect that seemed to affect only smaller wavelengths, in line with the observations made by [193] for the FP archetype.

High rise platform

R. Claus et al. [222] and M. Lopez et al. [223] worked on understanding the hydrodynamic performance of the high-rise platform (HRP) archetype with a tracking system. The specifics of both works

[222,223] can be seen in Table B.5. R. Claus et al. [222] conducted lab-scale experimental tests for a unit HRP archetype under both regular and irregular wave conditions. It was observed that the translational response was higher than the rotational response due to the stiffness of the mooring lines. Due to the low variations in the rotational response, the losses due to mismatch could be reduced significantly. It was also highlighted that the translational motions do not affect the energy produced by the farm but do impact the optimal distance between two archetypes when connected together. M. Lopez et al. [223] performed simulations with the same operating conditions and observed similar results to those of R. Claus et al. [222].

Vertical pipe truss

J. Song et al. [224], Z. Jiang et al. [225], J. Song et al. [226], and C. Yan [227] studied the hydrodynamic performance of the vertical pipe truss (VPIT) archetype. [224,226,227] performed simulations to observe the effect of currents, mooring lines, and installation angle (see Appendix B) on the response of the system. The takeaways from these studies are as follows: currents have a negligible effect on the system's response, the stiffness of the mooring dictates the damping of the system, and the number of connected archetypes dictates the stiffness of the mooring. It is recommended to maintain an installation angle of at least 15° to lower the overall system response. Z. Jiang et al. [225] conducted similar studies with a slight change in the archetype. Here, a multi-connected VPIT (MC-VPIT) archetype was interconnected via tension ropes (see Table B.5). It was observed that the difference in response between each unit archetype was minimal due to the interconnected ropes, potentially leading to low mismatch losses.

Triangular pontoon truss

W. Kang et al. [228] studied the HR of a triangular pontoon truss (TPT) archetype using numerical simulations (see Table B.5). The study highlighted that wave direction can have a strong effect on the response of this archetype, and they recommended an optimal installation angle of 0°. This is lower than the value (at least 15°) recommended by [224, 226,227] for the VPIT archetype, indicating that each archetype has specific operating parameters to ensure optimal system performance.

Up to this point, a summary of studies explaining the hydrodynamic analysis of different archetypes such as RP, FP, HPOT, HPIT, VPIT, and BUF has been provided. However, as mentioned at the beginning of this section, it is equally important to convert these HRs into EY predictions. It is found that there are not many studies that have worked on this aspect. However, few works that have quantified the EY due to motion are shown in Fig. 12 (c), some of which are explained below.

4.1.2. EY quantification of different FPV archetypes due to the effect of motion

In this part of the review, the effect of HRs discussed earlier are quantified in terms of EY to get an understanding of the most influential DoF.

Buoy floater

C. Wang et al. [229] investigated the impact of the hydrodynamic motion of the buoy floater (BUF) archetype on the EY of the system. Their study revealed a 2% to 5% difference in the irradiation received by the BUF archetype compared to a ground-mounted photovoltaic (GPV) system. They concluded that for every 5° increase in θ_t, an energy loss of 3% is expected.

Horizontal pontoon truss

K. Chen et al. [221] simulated the EY of the HPOT archetype due to wind-induced waves at three offshore locations (see Table B.5). The θ_t variations simulated in this work are shown in Fig. 12 (b). It was observed that when the modules have a pre-tilt angle (see Appendix B)($\theta_{pretilt} \in [0°, 10°]$), the relative difference in energy output was 1.5% compared to the EY at tilt angle of 0°. Consequently, when $\theta_{pretilt} \in [10°, 15°]$, the relative difference increases to 3% as shown in Fig. 12 (c).

Rigid pontoon

R. Bugeja et al. [230] and A. Kowsar et al. [231] have studied the EY aspect of the RP archetype. A. Kowsar et al. [231] compared a 50 MW FPV plant with a GPV system located in a marshland area in Bangladesh. The pre-tilt angles of both systems were 5° and 24.7°, respectively. They highlighted that the yearly EY of the FPV system was 7.22% lower than that of the GPV system (see Fig. 12 (c)). R. Bugeja et al. [230], on the other hand, studied the effect of motion on the insolation of OFPV systems. It was observed that the pitch response resulted in a 2.52% drop in insolation as it directly affects the tilt of the system. Yaw responses showed a very small effect, as it briefly affects the azimuth of the system (less than 0.38%). They concluded that roll motions could have a more significant effect as this motion affects both the tilt and the azimuth of the system.

Large rigid platform

A. Alcañiz et al. [232] and A. Magkouris et al. [233] have worked on estimating the EY of a large rigid platform (LRP) archetype (see Table B.5). A. Alcañiz et al. [232] predicted the motion (due to wind-generated waves) and DC/AC yield of the LRP archetype in the Dutch North Sea region. Highlights from the study were that a heavy rectangular floater with the widest side aligned towards the wind direction showed reduced response variations. The effect of this motion on EY reduction is negligible (0.1%) when compared to a GPV system at a θ_t of ($\theta_t = 0°$). This reduction can increase up to 14.6% when compared to a GPV system placed at an optimum θ_t as shown in Fig. 12 (c). This study also looked into the effect of motion on inverter efficiency and noted a loss of 2%. A. Magkouris et al. [233] performed similar studies in the Greek sea region and observed a decrement of 8%–9% in EY with the FPV system when compared to an optimally tilted GPV system. The study indicated that the module roll response has a strong influence on the energy generated by the system, similar to the study by [230].

Takeaways

This subsection provided insights into the current state of our understanding regarding the effects of motion on the EY. From the summary above, it can be deduced that although there is active research ongoing in understanding the HR of different FPV archetypes, there are certain associated limitations: (1) most studies focus on understanding the influence of specific factors (environmental or geometrical) on the system's translational (surge, sway, heave) and rotational (pitch, roll, yaw) response (which is important) but does not clearly address on which of the 6DoF actually influence the EY of the system; (2) the studies also do not fully portray the behavior of OFPV systems in practical offshore environments; (3) only a limited number of studies actually quantify the effect of HRs in terms of the EY by making certain critical assumptions. Finally, Based on the data compiled in this section (see Fig. 12 (c)), it can be inferred that an EY loss of ***0.4% to 15%*** can be expected due to the effect of motion. The above mentioned gaps in understanding the impact of motion on EY create uncertainties that tend to slowdown the progress of the field. Therefore, future research must address these uncertainties to enhance our understanding on the effect of motion on EY. Some of the key conclusions from this subsection are discussed later in Section 5.

4.2. Impact of cooling effect

This subsection deals with understanding the effect of cooling on the EY. Four important objectives will be covered in this subsection: (1) understanding how the process of cooling affects the EY, (2) reviewing current literature and compiling the different methods used to estimate the cooling effect, (3) factors that have an effect on the cooling process and (4) quantifying this effect in terms of EY. Fig. 13 shows the comparison of the heat transfer (HT) [234] (see Appendix B) mechanism between a GPV and an OFPV system. As seen from the figure, OFPVs have three additional HT mechanisms (process 4,5,6 as explained in the caption of Fig. 13) when compared to GPVs. These additional mechanisms contribute to the enhanced HT between the system and

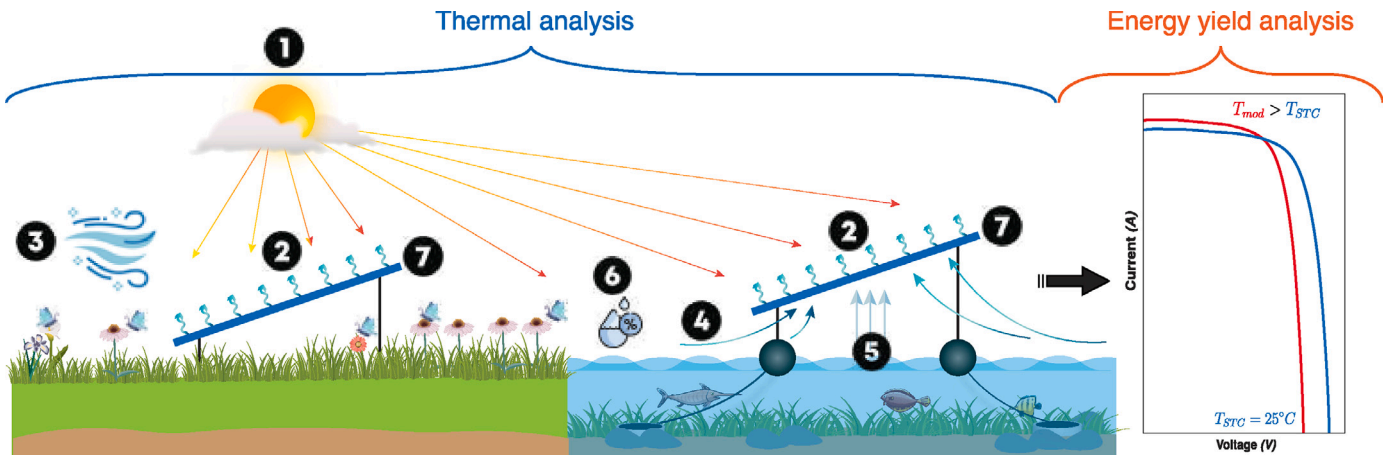

Fig. 13. The heat transfer (HT) process in photovoltaic systems. (1) Radiative heat transfer from the sun to the module layers, where solar radiation directly heats the module surfaces. (2) Radiative heat loss from the module to the surroundings, contributing to cooling. (3) Convective heat transfer due to wind flow over the PV module, which helps lower the module temperature due to forced convective heat transfer, with effectiveness dependent on site conditions. (4) Convective heat transfer occurring on both the upper and lower module surfaces in GPVs and OFPVs. However, in OFPVs, the presence of water in offshore conditions enhances cooling due to lower ambient temperatures. (5) Convective evaporative cooling in OFPVs, where moisture from the water surface evaporates, facilitating heat and mass transfer at the back of the modules, thereby enhancing cooling for archetypes in moderate to high elevation regimes, as shown in Fig. 7. (6) Convective heat transfer due to humidity, which plays a significant role in offshore conditions and can either increase or decrease module temperature depending on the location. (7) Conductive heat transfer within the module layers, affecting overall heat dissipation.

the environment which can potentially lower the module temperature (T_{mod}), thereby resulting in some cooling effect.

There are two types of analysis that need to be performed to evaluate the impact of cooling on OFPV systems: Thermal and EY (see Fig. 13). A thermal analysis involves evaluating the thermal behavior of PV modules by incorporating all the relevant heat transfer mechanisms. This needs to be conducted as this can affect system performance in two ways. Firstly, it alters the module temperature, which directly influences the EY of the system (lower T_{mod} leads to higher EY). Secondly, it influences the degradation rates of the modules due to thermal cycling.

In general, there are two ways of conducting the thermal analysis for FPV systems: (1) perform long-term site measurements or CFD studies to predict empirical correlations for T_{mod}, and (2) determine typical heat loss coefficients (U-values, see Appendix B) based on short-term site measurements, which can be used in the Faiman model [235] as shown in Eq. (1) to evaluate the T_{mod}, which is then used for the EY analysis.

$$T_{mod} = T_{amb} + \frac{G_{POA}}{U_c + U_v \cdot U_\infty} \tag{1}$$

Due to the nascent stage of the field, reliable long-term measurements are challenging, leading researchers to explore other alternatives such as proposing empirical correlations or U-values based on short-term temperature data (either from site measurements or CFD simulations). In the upcoming paragraphs, the methods used by different studies are summarized for each archetype (including both analysis as shown in Fig. 13), along with providing the corresponding T_{mod} correlations and U-values for various FPV archetypes. This summary will also provide an understanding of how these factors quantify the effect on EY.

4.2.1. Thermal analysis and EY quantification of different FPV archetypes

This part of the review deals with the different methodologies used in literature to evaluate the thermal behavior of different FPV archetypes and the factors that influence the cooling effect. The impact of the thermal behavior on the EY is also quantified in the summary below.

Horizontal pipe truss

G. Chowdhury et al. [236], T. Kjeldstad et al. [237], N. Elminshawy et al. [238–240], B. Amiot et al. [241], G. Tina et al. [242,243], M. Dörenkämper et al. [244] and H. Liu et al. [245] have studied the effect of cooling with the horizontal pipe truss archetype (HPIT). Kjeldstad et al. [237] and Dörenkämper et al. [244] have performed statistical analysis to determine the U-value of this archetype in three locations: Srilanka, Netherlands and Singapore using Eq. (2) as shown in Fig. 14. The study of [237] ignored the effect of wind speed on the estimation of the U-value, whereas [244] considered this effect. It was noted that wind speed is directly proportional to the heat loss of the system and is influenced by the type of archetype.

$$U = \frac{G_{POA} \cdot (\psi - \eta \cdot T_{mod})}{T_{mod} - T_{amb}}, U = U_c + U_\infty \cdot U_v \tag{2}$$

H. Liu et al. [245] and G. Tina et al. [242] have measured [245] and simulated [242] temperature parameters of monofacial and bifacial PV modules at a site in Singapore, Frankfurt and Catania with the HPOT and HPIT archetypes which were differentiated by varying the distance of the PV modules from the water surface and water surface coverage. Both studies determined the U-values for the above-mentioned systems and observed that free-standing and small footprint systems (see Appendix B) show a higher U-value indicating lower module temperatures (see Fig. 14). The takeaway from this study is that the effect of cooling depends on the archetype, distance of the PV modules from the water surface, and the weather condition at the site. It was also noted that irrespective of all the above-mentioned factors, the U-value of FPV systems is equal to or higher than well-ventilated ground or roof-mounted systems.

N. Elminshawy et al. [238–240] studied the thermal behavior of both floating and partially submerged PV systems using both experimental and computational approaches. A regression analysis was used to predict two equations for evaluating the T_{mod} as a function of multiple factors as shown in Eqs. (3) and (4). It was collectively observed that both wind speed and wind direction have a direct influence on the module temperature. The wind direction ($\theta = 90°, 180°$) showed the lowest module temperature [238–240]. The differences in the power outputs of the system with varying submerged ratios show that a threshold exists beyond which the performance starts to degrade (beyond 25%) as shown in Fig. 15.

$$T_{mod} = 71.62 + 25.6 \cdot t - 0.23 \cdot G_{POA} - 1.23 \cdot AF - 23 \cdot A_R - 8.9 \cdot T_{amb} + 6.64 \cdot A_R \cdot T_{amb} + 8.8 \times 10^3 \cdot G_{POA} \cdot T_{amb} - 1.05 \cdot t^2 + 2.2 \times 10^{-5} \cdot G_{POA}^2 \tag{3}$$

$$\ln(T_{mod}) = 3.62 - 0.0068 \cdot \theta_{wd} - 0.0549 \cdot U_\infty - 0.0109 \cdot U_\infty \cdot \theta_{wd} - 0.0598 \cdot \theta_{wd}^2 + 0.007 \cdot U_\infty^2 \tag{4}$$

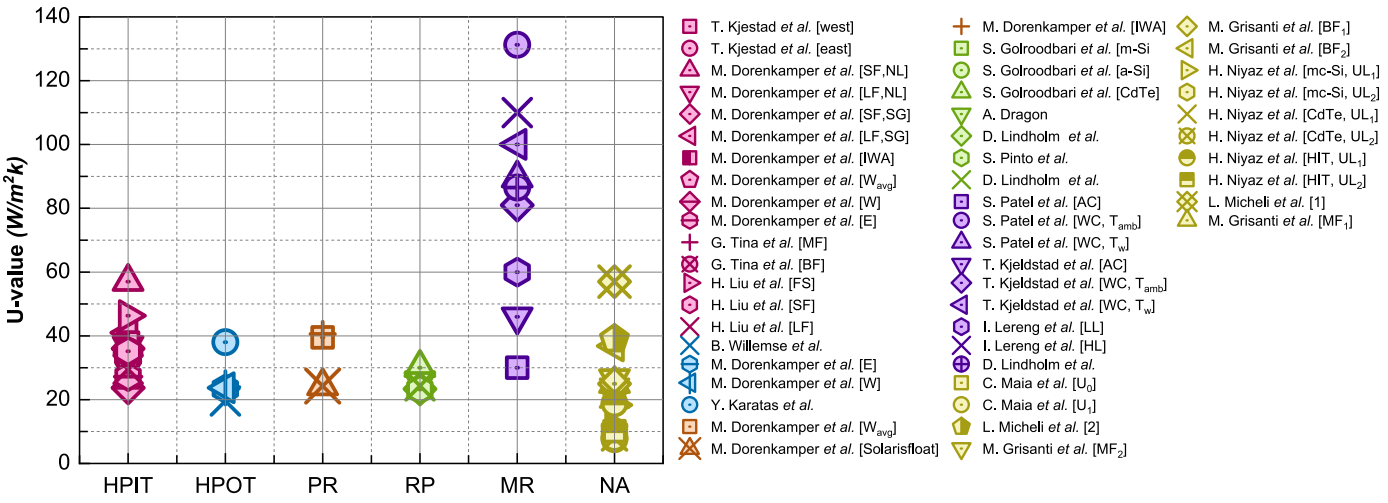

Fig. 14. Heat loss coefficients or U-values of different FPV archetypes. (abbreviations: NA — no archetype, SF — small footprint with open structure, LF — large footprint with closed structure, MF — monofacial modules, BF — bifacial modules, NL — Netherlands, SG — Singapore, SL — Srilanka, FS — free standing, AC — air-cooled, WC — water-cooled, LL — lower limit, HL — higher limit) *Data extracted using matlab digiplotter package [187] and the data values of this plot can be accessed in Appendix B.*

G. Chowdhury et al. [236], B. Amiot et al. [241], G. Tina et al. [242], and M. Dörenkämper et al. [244] used different HT techniques such as CFD [236], five-layer thermal model [241], and multilayer model [242] to study the thermal behavior of the HPIT archetype. Their studies revealed that relative humidity, water temperature, and θ_t had a lower influence on the T_{mod} compared to ambient temperature (showing a 0.85 °C change in T_{mod} per degree change in T_{amb}), wind speed, wind direction, and the distance above water (FPVs placed close to the water surface showed reduced performance due to low convective heat transfer).

B. Cheng et al. [220], B. Amiot et al. [246], B. Willemse et al. [247], M. Rahaman et al. [248], H. Nisar et al. [249], N. Kumar et al. [250], R. Radhiansyah et al. [251], Y. Karatas et al. [252], I. Peters et al. [253], W. Kamuyu et al. [254,255], D. Tryakin et al. [256] have studied the effect of module temperature variation for the horizontal pontoon truss type archetype (HPOT). B. Amiot et al. [246] have made use of a quantile regression model along with onsite measurement data to predict an equation for the median function of the U-value which is as shown in Eq. (5).

$$U_c = 3.05 \cdot U_\infty + 24.29 \tag{5}$$

B. Willemse et al. [247] and Y. Karatas et al. [252] used regression analysis with Eq. (6) alongside onsite measurements to determine the median U-values, which are shown in Fig. 14. It was noted that θ_t significantly influences the rate of heat convection on the back surface of the module. Once again, ambient temperature emerged as the major influencer, with a unit degree increase in ambient temperature leading to a 0.43% loss in energy.

$$(\tau \cdot \psi) \cdot G_{POA} = \eta \cdot G_{POA} + U_c \cdot (T_{mod} - T_{amb}) \tag{6}$$

B. Cheng et al. [220], M. Rahaman et al. [248], R. Radhiansyah et al. [251], Y. Karatas et al. [252], I. Peters et al. [253], W. Kamuyu et al. [254,255], and D. Tryakin et al. [256] used both experimental and computational approaches to predict T_{mod} equations. M. Rahaman et al. [248] studied the HT effects using three different models—simple thermal, empirical, and CFD. The T_{mod} correlations predicted using the simple thermal and the empirical model are shown in Eqs. (7) and (8) respectively which are similar to the full fluid dynamic model proposed by M. Fuentes [257] . It can be observed that both techniques yield a correlation that largely depends on the same set of parameters as inline with other studies discussed up until now which are: irradiance, ambient temperature, wind speed, and water temperature.

$$T_{mod} = \frac{h_{c_f} \cdot T_{amb} + h_{r_f} \cdot T_{amb} + h_{c_b} \cdot T_{wat} + h_{r_b} \cdot T_{wat}}{h_{c_f} + h_{c_b} + h_{r_f} + h_{r_b}} + \frac{-P_e + Q_g + \tau \cdot \psi \cdot G_{POA} + \frac{\alpha \cdot \Delta G_{POA}}{L}}{h_{c_f} + h_{c_b} + h_{r_f} + h_{r_b}} + T_{mod_0} \cdot e^L \tag{7}$$

$$T_{mod} = 2.052 - 0.053 \cdot RH + 0.965 \cdot T_{amb} + 0.0068 \cdot G_{POA} + 0.1364 \cdot T_{wat} - 0.495 \cdot U_\infty + 0.0028 \cdot U_{wd} + 0.0187 \cdot GHI \tag{8}$$

B. Cheng et al. [220] and Radhiansyah et al. [251] proposed T_{mod} correlations as shown in Eqs. (9) and (10) by processing real-time measurements from four offshore deployments (see Table B.5). It was noted that the wind speed above the water surface has the largest impact on the module temperature.

$$T_{mod} = T_{app} + c_1(1 + c_2 \cdot T_{app}) \cdot (1 - c_3 |U_\infty|) \cdot G_{POA} \tag{9}$$

$$T_{mod} = 0.943 \cdot T_{amb} + 0.0195 \cdot G_{avg} - 1.528 \cdot U_\infty + 0.353 \tag{10}$$

W. Kamuyu et al. [254,255], I. Peters et al. [253], and D. Tryakin et al. [256] have proposed T_{mod} correlations using regression analysis based on site data for the HPOT archetype in Hapcheon dam in South Korea (see Table B.5 for more information). The correlations proposed as a result of this study are shown in Eqs. (11), (12) [254,255], and (13) [256].

$$T_{mod} = 2.0458 + 0.9458 \cdot T_{amb} + 0.0215 \cdot G_{avg} - 1.2376 \cdot U_\infty \tag{11}$$

$$T_{mod} = 1.8081 + 0.9282 \cdot T_{amb} + 0.021 \cdot G_{avg} - 1.2210 \cdot U_\infty + 0.0246 \cdot T_{wat} \tag{12}$$

$$T_{mod} = T_{amb} + (T_{NOCT} - T_{amb,NOCT}) \cdot \left(\frac{G_{POA}}{G_{NOCT}}\right) \cdot \left(\frac{10.91}{8.91 + (2 \cdot U_\infty)}\right) \tag{13}$$

Eq. (11) shows a 1%–2% error when compared to experimental data, whereas Eq. (12) [254,255] displays a 4% difference, which is attributed to the inclusion of water temperature (T_{wat}). The correlation proposed by D. Tryakin et al. [256] highlights that a drop in T_{mod} is observed due to an increase in wind speed, which enhances natural convection, resulting in a 1.6% increase in EY.

N. Kumar et al. [250] simulated the effect of cooling for the HPOT archetype using three commercial PV simulation tools—PVsyst, SAM,

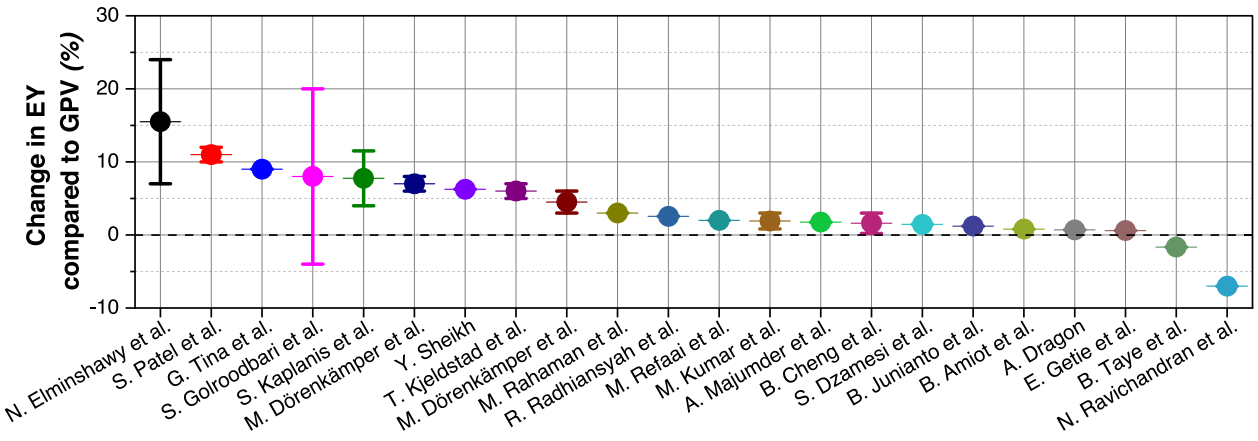

Fig. 15. EY gains reported by different studies due to the effect of cooling [220,237,238,243,244,246,248,250,251,258–271]. *Data extracted using matlab digiplotter package [187].*

and HelioScope. They used three temperature correlations in the simulation as shown in Eqs. (10), (11) and (12). The study observed that all the tools over-predicted the performance of FPV systems when compared to site measurements, indicating a need for a dedicated tool to accurately predict the EY of OFPV systems.

Horizontal pontoon truss & pontoon ring

M. Dörenkämper et al. [263,272] worked on evaluating the U-value for multiple FPV archetypes such as HPOT, HPIT, and pontoon ring (PR). A statistical linear regression analysis was used to predict the U-values by measuring critical environmental parameters onsite at different locations such as the Netherlands and Sri Lanka (see Table B.5). The proposed U-values are shown in Fig. 14.

In the work of [263], the effect of wind speed on the predicted U-value is analyzed. Two U-values are proposed for each location based on two methods of incorporating the wind speed: (1) average wind speed (U_{avg}), and (2) irradiance-weighted wind speed average (IWA). Results from both locations highlight that the IWA technique is more accurate. The study of [272] evaluates the effect of wind direction and water temperature. It was suggested that a water-temperature-dependent U-value component has to be included in the estimation of an overall U-value along with a wind-speed-related term to account for the water-induced effects. Ultimately, wind speed, ambient temperature, wind direction, and water temperature are deemed critical factors that affect the T_{mod} [263,272].

Rigid pontoon

S. Pinto et al. [273], S. Golroodbari et al. [258,259,274], A. Dragon [261], N. Ravichandran et al. [275], and D. Lindholm et al. [276] studied the effect of cooling for a rigid pontoon archetype (RP). S. Pinto et al. [273], S. Golroodbari et al. [258], and D. Lindholm et al. [276] used a combination of experimental data and computational methods to evaluate the U-values of this archetype. Each author used different correlations to evaluate the U-value as shown in Eqs. (14), (15), and (16) respectively.

$$U_c \cdot (T_{mod} - T_{amb}) = G_{POA} \cdot \tau \cdot \psi \cdot \left(1 - \frac{\eta}{\tau \cdot \psi}\right) \tag{14}$$

$$U_c = \frac{G_{POA}}{1500} + 2 \tag{15}$$

$$U_C = 17.7 + 5.5 \cdot U_{\infty} \tag{16}$$

A 0.31%–0.46% loss in energy production was observed by S. Pinto et al. [273] due to the large footprint of the system, as shown in Fig. 15. The study by D. Lindholm et al. [276] confirms that for large footprint systems, the water temperature has a small influence on the T_{mod}, whereas wind speed has a significant influence, projecting similar observations to other studies. The median U-values proposed as a result of [258,273,276] can be seen in Fig. 14.

A. Dragon [261] used onsite measurements from an FPV installation in France. The study aimed to provide T_{mod} correlations as a function of environmental parameters such as solar irradiation, ambient temperature, wind speed, and relative humidity to assess the major influencing factors. The four correlations proposed are shown via Eq. (17), (18), (19), and (20) respectively.

$$T_{mod} = 0.021 \cdot G_{POA} + 13.525 \quad (R^2 = 0.3277) \tag{17}$$

$$T_{mod} = 1.3982 \cdot T_{amb} + 0.0556 \quad (R^2 = 0.666) \tag{18}$$

$$T_{mod} = -0.9987 \cdot U_{\infty} + 26.49 \quad (R^2 = 0.0335) \tag{19}$$

$$T_{mod} = -0.2623 \cdot RH + 39.73 \quad (R^2 = 0.2148) \tag{20}$$

The R^2 values for each equation indicate the strength of the influence of each parameter on the module temperature. The results highlight that T_{mod} decreases with ambient temperature, wind speed, and relative humidity (RH). An extension of the work also estimates the median U-value, which is shown in Fig. 14.

Flexible pontoon

N. Ravichandran et al. [275] analyzed data from four active near-shore installations in Maldives with the flexible pontoon (FP) and RP archetypes and evaluated the EY using Helioscope (see Table B.5). The study quantified that the major loss in EY was due to temperature effects (compared to mismatch, soiling, and shading losses) and was about 4.8%, as shown in Fig. 15. They highlighted that the temperature loss using the FP archetype was lower than that of the RP archetype due to its direct contact with water.

Membrane ring

S. Patel [267], T. Kjeldstad et al. [237], D. Lindholm et al. [277], and I. Lereng [278] conducted studies quantifying the cooling effects of a membrane ring (MR) archetype. The works by S. Patel [267] and T. Kjeldstad et al. [237] made use of onsite measurements extracted by OceanSun at one of their installations in Skaftå, whereas I. Lereng [278] conducted a lab-scale experiment mimicking the OceanSun's MR archetype. Eq. (21) was used by [237,267,277,278] to determine T_{mod}.

$$T_{mod} = T_{BS} + \frac{G_{POA}}{G_{STC}} \cdot \Delta T \tag{21}$$

Three case studies were conducted to determine the U-values: (1) water-cooled system where the PV modules are directly placed on a polymer membrane with $T_{BS} = T_{wat}$, (2) water-cooled system where the PV modules are directly placed on a polymer membrane with $T_{BS} = T_{amb}$, and (3) air-cooled system where there is an air gap between the PV modules and the membrane with $T_{BS} = T_{amb}$.

The predicted U-values by [237,267,277,278] are shown in Fig. 14. The common conclusions drawn by each study are that a higher U-value is obtained when the PV module is in direct contact with the membrane with $T_{BS} = T_{wat}$, indicating that water is an efficient heat transportation medium (this configuration performs 3.17–7.32% better than air-cooled configurations in terms of EY). [277] noted that for water-cooled archetypes such as MR, wind speed has a relatively small impact on the T_{mod}, unlike other archetypes where wind speed is the major influencing parameter. Therefore, for U-values greater than 50 W/m^{2}K, FPV systems with the MR archetype can show up to 10-12% higher EYs compared to GPVs, as shown in Fig. 15.

No definitive FPV archetype

C. Maia et al. [279], M. Grisanti et al. [280], H. Niyaz et al. [281], L. Micheli et al. [282], C. Ramanan et al. [283], S. Kaplanis et al. [262], E. Getie et al. [284], A. Majumder et al. [268], B. Taye et al. [269], and L. Liu et al. [285] have worked on quantifying the effects of cooling for different PV technologies without a definitive FPV archetype. C. Maia et al. [279], M. Grisanti et al. [280], H. Niyaz et al. [281], and L. Micheli et al. [282] used different methods such as statistical analysis [281,282], machine learning [280], and heat transfer models [279] to predict the U-values of FPV systems. H. Niyaz et al. [281] proposed a T_{mod} correlation for three distinct types of PV technologies - mc-Si, Cadmium Telluride (CdTe), and hetro-junction with intrinsic thin layer (HIT), which is shown in Eq. (22).

$$T_{mod} = \frac{T_{amb} \cdot U_{L_1} + T_{wat} \cdot U_{L_2}}{U_{L_1} + U_{L_2} - \gamma_{pow} \cdot \eta_{ref} \cdot G_{POA}} + \frac{(\tau \cdot \psi - \eta_{ref} - \gamma_{pow} \cdot \eta_{ref} \cdot T_{ref}) \cdot G_{POA}}{U_{L_1} + U_{L_2} - \gamma_{pow} \cdot \eta_{ref} \cdot G_{POA}} \tag{22}$$

M. Grisanti et al. [280] used machine learning-based regression models to predict U-values for mono-facial and bi-facial PV modules, which were used in the Faiman and Sandia models [235,286] to determine T_{mod}. Different locations in Europe were simulated by L. Micheli et al. [282] to evaluate the potential of FPV in terms of performance. It was concluded that the southernmost countries of the continent showed an ideal FPV performance due to factors such as high sun elevations and enhanced cooling effects. However, the rates of cooling in each of these locations was not reported. The HT model of C. Maia et al. [279] highlighted that the instantaneous module temperature depends strongly on the incident solar irradiation, ambient temperature, and wind speed. But, the monthly average module temperature did not show significant variations throughout the year, indicating a balance of the aforementioned influencing factors. The U-values proposed by [279–282] are shown in Fig. 14.

S. Kaplanis et al. [262], E. Getie et al. [284] and B. Taye et al. [269] used both measurement data [269,284] and CFD [262] to provide a correlation for T_{mod}. S. Kaplanis et al. [262] performed both steady state and transient simulations to understand the dependency of module temperature on environmental parameters. The correlation proposed is given by Eq. (23).

$$T_{mod} = T_{amb} + f_R \cdot G_{POA}\ ,\ f_R = \frac{a + b \cdot U_\infty}{1 + c \cdot U_\infty + d \cdot U_\infty^2} \tag{23}$$

It was noted that module temperature and humidity are inversely related. A 4% increase in EY was observed in comparison to a GPV system due to difference in humidity levels as shown in Fig. 15. However, it is unclear on how the authors incorporated the effects of humidity in the temperature correlation (it is believed that the effect of humidity might be reflected in the values of the coefficients a, b, c, d).

E. Getie et al. [284] and B. Taye et al. [269] used theoretical [269] and modeling (PVsyst) [284] approaches along with onsite measured data to evaluate the cooling effect of a FPV plant on the Great Ethiopian Renaissance Dam (see Table B.5). Both works made use of the same equation as shown in Eq. (10). The studies collectively highlighted that ambient temperature and wind speeds are the main factors that affect the module temperature of the system.

The works of C. Ramanan et al. [283], A. Majumder et al. [268], and L. Liu et al. [285] focused on understanding the sensitivity of module temperature to certain environmental parameters. A CFD-based approach was used by [283,285] and a statistical approach by [268]. The reported results provide insights into the effects on module temperature due to variations in θ_t, wind speed, height of the module from the water surface, ambient temperature, and water temperature.

It was highlighted that water temperature needs to be 2 °C lower than the ambient temperature to facilitate the cooling effect. For variations in wind speed, the module temperature reduced by 1.2 °C when the ambient temperature due to wind flow was 5 °C warmer than the water temperature. Maximum cooling was observed when the modules were placed 1500 mm above the surface of the water with $\theta_t = 0°$. Similar observations were also made by A. Majumder et al. [268] and L. Liu et al. [285], where a reduction of 3.7 °C in the ambient temperature and an irradiance of 700–800 W/m^2 led to maximized cooling effects [268]. Overall, a 1.5 – 2 % increase in system efficiency could be obtained by optimizing the above-mentioned environmental factors [285].

Takeaways

This subsection provided insights into the current state of research on evaluating the cooling effect. From the above summary, it can be deduced that the progress made in understanding the cooling effect is better than the motion effects. However, challenges remain: (1) the duration of measurement data recorded, which are used to predict U-values and T_{mod}, is very short (some less than a day); (2) The method of coupling thermal analysis and EY analysis is done through the use of commercial PV simulation tools, which are currently only suitable for GPV systems; (3) Most predictions made are based on inland water conditions, and there is a strong need to re-evaluate the proposed numbers and equations for offshore environments. Therefore, from the current state of research it can be deduced that an EY gain of ***-4% to 20%*** can be expected due to the effect of cooling (see Fig. 15). Future research addressing these gaps is recommended to better understand the impact of cooling on the EY. Some of the key conclusion from this subsection are later mentioned in Section 5.

4.3. Impact of optical effects

This subsection deals with the understanding of the optical phenomena that affect the performance of OFPV systems. Fig. 16 illustrates the various optical processes that influence the performance of FPV systems, which are as follows:

1. **Effect of albedo:** This is the process where solar irradiation reflected from the surface of the water potentially returns to the rear side of the PV modules, thereby providing additional irradiation.
2. **Effect of partial shading:** Partial shading which tend to reduce the overall EY can occur in offshore environments in two distinct ways as shown in Fig. 16: (1) water overflow leading to partial submergence and (2) salt deposition due to water overflow.
3. **Effect of soiling:** In offshore conditions, the accumulation of bird droppings and ecological matter over time, as depicted in Fig. 16, can result in localized soiling on PV modules. When not cleaned regularly, this can create hotspots, causing module degradation and potentially reducing the overall energy EY of the system.

In this subsection, an overview of the results observed in the literature on the above-mentioned processes is provided, offering readers an insight into the impact of optical changes on the EY. As this area of research is relatively new, only a limited number of studies have evaluated the effects of each of the three processes on EY.

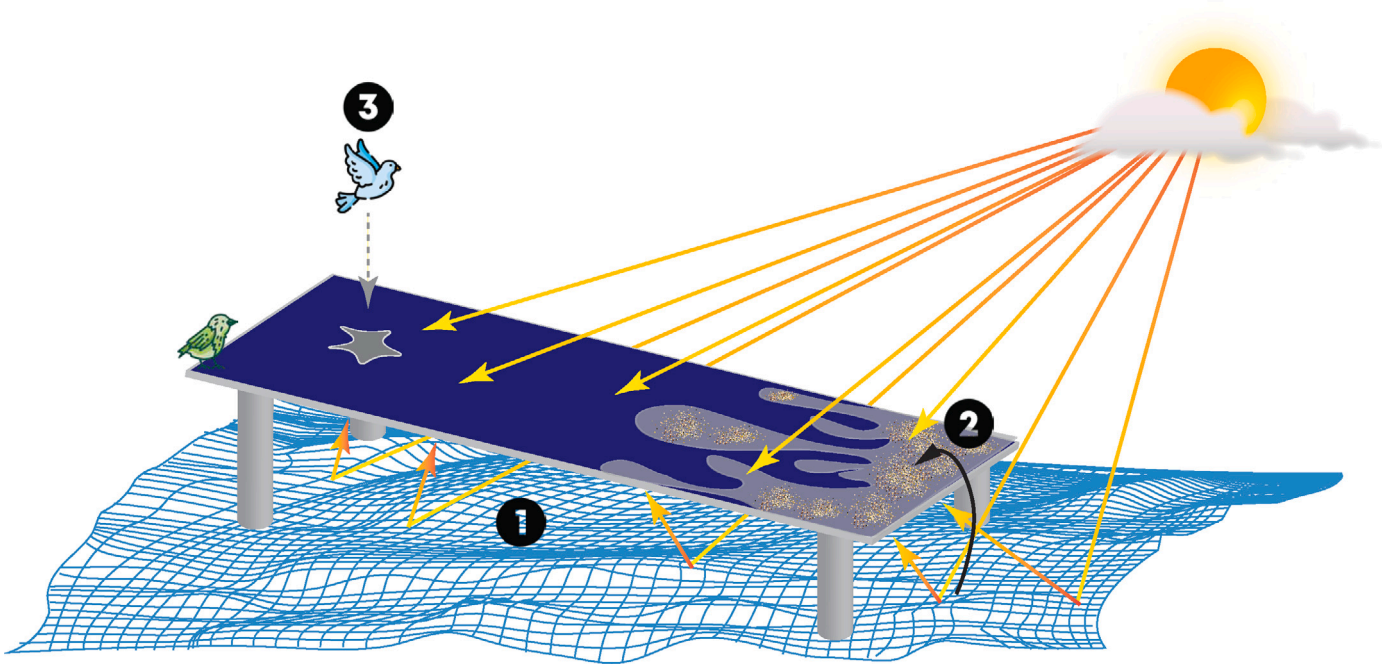

Fig. 16. Change in optical effects that influence the EY of OFPV systems. (1) albedo of sea-water surface, (2) shading due to water overflow and salt deposition, and (3) soiling due to bird dropping and concentrated algae growth.

4.3.1. Studies on understanding the effect of ocean surface albedo

This part of the review deals with providing an overview of the current understanding of evaluating the albedo of sea surfaces, commonly referred to as ocean surface albedo (OSA) [287] (see Appendix B). The following summary compiles various works of literature that have provided insights into: (1) methods (experimental and numerical) used to evaluate the albedo of sea water, (2) factors that affect OSA and (3) the quantification of OSA in terms of EY.

Initial studies on ocean surface albedo

Initial studies on measuring and proposing empirical correlations for the OSA began in the late 1900s and early 2000s, with significant contributions from researchers such as W. Sellers et al. [288], J. Willis [289], R. Payne [290], H. Gordon et al. [291], J. Simpson et al. [287], K. Katsaros et al. [292], B. Hannabas [293], J. Winckler et al. [294] and Z. Jin et al. [295]. These studies primarily focused on in-situ measurements of surface reflectance across various types of water bodies, such as lakes, ponds, and oceans.

The work by W. Sellers et al. [288] led to the proposal of an empirical correlation for the albedo of flat water surfaces, derived from in-situ measurements, as shown in Eq. (24). Although this proposed equation provides a good starting point for evaluating the albedo of water surfaces, there are certain limitations associated with it, such as: (1) the correlation must be calibrated to suit local conditions and serves only as a general estimate of the global albedo, and (2) it can only estimate the albedo of stagnant or flat water surfaces, while the albedo might be three times as high as the value proposed by Eq. (24) when there are waves.

$$\alpha_{flat\ water} = 50 \cdot \left\{ \frac{\sin^2(z - r_f)}{\sin^2(z + r_f)} + \frac{\tan^2(z - r_f)}{\tan^2(z + r_f)} \right\} \tag{24}$$

J. Willis [289], R. Payne [290], K. Katsaros et al. [292], and J. Simpson et al. [287] conducted in-situ albedo measurements at different offshore locations. The studies by [289,290] performed shortwave albedo measurements on a shipboard for two sea surfaces near Bermuda and in the mouth of Buzzards Bay in Massachusetts respectively. K. Katsaros et al. [292] measured the OSA using aircraft and ship data near the Tropical Atlantic Ocean as part of the JASIN experiment. J. Simpson et al. [287] conducted measurements from a floating instrument platform located in the North Pacific Ocean.

J. Willis [289] determined the OSA from radiation measurements taken over two days for varying wave heights ranging from 1 m to 3 m and solar heights ranging from 25° to 34°. The study concluded that solar elevation, wave height, bubbles below and on the water surface, water turbidity, salinity, and water depth are key parameters that strongly influence the albedo of the ocean surface. R. Payne [290] studied the effects of wind speed, water surface roughness, and the presence of whitecaps on the OSA, reporting that while wind speed and water surface roughness had a small effect, whitecaps significantly impacted albedo when wind speeds reached 15 m/s. K. Katsaros et al. [292] made similar observations, noting that clear or cloudy skies, breaking waves, and foam and bubbles in wind streaks also affect the OSA. J. Simpson et al. [287] observed that OSA decreases with increasing wind speed under clear skies with a solar altitude between 15° and 30°, but found no variation at higher solar altitudes, which contradicts the observations made by R. Payne [290]. The range of OSA reported by [287,289,290,292] are listed in Table 4.

H. Gordon et al. [291], J. Winckler et al. [294], B. Hannabas [293], and Z. Jin et al. [295] explored the effects of OSA through both in-situ measurements and computational modeling. H. Gordon et al. [291] estimated the influence of the ocean's optical properties and wind-induced sea foams (also known as whitecaps) on the OSA by solving the radiative transfer equation using a Monte Carlo method. This method considered the optical properties of various water bodies, including Crater Lake, San Vicente reservoir, and a totally absorbing ocean. The study found that the OSA of a clear ocean is at most 10% greater than that of a highly turbid ocean. Additionally, the presence of even a relatively small amount of foam on the ocean surface can significantly increase the OSA – more than doubling it – depending on the foam's reflectivity, the solar zenith angle, and wind speed as shown in Table 4.

J. Winckler et al. [294], on the other hand, conducted tests at Lake Hefner in Oklahoma and observed that cloudiness was a crucial factor to consider in empirical correlations for accurately estimating the OSA. The equation proposed by J. Winckler et al. [294] is presented in Eq. (25).

$$\alpha_{lake} = x \cdot B^y \tag{25}$$

B. Hannabas [293] proposed a single correlation for the surface albedo for different surfaces such as water, cotton, different colored plywood

Table 4
Reported albedo values for different water bodies as cited in the literature. *(The ranges are approximate values derived from each cited study. For precise value estimation, readers are encouraged to consult the original references listed in the table.)*

Waterbody	α_{OSA}(%)	Ref.	Waterbody	α_{OSA} (%)	Ref.
Sargasso Sea	7.7–8.2	[289]	Clear lake with frequentwhitecaps	2.7–30	[293]
Bermuda	14–49	[289]	Lakes with ripples upto 0.02 m,low turbidity, green water	7.6–22	[293]
Buzzards bay	3.5–28	[290]	Lakes with no waves, highturbidity, muddy water	11.7–19	[293]
Atlantic Ocean	2–14	[292]	Virginia beach, nearshore	3–40	[295]
Lake Washington	2–20	[292]	Open ocean	3–27	[296]
North Pacific ocean	0.9–40	[287]	Open ocean with sea grass	4–23	[296]
Crater Lake	8–39	[291]	Open ocean with ooid sand	9–34	[296]
San Vicenta reservoir	7.6–38.8	[291]	Open ocean with varyingturbidity (TSM : 50–1030 gm^{-3})	6–30	[296]
Totally absorbing ocean	7.5–38.8	[291]	South China sea	1–20	[297,298]
Clear lake, no waves	7.19–13	[293]	Open ocean	3–23	[299]
Clear lake with ripples upto 0.02 m	4.5–16	[293]	Open ocean with varyingturbidity (TSM : 50-1030 gm^{-3})	6–30	[299]
Clear lake with ripples>0.02 m,occasional whitecaps	3.6–23	[293]	North Sea	10–40	[300]

and white polyethylene as shown in Eq. (26) and pointed out that color, surface roughness and solar angle are important factors that needs to be included in the surface albedo correlations which were not considered in the study of J. Winckler et al. [294].

$$\alpha_{lake} = p^{C\cdot\sin(B)+1} \tag{26}$$

It was also noted that the wind speed profile plays a crucial role as it can influence the degree of surface roughness which inturn affects the surface albedo. The range of the surface albedo values proposed for different water bodies by [293] is shown in Table 4, and the average albedo for all the presented water surfaces is depicted in Fig. 17 (a). Z. Jin et al. [295,301] conducted a comprehensive OSA parameterization using measurements from a sea platform located 25 km east of Virginia Beach. The parameterization was conducted by separating different components of the OSA as shown in Eq. (27).

$$\alpha_{OSA} = \left[f_{dir}\cdot\alpha_{direct} + f_{dif}\cdot\alpha_{diffuse}\right] = \left[f_{dir}\cdot\alpha^{SR}_{direct} + f_{dir}\cdot\alpha^{WS}_{direct}\right] + \left[f_{dif}\cdot\alpha^{SR}_{diffuse} + f_{dif}\cdot\alpha^{WS}_{diffuse}\right] \tag{27}$$

Based on this parameterization, a lookup table for the OSA was developed using a validated coupled ocean-atmosphere radiative transfer model. The study concluded that OSA is highly variable and sensitive to five factors which are: solar zenith angle, wind speed, aerosol optical depth (AOD), atmospheric turbidity, and ocean turbidity (particularly chlorophyll concentration). It was observed that increasing AOD raises the OSA at high sun angles but lowers it at low sun angles. Wind speed exhibited minimal impact at high sun angles but significantly affected OSA at low sun angles, while ocean turbidity showed only a marginal effect on OSA. The average range of the OSA as a result of this study is shown in Table 4.

Recent studies on ocean surface albedo

Recent studies by M. Fogarty et al. [296], C. Huang et al. [297,298], S. Patel et al. [267,302,303], H. Liu et al. [245], A. Cosgun et al. [304], S. Golroodbari et al. [300], H. Ziar et al. [305,306] and J. Du et al. [299] have attempted to built upon the previous works to provide a more comprehensive understanding of the variation of surface albedos. The works of H. Liu et al. [245], A. Cosgun et al. [304] and H. Ziar et al. [306] deal with field measurements of the albedo at certain FPV installation zones in the Netherlands, Singapore and Turkey respectively. The studies have measured the variation of albedo only during certain months of the year as shown in Fig. 17 (a). On the other hand, S. Patel et al. [267,302,303], S. Golroodbari et al. [300] and H. Ziar et al. [305] have worked on providing physical/empirical models to evaluate the albedo. In the albedo model of S. Patel et al. [267,302,303], the water surface was assumed to be flat, smooth and only the surface layer refraction was considered. The effect of wavelength, water temperature and ambient temperature was studied. It was noted that the water surface albedo strongly depended on the wavelength of light and not on temperature.

M. Fogarty et al. [296] studied the surface albedo of dense water bodies with depths ranging from 0.8 to 3 m, following the methodology proposed in [301]. The purpose of this study was to address the gaps left by earlier research conducted in the 1900s and 2000s. The authors noted that studies by [287,290,292,293] provided reasonable estimates of water surface albedo, but only for shallow coastal waters with depths $\geq$ 1 m. This limitation was due to the exclusion of environments with bright sand bottoms or highly turbid waters where the total suspended matter (TSM) concentration is $\geq$ 50 gm^{-3}. The work of M. Fogarty et al. [296] found that factors such as ooid sand bottoms, seagrass canopies, and turbid waters with high TSM significantly increased the albedo of the water surface as shown in Table 4.

C. Huang et al. [297,298] proposed empirical correlations based on measurements taken from a fixed sea platform in the South China Sea over 152 days. The study covered a variety of atmospheric and oceanic conditions. It was observed that the solar zenith angle significantly influences the OSA under clear sky conditions, while its influence diminishes under cloudy sky conditions. The study also found that the OSA significantly increased with the solar zenith angle only at low sun angles, which aligns with the observations made by [295,301]. Other atmospheric and oceanic properties, such as wind speed, wave heights, and water vapor pressure, were also identified as critical factors affecting the OSA. The range of albedo values proposed in this work is listed in Table 4.

J. Du et al. [299] conducted measurements of lake water surface albedo in Northeast China to understand the driving parameters influencing albedo under clear sky conditions. The study concluded that lake water surface albedo is influenced by several factors, including solar altitude angle, water turbidity, and wind speed. Among these, solar altitude was identified as the primary influencer inline with other studies. Additionally, the study reported that higher surface albedo was observed in highly turbid lakes, consistent with observations made by [296] (see Table 4) and contradicting the observation made by [295,301]. The authors, therefore, recommend that albedo models should incorporate the effect of turbidity for more accurate albedo estimation.

S. Golroodbari et al. [300] on the other hand, modeled the dynamic OSA for North Sea conditions including the effect of waves and proposed a correlation according to Eq. (28) which is similar to the theory proposed by [295,301]. It was highlighted that the albedo depends on both atmospheric and oceanic properties such as solar zenith angle, ocean surface roughness, wind speed and optical wavelength inline with the observations made by [267,293,302,303]. The results also showed that the albedo had a non-linear relation with the wind speed.

$$\alpha_{North\ sea} = f_{dir}\cdot\alpha_{direct} + f_{dif}\cdot\alpha_{diffuse} \tag{28}$$

H. Ziar et al. [305] developed a physics based model that can evaluate the albedo as a function of location, time, geometry and weather conditions. The model can estimate the albedo for complex geometries with rough surfaces in urban environments. However, the suitability of this model for offshore conditions is yet unknown. The albedo predictions made by [245,267,300,302–306] can be seen in Fig. 17 (a).

EY quantification due to ocean surface albedo

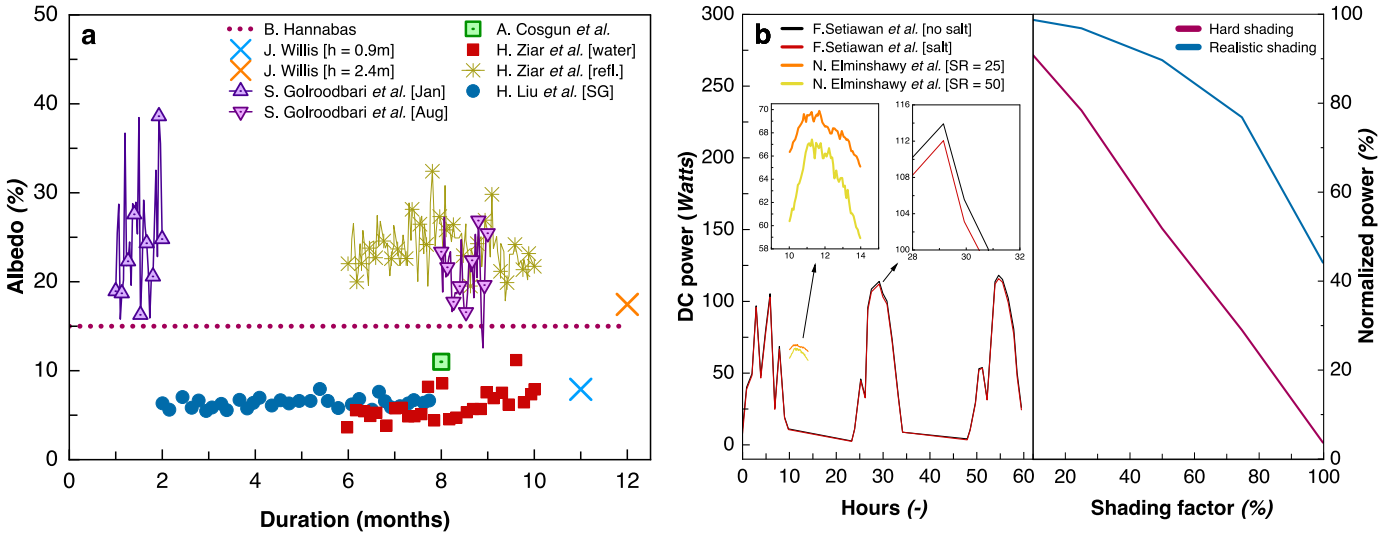

Fig. 17. The impact of optical effects on the performance of FPV systems. (a) Average albedo values for water surfaces, (b) impact on the EY due to salt deposition and bird droppings. *Data extracted using matlab digiplotter package [187].*

Up until now, the methods to evaluate the albedo was presented. But however, the quantification of this parameter with respect to EY is equally important. The results of S. Patel et al. [267,302,303] and S. Golroodbari et al. [300] showed a gain of approximately 1% in the EY of the system due to albedo. Studies by G. Tina et al. [242], A. Cosgun et al. [304], S. Pinto et al. [273], R. Yakubu et al. [307] and G. Rimon et al. [308] quantified the effect of albedo on the EY by varying the albedo from a lower value to a higher value (see Table B.5). G. Tina et al. [242] observed that monofacial PV modules are nearly insensitive to the changes in albedo whereas a gain of 5%–8% was observed in the case of bifacial modules (when the albedo is varied from 5%–20%). G. Rimon et al. [308] varied the albedo from 10%–90% and noted a bifacial gain of 4.5% compared to a monofacial PV module. A similar study by A. Cosgun et al. [304] surprisingly showed a 12% gain in the EY.

4.3.2. EY quantification due to the effect of shading

This part of the review deals with quantifying the effects of shading caused by salt deposition and water overflow on the EY of OFPV systems. N. Ravichandran et al. [275], N. Elminshawy et al. [238], B. Juniato et al. [271], A. Ates et al. [309], and F. Setiawan et al. [310] reported insights on the effects of shading and its impact on the EY. F. Setiawan et al. [310] conducted an experiment mimicking the event of sea salt deposition (see Table B.5) and observed a 2.46% drop in the EY when compared to a clean module, as shown in Fig. 17 (b). N. Elminshawy et al. [238], on the other hand, experimented with partially submerged PV panels in non-saline water. It was observed that at a submergence ratio of 25%, the EY of the system increased by 3.95% due to the cooling effect, but when the ratio increased to 50%, the EY decreased by 4.12% due to the effect of shading, as shown in Fig. 17 (b).

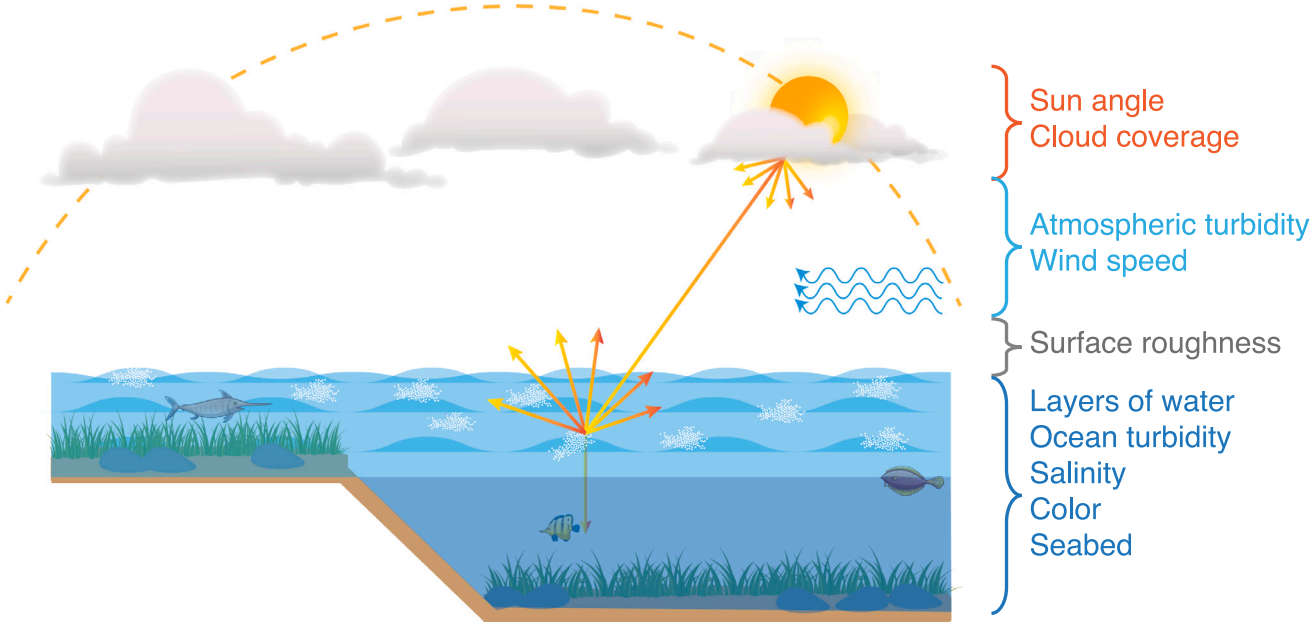

Fig. 18. Factors that needs to be considered to evaluate the ocean surface albedo.

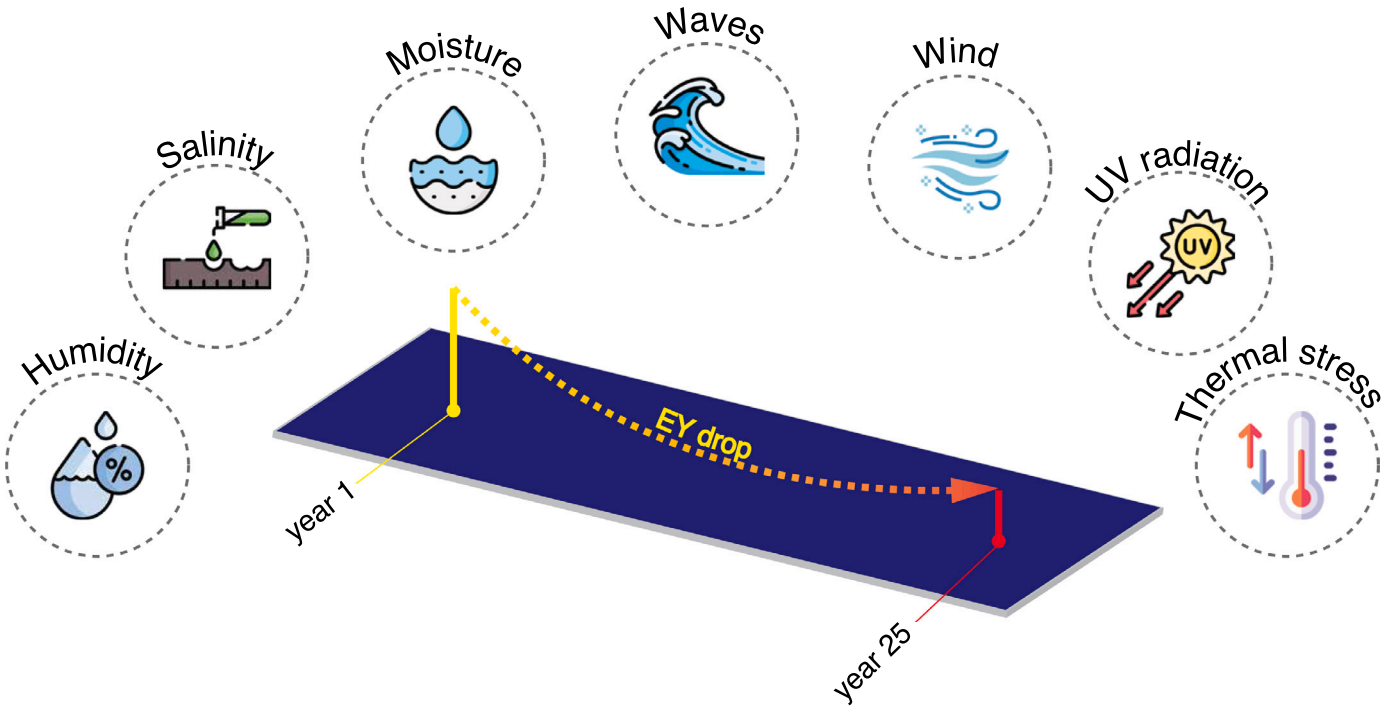

Fig. 19. Factors that influence the long term degradation of PV modules in offshore environments. Most common attributing factors are relative humidity, corrosion (due to seawater salinity), moisture ingress, mechanical stress (due to the combined action of wind and waves), UV radiation and thermal stress.

4.3.3. EY quantification due to the effect of soiling

This part of the review deals with quantifying the effect of soiling caused by bird droppings on the EY of OFPV systems. N. Ravichandran et al. [275], S. Pinto et al. [273], H. Liu et al. [245], X. Gao et al. [311], S. Ahn et al. [312] and H. Ziar et al. [306] worked on quantifying the effect of bird-droppings on the EY of FPV systems. H. Ziar et al. [306], H. Liu et al. [245] and S.H. Ahn et al. [312] worked on monitoring and detecting bird-droppings on FPV systems. Bird activity at a test site in the Netherlands with TPWT and RPWT archetypes was monitored by H. Ziar et al. [306]. They noticed bird droppings at several spots on the modules, especially those close to the water when placed at low tilt angle. This led to a drop in the effective albedo from 68% to 24% in 8 months, resulting in a loss in the EY. Similarly, a drop in the performance ratio over 10% was reported by H. Liu et al. [245] due to bird droppings at a test site in Singapore, and a drop in EY of 2% was reported by N. Ravichandran et al. [275] at a test site in the Maldives.

X. Gao et al. [311] developed a deep-learning based soiling detection tool which can detect and report the degree of bird-droppings in a given FPV farm. Similarly, S. Ahn et al. [312] modeled bird-droppings based on two situations — (1) hard shading ($\tau = 0$), (2) realistic shading ($\tau \neq 0$). The difference in the two cases in terms of loss in power (a relative difference of about 40% reported) can be visualized in Fig. 17 (b). This study shows the importance of modeling the bird-dropping as a partially-transmittive medium rather than a hard shading object.

Soiling effects also determine the operational and maintenance costs (O&M) of OFPVs (frequency of cleaning). Studies focusing on the cleaning frequency of GPV and IFPV systems suggest that manual cleaning is typically required every 7–20 days in dusty regions depending on the location [313–317]. However, the same frequency for OFPVs could significantly increase O&M costs. Therefore, innovative solutions such as self-cleaning coatings on PV modules could help extend the duration between cleaning cycles, reducing O&M costs. However, further research is needed to evaluate the feasibility and effectiveness of such coatings in offshore environments [318–320].

Takeaways

This subsection provided insights into the current state of research on evaluating the optical effects. From the summary above, it can be concluded that this area of research is still developing, with only a few initial but significant findings. Studies on OSA reveal mixed observations across different research efforts, creating ambiguity in fully understanding this effect. It remains unclear which parameters should be included in an albedo model to accurately predict OSA. To simplify this for the readers and to encourage further research, Fig. 18 is shown which illustrates the reported factors that need to be to considered when modeling OSA. Therefore, more experimental and validated models need to be developed to fully understand the effects of OSA, shading, and soiling on the EY of OFPV systems. Overall, reported results suggest: (1) a ***1% to 5%*** EY gain for bifacial PV modules due to seawater albedo [300,308] can be expected; (2) an EY loss of ***1% to 5%*** due to salt deposition and water overflow [238,310] can be expected; and (3) an EY loss of ***2% to 40%*** due to soiling from bird droppings [245,275,311] can be expected. Further key conclusions from this subsection are later discussed in Section 5.

4.4. Impact of long-term degradation

This subsection is dedicated to understanding the effects of long-term degradation on the OFPV module performance. Fig. 19 shows all the factors that contribute to degradation losses in OFPV systems. These factors collectively contribute to the overall degradation of OFPV systems, reducing their efficiency and lifespan. Similar to the area of optical effects, the field of analyzing degradation effects of FPV (for both IPFVs and OFPVs) systems is limited. However, few studies have been compiled in this review, which have solely focused on developing degradation models to predict the rates of degradation of FPV systems.

S. Golroodbari et al. [321], G. Mannino et al. [322], W. Luo et al. [323], W. Soppe et al. [40], M. Kumar et al. [324], A. Goswami et al. [325], and Z. Li et al. [326] studied the long-term degradation effects of FPV systems. W. Soppe et al. [40] conducted a lab-scale experimental study with flexible CIGS cells to determine the degradation rates caused by mechanical strains due to the effect of wave motion. Tests were performed with the cells oriented inline and oblique to

the wave direction. After testing 1.6 million cycles for each case, a power loss of 3.5% and 4%–5% were reported respectively. The losses increased to 20% in certain cases due to high cell temperatures. A. Goswami et al. [325] monitored a site with an FPV system for 17 months to quantify the effects of system degradation. Multiple factors led to module degradation in offshore conditions, such as temperature, wind speed, mechanical failures due to waves, humidity, and UV rays. Eq. (29) was used to determine the degradation rate of the system with inputs from real-time measurements.

$$DR = \frac{S \cdot 12}{I} \times 100 \tag{29}$$

It was noted that the degradation rate of FPV system was higher (4.4% higher) compared to a GPV system due to humidity, water corrosion and moisture ingression (2.06% lower power output of the FPV system [325]). M. Kumar et al. [324] used a similar correlation as Eq. (29) to determine the degradation rate for a canal top PV system and reported a value of $1.93 \pm 0.28\%/year$. S. Golroodbari et al. [321], G. Mannino et al. [322] and Z. Li et al. [326] have worked on different models to assess the degradation rate of FPV systems. A statistical approach based on historic data was used by [321] to predict EY of the system as shown in Eq. (30).

$$E_{PV,N_{year}} = \sum_{n=1}^{N_{year}} E_{PV,1} \cdot (1 - 0.005)^{n-1} \tag{30}$$

G. Mannino et al. [322] modeled the effect of module degradation on the EY for offshore conditions using existing degradation models (for GPV systems) proposed by I. Kaaya et al. [327] and B. Subramaniyan et al. [328] as shown in Eqs. (31) and (32).

$$DR = A_N \cdot (1 + k_H) \cdot (1 + k_P) \cdot (1 + k_{T_m}) - 1 \tag{31}$$

$$DR = \beta_0 \cdot e^{-\frac{\beta_1}{k_B \cdot T_{max}}} \cdot \left(\Delta T_{daily}\right)^{\beta_2} \cdot \left(\Delta UV_{daily}\right)^{\beta_3} \cdot \left(\Delta RH_{daily}\right)^{\beta_4} \tag{32}$$

The model included the effects of irradiance, temperature, relative humidity and wind speed [328]. However, [322] observed a lower degradation rate in offshore condition compared to inland which was deemed not realistic. Hence, the authors suggested that degradation models developed for GPV systems cannot be used for FPV systems. This is due to the fact that parameters such as effect of waves and salinity have not been included in these models [322]. Following up on this work, Z. Li et al. [326] proposed a weight based model to evaluate the degradation of FPV systems. This model includes factors such as irradiation, temperature cycling, humidity and wind speed which is similar to the two models shown in Eqs. (31) and (32), the difference being the inclusion of wind speed. The proposed correlation is given by Eq. (33).

$$DR = \eta_1 \cdot (1 + k_{RT}) \cdot (1 + k_{UV}) + \eta_2 \cdot (1 + k_{RT}) \cdot (1 + k_{TC}) + \eta_3 \cdot (1 + k_{TC}) \cdot (1 + k_{UV}) - \eta_1 - \eta_2 - \eta_3 \tag{33}$$

Takeaways

This subsection provided insights into the current state of research on evaluating the degradation effects of OFPV systems. From the above summary, it is clear that different degradation models have been developed to estimate the degradation rates of GPV systems. However, these models cannot be simply used for OFPV systems, and there is a strong need to adapt or develop models which can predict the degradation rates for OFPV systems, including all the relevant factors (see Fig. 19). Therefore from the above studies, it can be drawn that an EY loss of ***2% to 20%*** can be expected due to degradation effects [40]. Some of the key conclusions from this subsection are mentioned below in Section 5.

5. Conclusion

In this work, a comprehensive overview of FPV systems is provided with a prime focus on OFPV systems. Both technological and performance aspects of OFPV systems were discussed in great detail. Along with an overview, this work also provided a technical review of the different processes that effect the EY of OFPV systems thereby addressing both the review questions (RQ1 & RQ2) formulated in Section 2. Here, conclusions are given for each section by highlighting the most important takeaways which are as follows:

1. *RQ1: Technological overview of FPV system*

   - To the best of the authors' knowledge, this is the only review article that has proposed a classification matrix comprising 25 different FPV archetypes.
   - Among the FPV archetypes included in the classification, the majority of the designs currently target the moderate elevation regime, with loop floats and rigid floats being the most commonly used floaters.
   - The Technology Readiness Levels (TRLs) of inland FPVs are higher than those of offshore FPVs.
   - The average TRLs of OFPVs are between 4 and 5, indicating the need for further research and development.
   - Out of the 52 organizations reported in this work, 37% are focused on OFPVs, while the rest are involved in the IFPV sector.

2. *RQ2: Performance overview of FPV system*

   (a) *Impact of dynamic motion*

   - Factors such as wave height, wave period, wavelength, gap between connected archetypes, dimensions of the archetype, pre-tilt angles, installation angles, mooring stiffness, connector stiffness, and wave direction strongly influence the hydrodynamic response of the system and need to be considered in numerical simulations.
   - Out of all the environmental loads, wind and wave loads exert the strongest influence on the hydrodynamic response.
   - New concepts such as an external floating breakwater significantly depend on the FPV archetype, and their effect is not always beneficial indicating that each archetype has specific operating conditions to ensure optimal performance.
   - Studies noted that rotational responses affect the EY more than translational responses.
   - Overall, an EY loss of ***0.4% to 15%*** can be expected due to the motion effects, depending on the above-mentioned factors.

   (b) *Impact of cooling effect*

   - Factors such as ambient temperature, module tilt, relative humidity, water temperature, wind speed, wind direction, FPV archetype, and irradiance influence the strength of the cooling effect.
   - The U-values in general are higher for FPV system compared to a GPV indicating lower module temperatures.
   - Many studies have proposed empirical correlations tailored to specific locations under investigation, leading to a vast database of equations for module temperature. This proliferation of equations creates confusion, as even minor adjustments, such as the inclusion or exclusion of a single parameter, can result in the proposal of a new equation.
   - Overall, an EY gain of ***−4% to 20%*** can be expected due to the cooling effects, depending on the above-mentioned factors.

   (c) *Impact of optical effects*

- Factors such as the wavelength of light, cloudiness, solar zenith angle, atmospheric turbidity, surface roughness of the sea surface, wind speed, ocean turbidity and depth of the water significantly influence the surface albedo of water.
- The impact of salt deposition and partial submergence due to saline water overflow needs thorough investigation. The potential gains from cooling and the losses due to shading should be optimized to enhance overall system performance.
- Bird droppings should be modeled as partially transmittive elements rather than as non-transmittive elements to more accurately reflect their impact.
- Overall, reported results indicate that an EY gain of ***1% to 5%*** due to albedo effects can be expected with bifacial modules. Additionally, an EY loss of ***1% to 5%*** each can be expected from water submergence and salt deposition, and an EY loss of ***2% to 40%*** due to soiling from bird droppings.

(d) *Impact of long-term degradation*

- The degradation rates for PV modules in offshore conditions depend on the motion due to waves, temperature effects, wind speed, humidity, and UV rays.
- Current methods for evaluating degradation effects are based on models designed for GPVs, which significantly underestimate the rate of degradation for OFPV systems. This suggests that these models are not suitable for OFPVs and need to be adapted for offshore conditions.
- Overall, an EY loss of ***2% to 20%*** can be expected due to module degradation.

6. Outlook & future direction

Based on the above review, several viewpoints are projected to guide future research and to accelerate the growth of OFPVs. A few key outlooks are as follows:

- The current state of research reveals that our understanding of OFPV systems, particularly in quantifying energy yield (EY), is very limited. Therefore, increased efforts should be directed towards understanding the performance of OFPV systems, as energy output is the most critical aspect of any energy-generating system.
- Most EY quantifications reported in literature are either based on short-term experimental/in-situ measurements or on simulation results that are not well validated. This ultimately leads to ambiguity thereby slowing the field's progress.
- The majority of simulation work published, relies on commercial PV modeling tools that are primarily designed for evaluating EY for GPVs and RPVs, which do not yield realistic results for OFPVs.
- Publications that report experimental validation of numerical models need to place greater emphasis on both the experimental and numerical methodologies used, alongside the presentation of results.
- Increased collaboration between industry and research institutions is highly recommended to foster more effective advancements.

Overall, the outlook for OFPVs in terms of commercial application is promising, but achieving this potential requires a concentrated focus on research and development. The OFPV community should emphasize robust research practices and foster strong collaborations with industry partners. By doing so, the understanding of this field can be significantly accelerated, thereby increasing the TRL of various archetype technologies ultimately pushing OFPV towards large-scale commercialization.

Table B.5
Comprehensive review of studies investigating motion response, cooling effects, optical effects, and degradation effects across various floating photovoltaic archetypes and their influence on energy yield.

Study	Arch.[a]	Dimension [m][b]				Met.[c]		Control Parameters [SI units][d]							ME[e]							CE[f]				OE[g]			DE[h]	Tool	Dur.[i]	EY [%][j]	Val.[k]
															Loads				Response													
		L	W	H	D	S_i	E_x	U_∞	h	T_p, λ_w	$S(\omega)$	θ_p	PVT	T_a	T_{ai}	F_w	F_{WR}	IR	F_c	SB	MB	ML	E_a	E_{ai}	TC	UV	$Al.$	$Sh.$	$So.$				
[217]	HPOT(R)	29.99	22.41	–	–	✓	×	36–70	–	–	–	12	–	–	–	✓	×	×	×	×	×	×	×	×	×	×	×	×	×	×	ABAQUS	×	–	N
[329]	FP(F)	600	200	0.05	–	✓	×	25	14.8	212*	–	–	–	–	–	✓	✓	×	✓	✓	×	✓	×	×	×	×	×	×	×	×	SolidWorks	×	–	N
[330]	RP(R)	–	–	–	–	✓	×	45	0.1, 0.65	3.22,16.2*	–	6	–	–	–	✓	✓	×	×	✓	×	×	×	×	×	×	×	×	×	×	Ansys fluent, Aqwa	×	–	N
[331]	LRP(R)	–	–	–	–	✓	×	–	0.1, 0.4, 1.5	–	–	12	mc-Si	–	–	×	✓	×	×	×	✓	×	×	×	×	×	×	×	×	×	×	PVLib	1y	3-9↓	N
[211]	HPIT(R)	2	1	0.3	0.75–2	✓	×	–	0–10	8–23	–	–	–	–	–	×	✓	×	×	✓	×	×	×	×	×	×	×	×	×	×	Ansys fluent	×	–	Y_a
[218]	HPOT(R)	13.19	6.294	0.2	–	✓	×	6,25	0.2,0.75	1,4,8	JS	10	–	–	–	×	×	✓	×	✓	×	✓	×	×	×	×	×	×	×	×	Ansys Aqwa	×	–	Y_a
[230]	RP(R)	–	–	–	–	✓	×	–	–	–	–	0,30	mc-Si	–	–	×	×	×	×	×	×	×	×	×	×	×	×	×	×	×	Inhouse	1y	0.12–2.5↓	Y_a
[209]	RP(R)	7.10	4.6	0.4	–	✓	×	–	–	0–8	–	–	–	–	–	×	✓	×	×	✓	×	✓	×	×	×	×	×	×	×	×	Orcaflex, WAMIT	×	–	N
[226]	VPIT(R)	37	37	2.3	2	✓	×	–	5.5,8.7	1–30	JS	–	–	–	–	×	×	✓	×	×	✓	✓	×	×	×	×	×	×	×	×	Orcalfex, Orcawave	×	–	N
[208]	RP(R)	1.23	0.69	0.4	–	✓	×	40	0.9	0–25	JS	10	–	–	–	×	✓	✓	×	✓	×	✓	×	×	×	×	×	×	×	×	Orcaflex	×	–	N
[212]	HPIT(R)	–	0.965	–	0.11	✓	×	–	(0.025,0.05, 0.075)**	2,1.33,1	JS	–	–	–	–	×	×	✓	×	✓	×	×	×	×	×	×	×	×	×	×	OpenFOAM, WAFO	×	–	Y_a
[228]	TPT(R)	60	–	–	4	✓	×	46.1	4.5**	10 s	JS	–	–	–	–	✓	×	✓	✓	×	✓	✓	×	×	×	×	×	×	×	×	Inhouse	×	–	N
[332]	RP(R)	2.5	2.5	0.4	–	✓	×	–	(0.5–5)**	2.8–8.9	JS	0	–	–	–	×	×	✓	×	×	✓	×	×	×	×	×	×	×	×	×	HydroStar	×	–	N
[204]	HPOT(R)	12	4.4	0.8	–	✓	×	25	0.5**	1–20	JS	–	–	–	–	✓	×	✓	✓	✓	✓	✓	×	×	×	×	×	×	×	×	SeSam	×	–	N
[205]	RP(R)	0.4	0.25	0.2	–	✓	×	–	–	0.44–3.04*	–	–	–	–	–	×	✓	×	×	×	✓	✓	×	×	×	×	×	×	×	×	MHydro	×	–	Y_a
[227]	VPIT(R)	49.3	49.3	14	4	✓	×	–	1.9,5.69**	4.9,13.72	JS	10	–	–	–	×	×	✓	×	×	✓	✓	×	×	×	×	×	×	×	×	SIMA	×	–	N
[229]	BUF(R)	–	–	1.5	3	✓	×		0.012–1.2	1.2–10.6	–	30	mc-Si	–	–	×	✓	×	×	✓	×	×	×	×	×	×	×	×	×	×	Ansys Aqwa, Inhouse	–	3↓	Y_a
[333]	RP(R)	1	0.4	0.2	–	✓	×	–	–	3,4,5	–	–	–	–	–	×	✓	×	×	×	×	×	×	×	×	×	×	×	×	×	Matlab	×	–	Y_s
[224]	LPWT(R)	–	–	2	2	✓	×	–	1.5**	3.48	JS	–	–	–	–	×	×	✓	×	✓	×	✓	×	×	×	×	×	×	×	×	Ansys Aqwa, Orcaflex	×	–	N
[334]	LPWT(R)	10	10	2.43	1.5	✓	×	5	0.5–2.3	4.2–17.1	–	–	–	–	–	✓	✓	×	✓	×	✓	✓	×	×	×	×	×	×	×	×	Ansys Aqwa	×	–	N
[225]	VPIT(R)	4.7	2.9	0.6	–	✓	×	–	1.9–15.3**	7.8–12	PM	–	–	–	–	×	✓	✓	×	×	✓	✓	×	×	×	×	×	×	×	×	Orcaflex	×	–	Y_a
[335]	HPIT(R)	4.5	1.16	0.11	0.11	×	✓	–	0.056–0.11	0.8–2	JS	–	–	–	–	×	✓	✓	×	✓	×	×	×	×	×	×	×	×	×	×	Exp.	×	–	–
[219]	HPOT(R)	1.27	1.21	0.495	–	×	✓	–	0.1–0.5	1.12–3.15	JS	12	–	–	–	×	✓	✓	×	×	✓	✓	×	×	×	×	×	×	×	×	Exp.	×	–	–
[336]	HPOT(R)	1.3	0.86	0.23	–	✓	×	55	0.625	3.48	PM	15	–	–	–	✓	✓	✓	×	×	✓	✓	×	×	×	×	×	×	×	×	Ansys CFX, Ansys Aqwa	×	–	Y_a
[337]	BF(R)	8.6	8.6	1.3	–	✓	×	7–10	–	0.8–1.2rad/s	MS	–	pc-Si	–	–	×	×	✓	×	✓	×	✓	×	×	×	×	×	×	×	×	SeSam	×	–	N
[338]	RP(R)	500	100	–	–	✓	✓	2.2,13.6	0.03–0.2**	0.6–3	JS	10	–	–	–	×	✓	✓	✓	✓	✓	✓	×	×	×	×	×	×	×	×	WAMIT, NEMOH, WECSim, PVWatts	1y	2-14↕	Y_a
[188]	FP(F)	300	60	2	–	✓	×	–	0.75–3.25**	5.45–8.29	JS	0	–	–	–	×	✓	✓	×	×	✓	✓	×	×	×	×	×	×	×	×	Capytaine	×	–	Y_a, Y_s
[221]	HPOT(R)	–	–	–	–	✓	×	–	0.1-1**	3	–	33	–	–	–	×	✓	×	×	×	✓	✓	×	×	×	×	×	×	×	×	Ansys Aqwa, Orcaflex	1y	1.4-15↓	N
[202]	HPOT(R)	80.62	50.7	–	–	✓	×	10	4**	10	JS	–	–	–	–	✓	×	✓	×	×	✓	✓	×	×	×	×	×	×	×	×	Ansys Aqwa, Orcaflex	×	–	Y_a
[215]	HPIT(R)	36	7	–	1	✓	×	0,30	0.5,1	5,7	–	30	–	–	–	✓	✓	×	×	✓	✓	✓	×	×	×	×	×	×	×	×	Ansys Aqwa	×	–	N

(*continued on next page*)

Table B.5 (*continued*).

Study	Arch.[a]	Dimension [m][b]				Met.[c]			Control Parameters [SI units][d]							ME[c]							CE[f]				OE[g]			DE[h]	Tool	Dur.[i]	EY [%][j]	Val.[k]
																Loads				Response														
		L	W	H	D	S_i	E_s	U_∞	h	T_p,λ_w	$S(\omega)$	θ_p	PVT	T_a	T_w	F_w	F_{wcc} R	F_{wcc} IR	F_c	SB	MB	ML	E_a	E_w	TC	UV	Al	Sh	So					
[339]	MR(F)	–	–	0.0011	1	✓	×	–	0.5	0–2 rad/s	–	–	–	–	–	×	✓	×	×	✓	×	×	×	×	×	×	×	×	×	×	WAMIT,Matlab	×	–	Y_e
[340]	MR(F)	–	–	0.0011	1	✓	✓	–	$\frac{h}{\lambda}=\frac{1}{50},\frac{1}{60}$	–	–	–	–	–	–	×	✓	✓	×	✓	×	✓	×	×	×	×	×	×	×	×	WAMIT	×	–	Y_e
[341]	FP(F)	300	–	5	–	✓	×	–	–	2–20	–	–	–	–	–	×	✓	×	×	×	✓	×	×	×	×	×	×	×	×	×	Inhouse	×	–	N
[342]	RP(R)	100	50	5	–	✓	×	–	–	1.45–2.06	–	–	–	–	–	×	✓	×	×	×	✓	✓	×	×	×	×	×	×	×	×	Ansys Aqwa	×	–	Y_s
[210]	RP(R)	100	50	5	–	✓	×	–	2	0.01–2.41rad/s	–	–	–	–	–	×	✓	×	×	×	✓	✓	×	×	×	×	×	×	×	×	Ansys Aqwa, inhouse	×	–	Y_s
[343]	SP(R)	4.7	2.9	0.6	1.3	✓	×	–	2.1–5.1	3.9–14	–	–	–	–	–	×	✓	×	×	×	✓	✓	×	×	×	×	×	×	×	×	Orcaflex	×	–	Y_s
[207]	RP(R)	38	5	2.5	–	×	✓	–	(0.67,1.01,3.06)**	2.4–11.8	WN,JS	0	–	–	–	×	×	✓	×	×	✓	✓	×	×	×	×	×	×	×	×	Exp.	×	–	–
[344]	VPIT(R)	4.7	2.9	0.6		×	✓	–	0.156	1.83	–	–	–	–	–	×	✓	×	×	×	✓	✓	×	×	×	×	×	×	×	×	Exp.	×	–	–
[206]	RP(R)	16.5	5.8	1.3	–	✓	×	20,39.1	0.2,0.88	4	–	–	–	–	–	✓	✓	×	✓	✓	×	✓	×	×	×	×	×	×	×	×	Inhouse	×	–	N
[213,214]	HPIT(R)	3	3	6	0.5–1	✓	×	–	0.25, 1**	2–8	JS	–	–	–	–	×	✓	✓	×	✓	×	✓	×	×	×	×	×	×	×	×	Riflex	×	–	Y_e
[213,216]	HPIT(R)	4.58	–	0.11	0.11	✓	✓	–	(0.049–0.056)**	0.8–2	JS	–	–	–	–	×	✓	✓	×	✓	×	×	×	×	×	×	×	×	×	×	Inhouse	×	–	Y_e
[345]	LPWT(R)	50	50	4.5	–	✓	×	30	7,10,13	1–20	JS	–	–	–	–	✓	✓	✓	✓	✓	×	✓	×	×	×	×	×	×	×	×	HydroD, Orcaflex	×	–	N
[346]	PR(F)	–	–	–	–	✓	×	–	0-0.05	0–7.5*	–	–	–	–	–	×	✓	×	×	✓	×	×	×	×	×	×	×	×	×	×	Inhouse	×	–	Y_e
[347]	PR(F)	–	–	–	–	✓	×	–	0-0.06	0.1–20 rad/s	–	–	–	–	–	×	✓	×	×	✓	×	×	×	×	×	×	×	×	×	×	Inhouse	×	–	Y_e
[222]	HRP(R)	0.2	0.2	0.69	–	×	✓	–	4–8	0.7–5.11	JS	–	–	–	–	×	✓	✓	×	✓	×	✓	×	×	×	×	×	×	×	×	Exp.	×	–	–
[193]	FP(F)	60	60	2	–	✓	×		–	2.7–8.3	–	–	–	–	–	×	✓	×	×	✓	×	✓	×	×	×	×	×	×	×	×	WAMIT, Abaqus	×	–	N
[203]	PR(R)	–	–	–	100	✓	×	–	0.1	1	–	–	–	–	–	×	✓	×	×	✓	×	✓	×	×	×	×	×	×	×	×	OpenFOAM	×	–	N
[348]	FP(F)	1200–4800	1000	2	–	✓	×	–	–	(38.9–271)*	–	–	–	–	–	×	✓	×	×	✓	×	✓	×	×	×	×	×	×	×	×	Inhouse	×	–	Y_e
[349]	FP(F)	5000	1000	5	–	✓	×	–	–	(125–250)*	–	–	–	–	–	×	✓	×	×	✓	×	×	×	×	×	×	×	×	×	×	Inhouse	×	–	N
[189]	FP(F)	5000	1000	5	–	✓	×	–	–	(100–250)*	–	–	–	–	–	×	✓	×	×	✓	×	×	×	×	×	×	×	×	×	×	Inhouse	×	–	Y_s
[350]	PR(F)	–	–	2–5	50–200	✓	×	–	–	50*	–	–	–	–	–	×	✓	×	×	✓	×	×	×	×	×	×	×	×	×	×	Fortran	×	–	N
[190]	FP(F)	400	60	3.7	–	✓	✓	–	2**	5.6	JS	–	–	–	–	×	×	✓	×	✓	×	✓	×	×	×	×	×	×	×	×	Inhouse	×	–	Y_e
[351]	PR(F)	–	–	–	4	✓	×	–	–	2.09*	–	–	–	–	–	×	✓	×	×	✓	×	×	×	×	×	×	×	×	×	×	Matlab	×	–	N
[352]	RP(R)	2/10	0.5	0.038	–	✓	×	–	0.02	0.5–2	–	–	–	–	–	×	✓	×	×	×	✓	×	×	×	×	×	×	×	×	×	Inhouse	×	–	Y_e
[191]	FP(F)	4	1	0.03	–	✓	×	–	(0.04–0.06)**	0.8	BM	–	–	–	–	×	×	✓	×	✓	×	✓	×	×	×	×	×	×	×	×	Inhouse	×	–	Y_e
[353]	FP(F)	10	0.8	0.01,0.02	–	✓	×	–	3–5	0.8–16	JS	–	–	–	–	×	✓	✓	×	✓	×	×	×	×	×	×	×	×	×	×	Inhouse	×	–	Y_e
[197]	RP(R)	3	0.6	0.04	–	✓	✓	–	–	1.8*	–	–	–	–	–	×	✓	×	×	×	✓	✓	×	×	×	×	×	×	×	×	Inhouse	×	–	Y_e
[354]	FP(F)	4.95	1.02	0.005	–	×	✓	–	0.02–0.04	0.563,0.796	–	–	–	–	–	×	✓	×	×	✓	×	✓	×	×	×	×	×	×	×	×	Exp.	×	–	–
[198]	RP(R)	300	60	2	–	✓	×	–	(0.75–3.25)**	5.45–8.29	JS	–	–	–	–	×	✓	✓	×	×	✓	✓	×	×	×	×	×	×	×	×	Inhouse	×	–	Y_e , Y_s
[199]	RP(R)	300	60	2	–	✓	×	–	–	0–2 rad/s	–	–	–	–	–	×	✓	×	×	×	✓	×	×	×	×	×	×	×	×	×	WAMIT, ABAQUS	×	–	Y_e
[192]	FP(R)	300	60	2	–	✓	×	–	–	(120–240)*	–	–	–	–	–	×	✓	×	×	✓	×	×	×	×	×	×	×	×	×	×	Inhouse	×	–	Y_e , Y_s
[200]	RP(R)	300	60	2	–	✓	×	–	2	(60–300)*	–	–	–	–	–	×	✓	×	×	×	✓	✓	×	×	×	×	×	×	×	×	Ansys Aqwa	×	–	Y_e , Y_s
[201]	RP(R)	300	60	2	–	✓	×	–	0.5	(120–300)*	–	–	–	–	–	×	✓	×	×	×	✓	✓	×	×	×	×	×	×	×	×	Ansys Aqwa	×	–	Y_e , Y_s
[194]	RP(R), FP(R)	300	60	2	–	✓	✓	–	–	(60–300)*	–	–	–	–	–	×	✓	×	×	×	✓	✓	×	×	×	×	×	×	×	×	Inhouse	×	–	Y_e
[232]	LRP(R)	32	32	0.4	–	✓	×	0–25	0–19.3	0–13.9	JS	0	mc-Si	–	–	×	×	✓	×	✓	×	×	✓	×	×	×	×	×	×	×	Matlab, PVMDtoolbox	1y	18-32↓	Y_e
[233]	LRP(R)	45	15	15	–	✓	×	–	0.25,0.79	1.63–9.4	JS	0	mc-Si	–	–	×	×	✓	×	✓	×	×	✓	×	×	×	×	×	×	×	Inhouse	1y	8-9↓	N
[231]	RP(R)	–	–	0.6	–	✓	×	–	–	–	–	5	mc-Si	–	–	×	×	×	×	×	×	×	✓	×	×	×	×	×	×	×	PVsyst	1y	8↓	N
[258]	RP(R)	–	–	–	–	✓	×	–	–	–	–	–	mc-Si	M	–	×	×	×	×	×	×	×	✓	✓	×	×	×	×	×	×	inhouse	1y	4↓- 20↑	N
[259]	RP(R)	–	–	–	–	✓	×	5.55–25	0.5–19.3	3.2–13.9	JS	0	mc-Si	–	–	×	×	✓	×	✓	×	×	✓	×	✓	×	×	×	×	×	Matlab	1y	13↑	N
[220]	HPOT(R)	–	–	–	–	✓	×	5.5–16.6	0.5–7.1**	3.2–9.9	–	0–15	mc-Si	–	–	×	✓	✓	×	✓	×	✓	×	✓	×	×	×	×	×	×	Matlab	1 h	0.2-3↑	N
[223]	HRP(R)	6	6	30	–	✓	×	5,30	1,4	7,14	JS	40	mc-Si	–	–	✓	×	✓	×	✓	×	✓	✓	×	×	×	×	×	×	–	Ansys Aqwa,PVGIS	×	–	N

(*continued on next page*)

Table B.5 (*continued*).

Study	Arch.[a]	Dimension [m][b]				Met.[c]		Control Parameters [SI units][d]									ME[e]										CE[f]					OE[g]				DE[h]	Tool	Dur.[i]	EY [%][j]	Val.[k]
																	Loads			Response																					
		L	*W*	*H*	*D*	S_i	E_x	U_∞	*h*	T_p, λ_w	$S(\omega)$	θ_p	*PVT*	T_a	T_w		F_w	F_{wc}		F_c	*SB*	*MB*	*ML*	E_a	E_u	*TC*	*UV*	*Al.*	*Sh.*	*So.*								
																		R	*IR*																				
[283]	⌣	–	–	0.25–3	–	✓	×	1–5	–	–	–	0–75	mc-Si	20–40	20–40		×	×	×	×	×	×	×	×	✓	✓	×	×	×	×	×	×		Ansys fluent	–	–	Y_a
[279]	⌣	–	–		–	✓	×	1-3.9	–	–	–	27	mc-Si	20–27.8	–		×	×	×	×	×	×	×	×	✓	×	✓	×	×	×	×	×		Inhouse	1y	–	N
[260]	RP(R)	–	–	–	–	×	✓	M	–	–	–	5	mc-Si	M	M		×	×	×	×	×	×	×	×	✓	✓	×	×	×	×	×	×		–	1y	1.44↑	–
[261]	RP(R)	–	–	–	–	✓	✓	2.78	–	–	–	11	mc-Si	M	M		×	×	×	×	×	×	×	×	✓	✓	✓	✓	×	×	×	×		PVsyst	9 m	0.7↑	N
[246]	HPOT(R)	–	–	–	–	✓	✓	M	–	–	–	30	mc-Si	M	–		×	×	×	×	×	×	×	×	✓	×	×	✓	×	×	×	×		Open Modelica	24d	0.8↑	Y_r
[247]	HPOT(R)	–	–	–	–	×	✓	1.39	–	–	–	16	mc-Si	16.6	–		×	×	×	×	×	×	×	×	✓	×	×	✓	×	×	×	×		–	1d	–	–
[248]	HPOT(R)	–	–	–	–	✓	×	0.96–1.64	–	–	–	150	mc-Si	11.70–21.19	15.62–25.04		×	×	×	×	×	×	×	×	✓	✓	✓	×	×	×	×	×		Comsol	1y	3↑	Y_a
[262]	–	–	–	–	–	✓	✓	M	–	–	–	M	mc-Si	M	M		×	×	×	×	×	×	×	×	✓	✓	✓	×	×	×	×	×		Inhouse	–	11.5↑	Y_a
[280]	–	–	–	–	–	✓	×	–	–	–	–	–	MF,BF	–	–		×	×	×	×	×	×	×	×	✓	×	×	×	×	×	×	×		Inhouse	–	–	N
[263]	PR(R) HPIT(R)	–	–	–	–	✓	✓	M	–	–	–	–	mc-Si PERC	–	–		×	×	×	×	×	×	×	×	✓	×	×	✓	×	×	×	×		PVsyst Sandia	1y	6-8‡	Y_r
[236]	HPIT(R)	–	–	0.2	–	✓	×	4	–	–	–	10	mc-Si	25	22		×	×	×	×	×	×	×	×	✓	✓	×	×	×	×	×	×		Comsol	–	–	N
[355]	TR(R)	–	–	–	–	✓	×	–	–	–	–	–	–	–	–		×	×	×	×	×	×	×	×	✓	✓	×	✓	×	×	×	×		Inhouse	–	–	N
[264]	RP(R)	–	–	–	–	✓	×	1.5	–	–	–	–	pc-Si	28	–		×	×	×	×	×	×	×	×	✓	✓	×	×	×	×	×	×		Ansys fluent	1y	2↑	N
[275]	RP(R)	–	–	–	–	✓	×	2–6	0.7–1	–	–	5–10	mc-Si	M	M		?	?	?	?	?	?	?	?	✓	×	×	×	×	✓	✓	×		Helioscope	1y	7↓	N
[249]	HPOT(R)	–	–	–	–	×	✓	M	–	–	–	0,15,30	mc-Si pc-Si	M	M		×	×	×	×	×	×	×	×	✓	✓	×	×	×	×	×	×		–	4d	10-17↓	–
[276]	RP(R)	–	–	–	–	✓	×	1–5	–	–	–	15	mc-Si	25,30	20,25,30		×	×	×	×	×	×	×	×	✓	✓	×	✓	×	×	×	×		Ansys fluent	–	–	Y_a
[250]	HPOT(R)	–	–	–	–	✓	✓	M	–	–	–	16	mc-Si	M	C		×	×	×	×	×	×	×	×	✓	⌣	✓	×	×	×	×	×		PVsyst SAM Helioscope	1y	0.83-3‡	N
[265]	HPIT(R)	–	–	–	–	✓	✓	1–7	–	–	–	15	pc-Si	M	10,30		×	×	×	×	×	×	×	×	✓	✓	×	✓	×	×	×	×		PVsyst	4 m	0.6↑	Y_r
[284]	–	–	–	–	–	✓	×	3.62	–	–	–	–	mc-Si	25.05	C		×	×	×	×	×	×	×	×	✓	✓	✓	×	×	×	×	✓		PVsyst	1y	–	N
[266]	HPOT(R)	–	–	–	–	×	✓	3–5				15	pc-Si	31–32	31–32.5		×	×	×	×	×	×	×	×	✓	✓	×	×	×	×	×	×		–	1d	10↑	–
[239]	HPIT(R)	–	–	–	–	×	✓	0.32–0.43	–	–	–	25	pc-Si	20–21	20–21		×	×	×	×	×	×	×	×	✓	✓	×	×	×	✓	×	×		–	1d	24↑	–
[238]	HPIT(R)	–	–	–	–	✓	×	–	–	–	–	25	pc-Si	20–21.8	17.5–18.3		×	×	×	×	×	×	×	×	✓	✓	×	×	×	✓	×	×		Ansys fluent, Matlab	5 h	7↑	Y_r
[241]	HPIT(R)	–	–	–	–	✓	×	0–2	–	–	–	30	pc-Si	16–30	23.5–26		×	×	×	×	×	×	×	×	✓	✓	✓	×	×	×	×	×		Inhouse	–	–	N
[356]	HPOT(R)	–	–	–	–	✓	×	M	–	–	–	–	–	M	M		×	×	×	×	×	×	×	×	✓	✓	×	×	×	×	×	×		Matlab	–	–	Y_r
[243]	HPIT(R)	–	–	–	–	✓	×	–	–	–	–	20	MF,BF	M	14.85–59.85		×	×	×	×	×	×	×	×	✓	✓	×	×	×	×	×	×		Inhouse	1y	9↑	Y_r
[242]	RP(R)	–	–	0–1.5	–	✓	×	–	–	–	–	5–30	MF,BF	10–26.6	–		×	×	×	×	×	×	×	×	✓	⌣	✓	×	✓	×	×	×		PVsyst, SAM	5d	3.4–7.3↑	Y_r
[251]	HPOT(R)	–	–	–	–	✓	×	C	–	–	–	–	mc-Si	C	C		×	×	×	×	×	×	×	×	✓	×	✓	×	×	×	×	×		Matlab	12 h	2.54↑	N
[267]	MR(R)	–	–	–	–	✓	×	M	–	–	–	0–60	mc-Si	M	20		×	×	×	×	×	×	×	×	✓	✓	×	✓	×	×	×	×		PVsyst	8 m	10-12↑	N
[281]	–	–	–	–	–	✓	×	M	–	–	–	26	mc-Si, HIT,CdTe	M	M		×	×	×	×	×	×	×	×	✓	✓	✓	×	×	×	×	×		Inhouse	–	–	Y_r
[268]	–	–	–	0.075	–	✓	×	M	–	–	–	–	–	M	M		×	×	×	×	×	×	×	×	✓	✓	×	×	×	×	×	×		Inhouse	4 m	1.75↑	N
[277]	MR(R), HPIT(R)	–	–	–	–	✓	×	M	–	–	–	–	–	M	M		×	×	×	×	×	×	×	×	✓	✓	×	×	×	×	×	×		Inhouse	–	–	Y_r
[237]	MR(R)	–	–	–	–	✓	✓	M	–	–	–	0	mc-Si	M	M		×	×	×	×	×	×	×	×	✓	✓	×	✓	×	×	×	×		PVsyst	3 m	5-7↑	Y_r
[252]	HPOT(R)	–	–	–	–	×	✓	0.05–15	–	–	–	13–31	pc-Si	−5 to 33	–		×	×	×	×	×	×	×	×	✓	⌣	×	✓	×	×	×	×		–	6 m	0.43‡	–
[240]	HPIT(R)	–	–	–	–	×	✓	0.08–4.16	–	–	–	30	pc-Si	M	M		×	×	×	×	×	×	×	×	✓	⌣	×	×	×	✓	×	×		–	13 h	11↑	–
[244]	HPIT(R)HPOT(R)	–	–	–	–	✓	✓	M	–	–	–	7–12	pc-Si	M	M		×	×	×	×	×	×	×	×	✓	✓	×	✓	×	×	×	×		PVsyst	1y	3-6↑	–
[357]	HPOT(R)	–	–	1	–	✓	×	M	–	–	–	0–15	MF,BF	–	–		×	×	×	×	×	×	×	×	⌣	⌣	×	×	×	×	×	×		PVsyst	5 m	8.76↑	N
[269]	–	–	–	–	–	✓	×	6.72	–	–	–	–	mc-Si	28.75	C		×	×	×	×	×	×	×	×	✓	✓	✓	×	×	×	×	×		Matlab Simulink	1y	1.66↓	N
[270]	HPOT(R)	–	–	–	–	✓	×	1	–	–	–	10	mc-Si	10–35	10–15		×	×	×	×	×	×	×	×	✓	✓	✓	×	×	×	×	×		Comsol	13 h	6.25↑	N
[253]	HPOT(R)	–	–	–	–	×	✓	M	–	–	–	–	–	M	M		×	×	×	×	×	×	×	×	✓	✓	×	×	×	×	×	×		Inhouse	–	–	N
[273]	PR(R),RP(R)	–	–	–	–	✓	×	M	–	–	–	0–22	mc-Si	M	M		×	×	×	×	×	×	×	×	✓	✓	×	×	✓	×	✓	×		PVsyst	1y	1.8–2.5↑0.3–0.46↑	N
[271]	RP(R)	–	–	–	–	×	✓	M	–	–	–	10	pc-Si	M	M		×	×	×	×	×	×	×	×	✓	✓	×	×	×	⌣	×	×		–	14 h	1.2↑	N

(*continued on next page*)

Table B.5 (*continued*).

Study	Arch.[a]	Dimension [m][b]				Met.[c]		Control Parameters [SI units][d]								*ME*[e]									*CE*[f]				*OE*[g]			*DE*[h]	Tool	Dur.[i]	EY [%][j]	Val.[k]
																Loads			Response																		
		L	*W*	*H*	*D*	S_i	E_x	U_∞	*h*	T_p, λ_w	$S(\omega)$	θ_p	*PVT*	T_a	T_w	F_w	F_{wv}	*R*	*IR*	F_c	*SB*	*MB*	*ML*	E_a	E_w	*TC*	*UV*	*Al.*	*Sh.*	*So.*					
[245]	HPIT(R)HPOT(R)	–	–	–	–	×	✓	M	–	–	–	5–15	MF,BF	M	M	×	×	×	×	×	×	×	×	✓	✓	×	✓	✓	×	✓	×	–	–	5-10↑	–
[278]	MR(R)	–	–	–	–	✓	✓	1.92–6.96	–	–	–	0	mc-Si	M	4	×	×	×	×	×	×	×	×	✓	✓	✓	✓	×	×	×	×	PVsyst TRNSYS	–	2-6↑	N
[255]	HPOT(R)	–	–	–	–	×	✓	M	–	–	–	–	–	M	M	×	×	×	×	×	×	×	×	✓	✓	✓	×	×	×	×	×	–	–	–	–
[254]	HPOT(R)	–	–	–	–	×	✓	M	–	–	–	–	mc-Si	M	M	×	×	×	×	×	×	×	×	✓	✓	✓	×	×	×	×	×	–	–	10↑	–
[285]	–	–	–	–	–	✓	×	1	–	–	–	–	mc-Si	25	–	×	×	×	×	×	×	×	×	✓	×	×	×	×	×	×	×	Ansys fluent	–	2↑	N
[256]	HPOT(R)	–	–	–	–	✓	×	1.1–3.3	–	–	–	15	–	10–40	–	×	×	×	×	×	×	×	×	✓	×	✓	×	×	×	×	×	MS Excel	–	–	N
[272]	PR(R)HPIT(R)	–	–	–	–	×	✓	M	–	–	–	12,15,25	mc-Si	M	M	×	×	×	×	×	×	×	×	✓	✓	×	✓	×	×	×	×	–	–	–	–
[274]	RP(R)	–	–	–	–	✓	×	E	–	–	–	0	–	E	E	×	×	×	×	×	×	×	×	✓	✓	✓	×	×	×	×	×	PVlib	–	–	N
[282]	–	–	–	–	–	✓	×	E	–	–	–	10,20	–	E	E	×	×	×	×	×	×	×	×	✓	✓	×	×	×	×	×	×	PVlib	–	–	N
[311]	–	–	–	–	–	✓	×	–	–	–	–	–	–	–	–	×	×	×	×	×	×	×	×	×	×	×	×	×	×	✓	×	Inhouse	–	–	Y_e
[304]	LRP(R)	–	–	1	–	×	✓	2.1–3	–	–	–	36	MF,BF	0.2–25.2	–	×	×	×	×	×	×	×	×	✓	✓	×	×	✓	×	×	×	PVsyst	1y	12.04↑	N
[312]	–	–	–	–	–	✓	×	–	–	–	–	–	mc-Si	–	–	×	×	×	×	×	×	×	×	×	×	×	×	×	×	✓	×	Matlab	–	–	Y_a
[307]	RP(R)	–	–	0	–	✓	×	M	–	–	–	5	MF,BF	M	M	×	×	×	×	×	×	×	×	✓	×	×	×	✓	×	×	×	Inhouse	–	14-24↑	N
[308]	RP(R)	–	–	–	–	✓	×	E	–	–	–	15	MF,BF	E	–	×	×	×	×	×	×	×	×	✓	×	×	×	✓	×	×	×	PurdueView Factor	6 m	2-6↑	N
[300]	RP(R)	–	–	–	–	✓	×	5.55–25	0.5–19.3	3.2–13.9	JS	0	mc-Si	E	–	×	×	✓	×	✓	×	×	×	✓	×	×	×	✓	×	×	×	Inhouse	1y	1.03↑	N
[309]	–	–	–	–	–	✓	×	–	–	–	–	–	mc-Si	–	–	×	×	×	×	×	×	×	×	×	×	×	×	×	✓	×	×	Inhouse	1y	4-30↓	N
[306]	TPWT(R)RPWT(R)	4.55 6.62	2.02 7.78	2.01	–	×	✓	M	–	–	–	15	MF,BF	M	–	×	×	×	×	×	×	×	×	✓	×	×	×	✓	✓	✓	×	PVMD toolbox	1y	17.3↑	–
[302]	–	–	–	–	–	✓	×	–	–	–	–	33.5	–	–	–	×	×	×	×	×	×	×	×	×	×	×	×	✓	×	×	×	Inhouse	–	–	N
[310]	–	–	–	–	–	×	✓	M	–	–	–	–	mc-Si	25–34	–	×	×	×	×	×	×	×	×	✓	×	×	×	✓	✓	×	–	3d	1.3W ↑	–
[303]	–	–	–	–	–	✓	×	–	–	–	–	–	–	–	–	×	×	×	×	×	×	×	×	×	×	×	×	✓	×	×	×	Inhouse	–	–	–
[321]	RP(R)	–	–	–	–	✓	×	M	–	–	–	–	mc-Si	M	–	×	×	×	×	×	×	×	×	✓	×	×	×	×	×	×	✓	Inhouse	1y	–	N
[322]	–	–	–	–	–	✓	×	E	–	–	–	–	mc-Si	E	–	×	×	×	×	×	×	×	×	✓	×	×	×	×	×	×	✓	Inhouse	1y	–	N
[323]	HPOT(R)	–	–	–	–	×	✓	M	–	–	–	7–12	mc-Si	M	M	✓	×	×	×	×	✓	×	×	✓	✓	×	×	×	✓	✓	✓	–	3y	0.5–1.1↓	–
[40]	FP(R)	–	–	–	–	×	✓	–	0.8–13	4.5–58.2	NorthSea	0	CIGS	–	–	×	×	✓	×	✓	×	×	×	×	×	×	×	×	×	×	✓	–	–	>1.5↓	–
[324]	–	–	–	–	–	✓	✓	M	–	–	–	26	mc-Si	M	–	×	×	×	×	×	×	×	×	✓	×	×	×	×	×	×	✓	Matlab	16 m	1.5↓	Y_e
[358]	HPIT(R)	–	–	–	–	×	✓	M	–	–	–	–	mc-Si	M	M	×	×	×	×	×	×	×	×	✓	✓	×	×	×	×	×	✓	–	–	–	–
[325]	VPIT(R)	–	–	–	–	×	✓	M	–	–	–	–	mc-Si	M	–	×	×	×	×	×	×	×	×	✓	×	×	×	×	✓	✓	✓	–	17m	–	–
[326]	–	–	–	–	–	✓	×	M	–	–	–	–	mc-Si	M	–	×	×	×	×	×	×	×	×	✓	×	×	×	×	×	×	✓	Inhouse	–	–	Y_e

[a] *Arch.*: FPV Archetypes, Abbreviations according to Fig. 7

[b] *L*: Length, *W*: Width, *H*: Height, *D*: Diameter

[c] S_i: Simulation based study, E_x: Experimental study

[d] U_∞: Wind speed (m/s)- M: measured based on the location, C: calculated using correlations, *h*: Wave height (m) — numbers with ** represent the significant wave height, T_p: Wave period (s) — numbers marked with * refer to the wavelength, λ_w in (m), λ: Wavelength (m), ω: Wave frequency (rad/s), $S(\omega)$: Wave spectrums — JS: JONSWAP spectrum, PM: Pierson–Moskowitz spectrum, MS: Mediterranean Sea wave spectrum, BM: Bretschneider-Mitsuyasu spectrum, θ_p: Pre-tilt angle (deg) — numbers with superscripts 'v' and 't' indicate tracker system and varied tilt angle respectively, *PVT*.: PV technology — mc-Si: Monocrystalline silicon module, pc-Si: Polycrystalline module, MF: monofacial panels, BF: bifacial panels, T_a,T_w: Ambient and water temperature in Celsius respectively.

[e] *ME*: Motion Effects, F_w: wind load, F_{wv}: wave loads, *R*: regular waves, *IR*: irregular waves, F_c: current loads, *SB*: response of a single unit archetype, *MB*: response of multi-connected archetypes, *ML*: mooring line inclusion.

[f] *CE*:Cooling Effects, E_a: effects of ambient conditions considered, E_w: effects of water considered, *TC*: temperature correlations proposed, *UV*: U-value proposed.

[g] *OE*: Optical Effects, *Alb.*: effect of changes in albedo, *Shad.*: effect of shading, *Soil*: effect of soiling

[h] *DE*: Degradation Effects, ⇝: An approximation is made to account for the degradation losses.

[i] *Dur.*: Duration of simulation. h — hours, d — days, m — months, y — years

[j] The gain or loss of EY observed due to each of the four processes

[k] *Val.*:Study validation, Y_e: Experimental validation performed, Y_a: Analytical validation performed, Y_i: Simulation validation performed, N: No validation performed.

Declaration of competing interest

The authors declare that they have no known competing financial interests or personal relationships that could have appeared to influence the work reported in this paper.

Acknowledgment

The authors gratefully acknowledge Dr. Elizabeth Endler, Chief Scientist – Energy Storage & Integration at Shell for their valuable review of this work.

Appendix A. Compilation of articles reviewed in this work

The compilation of all the articles reviewed in this work is encapsulated in a look up table as shown in Table B.5.

Appendix B. Supplementary data

Supplementary material related to this article can be found online at https://doi.org/10.1016/j.rser.2025.115596.

Data availability

Data will be made available on request.

References

[1] International Energy Agency (IEA). Renewables 2023: Analysis and forecast to 2028. 2023, https://www.iea.org/. [Accessed 03 March 2024].
[2] International Renewable Energy Agency (IRENA). Tripling renewable power by 2030: The role of the G7 in turning targets into action. 2024, https://www.irena.org/. [Accessed 03 March 2024].
[3] International Renewable Energy Agency (IRENA), Global Renewables Alliance (GRA). Tripling renewable power and doubling energy efficiency by 2030: Crucial steps towards $1.5°C$. 2023, https://www.irena.org/. [Accessed 03 March 2024].
[4] International Panel on Climate Change (IPCC). Climate change 2023: Synthesis report. Contribution of working groups I, II and III to the sixth assessment report of the intergovernmental panel on climate change. 2023, https://www.ipcc.ch/. [Accessed 03 March 2024].
[5] Chatzipanagi A, Taylor N, Jaeger-Waldau A. Overview of the potential and challenges for agri photovoltaics in the European union. 2023, https://joint-research-centre.ec.europa.eu/. [Accessed 03 March 2024].
[6] Wood Mackenzie. Floating solar landscape 2021. 2021, https://www.woodmac.com/. [Accessed 03 March 2024].
[7] rKeizo K. Floated on water surface solar-ray power generation apparatus. 1982, JPS5989471A.
[8] Ramanan CJ, Lim KH, Kurnia JC, Roy S, Bora BJ, Medhi BJ. Towards sustainable power generation: Recent advancements in floating photovoltaic technologies. Renew Sustain Energy Rev 2024;194:114322, https://doi.org/10.1016/j.rser.2024.114322.
[9] Trapani K, Santafé M. A review of floating photovoltaic installations: 2007–2013. Prog Photovolt Res Appl 2014;23:524–32. http://dx.doi.org/10.1002/pip.2466.
[10] Global data. Inside the world's largest dam-based floating solar power project. 2021, https://power.nridigital.com/future_power_technology_feb21/hapcheon_dam_based_floating_solar. [Accessed 03 March 2024].
[11] DNV. The future of floating solar: Drivers and barriers to growth. 2022, https://www.dnv.com/. [Accessed 03 March 2024].
[12] SolarPower Europe. Floating PV: Best practice guidelines. 2023, https://www.solarpowereurope.org/. [Accessed 03 March 2024].
[13] Misra D. Floating photovoltaic plant in India: Current status and future prospect. In: Advances in thermal engineering, manufacturing, and production management. 2021, p. 219–32.
[14] Mukhopadhyay S. Solar energy and gasification of MSW: Two promising Green energy options. In: Singh VK, Bangari N, Tiwari R, Dubey V, Bhoi AK, Babu TS, editors. Green energy systems. Academic Press; 2023, p. 93–125, https://doi.org/10.1016/B978-0-323-95108-1.00003-3.
[15] Ghosh A. A comprehensive review of water based PV: Flotavoltaics, under water, offshore & canal top. Ocean Eng 2023;281:115044, https://doi.org/10.1016/j.oceaneng.2023.115044.
[16] Wang J, Lund PD. Review of recent offshore photovoltaics development. Energies 2022;15:7462, https://doi.org/10.3390/en15207462.
[17] Essak L, Ghosh A. Floating photovoltaics: A review. Clean Technol 2022;4:752–69, https://doi.org/10.3390/cleantechnol4030046.
[18] Kumar M, Niyaz HM, Gupta R. Challenges and opportunities towards the development of floating photovoltaic systems. Sol Energy Mater Sol Cells 2021;233:111408, https://doi.org/10.1016/j.solmat.2021.111408.
[19] Oliveira-Pinto S, Stokkermans J. Marine floating solar plants: An overview of potential, challenges and feasibility. Proc Inst Civ Eng - Marit Eng 2020;173:120–35, https://doi.org/10.1680/jmaen.2020.10.
[20] Sahu A, Yadav N, Sudhakar K. Floating photovoltaic power plant: A review. Renew Sustain Energy Rev 2016;66:815–24, https://doi.org/10.1016/j.rser.2016.08.051.
[21] Hermann C, Dahlke F, Focken U, Trommsdorff M. Aquavoltaics: Dual use of natural and artificial water bodies for aquaculture and solar power generation. In: Gorjian S, Campana PE, editors. Solar energy advancements in agriculture and food production systems. Academic Press; 2022, p. 211–36.
[22] Ravichandran N, Ravichandran N, Panneerselvam B. Review on the structural components of floating photovoltaic covering systems. In: Reddy ANR, Marla D, Favorskaya MN, Satapathy SC, editors. Intelligent manufacturing and energy sustainability, Vol. 265. Singapore: Springer; 2022, p. 125–33.
[23] Mina M, Zsolt S. Top 200 operational floating solar projects. 2020, https://www.solarplaza.com/. [Accessed 03 March 2024].
[24] World Bank Group. Where sun meets water: Floating solar handbook for practitioners. 2019, https://www.worldbank.org/en/home. [Accessed 03 March 2024].
[25] International Energy Agency. Net zero roadmap: A global pathway to keep the 1.5 °C goal in reach. Paris: IEA; 2023, [accessed 03 March 2024].
[26] National Renewable Energy Laboratory. The renewable energy potential (reV) model: A geospatial platform for technical potential and supply curve modelling. Golden, CO: National Renewable Energy Laboratory; 2021.
[27] Aversen A, et al. Deriving life cycle assessment coefficients for application in integrated assessment modelling. Env Model Softw 2018;111–25, https://doi.org/10.1016/j.envsoft.2017.09.010.
[28] Smil V. Power density primer: Understanding the spatial dimension of the unfolding transition to renewable electricity generation (part I–definitions). 2010, http://www.vaclavsmil.com/wp-content/uploads/docs/smil-article-power-density-primer.pdf. [Accessed 03 March 2024].
[29] United Nations Economic Commission for Europe. Carbon neutrality in the UNECE region: Integrated life cycle assessment of electricity generation options. Geneva: United Nations; 2022.
[30] Ong S, Campbell C, Denholm P, Margolis R, Heath G. Land-use requirements for solar power plants in the United States. 2013, https://www.osti.gov/. [Accessed 03 March 2024].
[31] World Economic Forum. How much of Earth's surface is covered by each country. 2021, https://www.weforum.org/. [Accessed 03 March 2024].
[32] Christakou N, Heineke F, Janecke N, Klärner H, Kühn F, Tai H, et al. Renewable-energy development in a net-zero world: Land, permits, and grids. 2022, https://www.mckinsey.com/. [Accessed 03 March 2024].
[33] Swift DJP. Nearshore hydrodynamics and sedimentation. Springer US; 1984, p. 563–8.
[34] du Fornel E, Le Cadre Loret E, Mertens J, Keustermans J-P, Denis C, Sala O. Emerging sustainable technologies. 2024, https://innovation.engie.com/en/emerging-sustainable-technologies-2024. [Accessed 03 March 2024].
[35] TNO. Floating solar panels: Harnessing solar power on water. 2024, https://www.tno.nl/en/. [Accessed 03 March 2024].
[36] RWE. Offshore solar: Innovative solar energy projects. 2024, https://www.rwe.com/en/. [Accessed 03 March 2024].
[37] POM West-Vlaanderen, Ocean Energy Europe, Parkwind, Lappeenrannan-Lahden Teknillinen Yliopisto LUT, INNOSEA, RWE Renewables GmbH, et al. EU-SCORES: European scalable offshore renewable energy source. 2023, https://euscores.eu/. [Accessed 03 March 2024].
[38] International Energy Agency Photovoltaic Power Systems Programme (IEA PVPS). Carbon footprint analysis of floating PV systems. 2024, https://iea-pvps.org/. [Accessed 03 March 2024].
[39] Pouran HM, Padilha Campos Lopes M, Nogueira T, Alves Castelo Branco D, Sheng Y. Environmental and technical impacts of floating photovoltaic plants as an emerging clean energy technology. IScience 2022;25:105253, https://doi.org/10.1016/j.isci.2022.105253.
[40] Soppe W, Kingma A, Roosen D. Mechanical degradation studies on flexible CIGS cells and modules for floating PV. In: IEEE 49th photovoltaics specialists conference, 49. 2022, p. 1258–61, https://doi.org/10.1109/PVSC48317.2022.9938570.
[41] Friel D, Karimirad M, Whittaker T, Doran J, Howlin E. A review of floating photovoltaic design concepts and installed variations. 2019, Paper presented at 4th International Conference on Offshore Renewable Energy. CORE2019 proceedings, Glasgow: ASRANet Ltd, UK, 30 Aug 2019.
[42] Ma C, Wu RZ, Su H. Design of floating photovoltaic power plant and its environmental effects in different stages: A review. J Renew Sustain Energy 2021;13(6):062701, https://doi.org/10.1063/5.0065845.
[43] Shi W, Yan CJ, Ren ZR, Yuan ZM, Liu YY, Zheng SM, et al. Review on the development of marine floating photovoltaic systems. Ocean Eng 2023;286:115560, https://doi.org/10.1016/j.oceaneng.2023.115560.

[44] Gorjian S, Sharon H, Ebadi H, Kant K, Scavo FB, Tina GM. Recent technical advancements, economics and environmental impacts of floating photovoltaic solar energy conversion systems. J Clean Prod 2021;278:124285, https://doi.org/10.1016/j.jclepro.2020.124285.
[45] Vo TTE, Ko H, Huh J, Park N. Overview of possibilities of solar floating photovoltaic systems in the offshore industry. Energies 2021;14(21):6988, https://doi.org/10.3390/en14216988.
[46] Mishra S, Harish V, Saini G. Developing design topologies and strategies for the integration of floating solar, hydro, and pumped hydro storage system. Sustain Cities Soc 2023;95:104609, https://doi.org/10.1016/j.scs.2023.104609.
[47] Xiong L, Le C, Zhang P, Ding H, Li J. Harnessing the power of floating photovoltaic: A global review. J Renew Sustain Energy 2023;15:052701, https://doi.org/10.1063/5.0159394.
[48] Vidović V, Krajačić G, Matak N, Stunjek G, Mimica M. Review of the potentials for implementation of floating solar panels on lakes and water reservoirs. Renew Sustain Energy Rev 2023;178:113237, https://doi.org/10.1016/j.rser.2023.113237.
[49] Katare P, Bopche S, Tamkhade P, Gurav R, Nalavade S, Awad MM. Technological feasibility and challenges of hybrids: Wave, hydro, offshore-wind and floating solar energy harnessing. Multidiscip Rev 2024;7:2024054.
[50] Wu S, Jiang N, Zhang S, Zhang P, Zhao P, Liu Y, et al. Discussion on the development of offshore floating photovoltaic plants, emphasizing marine environmental protection. Front Mar Sci 2024;11:1336783.
[51] Lim SC, Dawoud MM, Hoe KY, Wong WY. Recent progress in floating solar photovoltaic systems: A review from Malaysia's perspective. J Eng Technol Appl Phys 2024;6:1–5.
[52] David TM, de Souza TM, Rizol PMSR. Photovoltaic systems: A review with analysis of the energy transition in Brazilian sulture, 2018–2023. Energy Inf 2024;7:1–24.
[53] Garrod A, Hussain SN, Ghosh A, Nahata S, Wynne C, Paver S. An assessment of floating photovoltaic systems and energy storage methods: A comprehensive review. Results Eng 2024;21:101940.
[54] Sun Z, Zhang L, Liu L, Chen W, Xie G, Zha J, et al. Optimal design for floating solar still by structural modification: A review. Desalination 2023;566:116937, https://doi.org/10.1016/j.desal.2023.116937.
[55] Huang G, Tang Y, Chen X, Chen M, Jiang Y. A comprehensive review of floating solar plants and potentials for offshore applications. J Mar Sci Eng 2023;11:2064, https://doi.org/10.3390/jmse11112064.
[56] Charles Rajesh Kumar J, Majid M. Floating solar photovoltaic plants in India – A rapid transition to a Green energy market and sustainable future. Energy Env 2023;34:304–58, https://doi.org/10.1177/0958305X211057185.
[57] Niccolai A, Grimaccia F, Lorenzo GD, Araneo R, Ughi F, Polenghi M. A review of floating PV systems with a techno-economic analysis. IEEE J Photovolt 2024;14:23–34, https://doi.org/10.1109/JPHOTOV.2023.3319601.
[58] Aweid RS, Ahmed OK, Algburi S. Recent developments of floating photovoltaic power plants: A review. AIP Conf Proc 2024;2885:020002, https://doi.org/10.1063/5.0182625.
[59] Kumar Dalapati G, Ghosh S, Sherin P A T, Ramasubramanian B, Samanta A, Rathour A, et al. Maximizing solar energy production in ASEAN region: Opportunity and challenges. Results Eng 2023;20:101525, https://doi.org/10.1016/j.rineng.2023.101525.
[60] Ahmed A, Elsakka M, Elminshawy N, Mohamed A, Sundaram S. Recent advances in floating photovoltaic systems. Chem Rec 2023;23:e202300229, https://doi.org/10.1002/tcr.202300229.
[61] Banik A, Sengupta A. Scope, challenges, opportunities and future goal assessment of floating solar park. Innov Energy Manag Renew Resour IEEE 2021;52042:1–5, https://doi.org/10.1109/IEMRE52042.2021.9386735.
[62] Ranjbaran P, Yousefi H, Gharehpetian GB, Astaraei FR. A review on floating photovoltaic (FPV) power generation units. Renew Sustain Energy Rev 2019;110:332–47, https://doi.org/10.1016/j.rser.2019.05.015.
[63] Cuce E, Cuce PM, Saboor S, Ghosh A, Sheikhnejad Y. Floating PVs in terms of power generation, environmental aspects, market potential, and challenges. Sustainability 2022;14:2626, https://doi.org/10.3390/su14052626.
[64] Pourgholami Markieh H, Kp A, Khorasanchi M, Oguz E. A review on conceptual design of support structures for floating solar power plants. In: 7th offshore energy storage symposium. 2023, p. 80–6, https://doi.org/10.1049/icp.2023.1557.
[65] Ma C, Liu Z. Water-surface photovoltaics: Performance, utilization, and interactions with water eco-environment. Renew Sustain Energy Rev 2022;167:112823, https://doi.org/10.1016/j.rser.2022.112823.
[66] Nobre R, Boulêtreau S, Colas F, Azemar F, Tudesque L, Parthuisot N, et al. Potential ecological impacts of floating photovoltaics on lake biodiversity and ecosystem functioning. Renew Sustain Energy Rev 2023;188:113852, https://doi.org/10.1016/j.rser.2023.113852.
[67] Li M, Luo H, Zhou S, Senthil Kumar GM, Guo X, Law TC, et al. State-of-the-art review of the flexibility and feasibility of emerging offshore and coastal ocean energy technologies in East and Southeast Asia. Renew Sustain Energy Rev 2022;162:112404, https://doi.org/10.1016/j.rser.2022.112404.
[68] Vivar M, H. S, Fuentes M. Photovoltaic system adoption in water related technologies – a review. Renew Sustain Energy Rev 2024;189:114004, https://doi.org/10.1016/j.rser.2023.114004.
[69] Cazzaniga R, Cicu M, Rosa-Clot M, Rosa-Clot P, Tina G, Ventura C. Floating photovoltaic plants: Performance analysis and design solutions. Renew Sustain Energy Rev 2018;81:1730–41, https://doi.org/10.1016/j.rser.2017.05.269.
[70] Benjamins S, Williamson B, Billing S-L, Yuan Z, Collu M, Fox C, et al. Potential environmental impacts of floating solar photovoltaic systems. Renew Sustain Energy Rev 2024;199:114463, https://doi.org/10.1016/j.rser.2024.114463.
[71] Roland E, Markus H. HelioFloat – a floating lightweight platform. 2016, Report published in the official website of Vienna University of Technology (TU Wien).
[72] Infratech Industries. Floating solar gen 1. 2022, https://infratechindustries.com/. [Accessed 03 March 2024].
[73] Bluewater. Renewable energy solutions. 2021, https://www.bluewater.com/. [Accessed 03 March 2024].
[74] Van Der Nat C, Gerardus JM, Van Den Berg B. Floating assembly for generating solar power and method for installing it. 2023, WIPO | PCT WO 2023/ 061600 A1.
[75] Van Der Nat C, Gerardus JM, Van Den Berg B. Floating assembly for generating solar power. 2023, WIPO | PCT WO 2023/ 061597 A1.
[76] DNV. DNV-RP-0584 design, development and operation of floating solar photovoltaic systems. 2021, https://www.dnv.com/. [Accessed 03 March 2024].
[77] Floating Solar BV. Floating solar parks. 2024, https://www.floatingsolar.nl/. [Accessed 03 March 2024].
[78] Swimsol. Floating solar PV for the sea. 2023, https://swimsol.com/. [Accessed 03 March 2024].
[79] Alexander P, Thomas M, Martin P. Floating platform. 2018, European Patent Office EP3237277B1.
[80] Akuo Energy. O'MEGA1 - renewable energy project on floating solar. 2022, https://www.akuoenergy.com/en. [Accessed 03 March 2024].
[81] BayWa re. The next generation of floating solar power. 2018, https://www.baywa-re.com/en/. [Accessed 03 March 2024].
[82] Bouygues Energies. O'MEGA1: First floating solar power plant in France. 2023, https://www.bouygues-es.com/. [Accessed 03 March 2024].
[83] Bryo Spa. Bryo and the new frontier of floating photovoltaics. 2023, https://www.bryo-spa.it/. [Accessed 03 March 2024].
[84] Chenya Energy. World's largest solar power plant. 2022, https://www.chenya-energy.com/. [Accessed 03 March 2024].
[85] Groenleven. Floating solar park oosterwolde. 2022, https://groenleven.nl/. [Accessed 03 March 2024].
[86] HelioRec. Simple, powerful floating solar technology. 2023, https://www.heliorec.com/. [Accessed 03 March 2024].
[87] Polina Igorevna V, Aleksandr Vladimirovich G. Floating module for photovoltaic panels. 2023, European Patent Office EP4286266A1.
[88] HelioRec. Floating module for photovoltaic panel. 2022, WIPO (PCT) WO2022010373A1.
[89] Innosea. Bringing marine renewable energies to life. 2022, https://innosea.fr/. [Accessed 03 March 2024].
[90] Intech Clean Energy. Floating solar system. 2021, https://intechcleanenergy.com/. [Accessed 03 March 2024].
[91] Kyoraku Co, Ltd. Floating solar power generation "minamo solar system". 2014, https://www.krk.co.jp/en/. [Accessed 03 March 2024].
[92] Kyoraku Co Ltd. Float systems. 2020, European Patent Office JP2023163007A.
[93] Kyoraku Co Ltd. Solar panel float and connected member thereof. 2019, European Patent Office US20190341877A1.
[94] LSElectric Co. Floating photovoltaic system. 2016, https://www.ls-electric.com/. [Accessed 03 March 2024].
[95] LSElectric Co Ltd. Supporting devices for solar panels. 2014, China National Intellectual Property Administration CN104702200A.
[96] Masdar. Cirata floating photovoltaic (FPV) plant. 2020, https://masdar.ae/en/. [Accessed 03 March 2024].
[97] Isifloating by Isigénère. Floating solar systems. 2008, https://www.isifloating.com/. [Accessed 03 March 2024].
[98] Pons Puig E, Ferrero Silvestre V, Redon Santafe M. Floating system for photovoltaic panels and floating installation comprising several floating systems for photovoltaic panels. 2024, WIPO (PCT) WO2024023374A1.
[99] Juan Ángel López M, Pons Puig E, Miguel Redón S, Hugo Coll C. Structure made up of floating photovoltaic panels. 2023, WIPO (PCT) WO2023084141A1.
[100] Mibet Energy. Floating PV system. 2012, https://www.mibetsolar.com/. [Accessed 03 March 2024].
[101] Narime. Capability profile in supplying floating and anchoring systems for solar power plant projects. 2019, http://narime.gov.vn/. [Accessed 03 March 2024].
[102] NEMO ENG Co, Ltd. Metal floating solar plant: The first metal floating system in the world. 2015, http://www.nemoeng.com/. [Accessed 03 March 2024].
[103] Nova Innovation. Powering a better future. 2023, https://novainnovation.com/. [Accessed 03 March 2024].
[104] NPSolar. Floating solar panels across the UK. 2021, https://np-solar.co.uk/. [Accessed 03 March 2024].
[105] NP: National Pontoon. Creating connections on water. 2024, https://nationalpontoon.co.uk/. [Accessed 03 March 2024].
[106] NRGenergia. Renewable energy and environment. 2024, https://nrg-energia.com/. [Accessed 03 March 2024].

[107] Loris S, Simone P. Floating element to make floating structures to support photovoltaic panels and method to produce said floating element. 2019, Spanish Patent and Trademark Office ES2742236T3.
[108] Giorgio T. Profile for fixing a photovoltaic panel to a support. 2013, Italian Patent and Trademark Office ITBO20110692A1.
[109] Giorgio T. Floating structure to support photovoltaic panels. 2013, Italian Patent and Trademark Office ITBO20120018A1.
[110] Profloating. FLOTAR floating PV system. 2018, https://www.profloating.nl/. [Accessed 03 March 2024].
[111] Vincent Daniel Gijsberthus Van D. Anchoring Device for Anchoring a Floating Solar Panel Assembly and Solar Panel Assembly, European Patent Office EP4107444A1 (Pending).
[112] Vincent Daniel Gijsberthus Van D. Method for manufacturing a design of a floating photovoltaic installation. 2022, WIPO (PCT) WO2022045893A1.
[113] Vincent Daniel Gijsberthus Van D. Solar float with a self-locking cap. 2022, Netherlands Patent Office NL2026458B1.
[114] Vincent Daniel Gijsberthus Van D. Solar float with a breathable cap. 2022, Netherlands Patent Office NL2026459B1.
[115] Solinoor B. Sun on water. 2023, https://solinoor.nl/. [Accessed 03 March 2024].
[116] ZIMMERMANN PV-Floating BV. Floating PV system. 2021, https://pv-floating.com/. [Accessed 03 March 2024].
[117] Sumitomo Mitsui Construction Co, Ltd. Float system for solar power generation. 2024, https://pv-float.com/. [Accessed 03 March 2024].
[118] Yukiro T, Wakaki T, Yoshiaki M, Kunio N. Solar float unit. 2023, Japan Patent Office JP2023102257A.
[119] Makoto K, Hitoshi S, Sei T, Kentaro T. Floating platform for solar panel installation. 2017, Taiwan Intellectual Property Office TWD186049S.
[120] Innovation S. Floating solar solutions. 2020, https://www.scg.com/innovation/en/. [Accessed 03 March 2024].
[121] Narisa W, Suwat W, Kriengkrai S, Attawut K, Kittimasak C, Pontawit K, et al. A floating structure for solar panel installation. 2018, WIPO (PCT) WO2018030965A1.
[122] Kok Boon H, Natthawoot P, Varith P, Natthakarn H. Floating Arrangement for Supporting Solar Panels, United States Patent and Trademark Office US20220289344A1 (Pending).
[123] Tanboon-Ek S, Surakit C, Tangpojthaweeporn P, Anuchitanukul R. A solar energy board float. 2018, Intellectual Property Office of Singapore SG10201710335SA.
[124] Kok Boon H, Pisan U, Varith P, Natthawoot P, Amorndech K. Floatation assembly and floating arrangement. 2023, WIPO (PCT) WO2023048655A1.
[125] Sungrow. Floating PV system. 2023, https://en.sungrowpower.com/. [Accessed 03 March 2024].
[126] Vikram Solar Ltd. Solar energy and engineering excellence: Building the future. 2017, https://www.vikramsolar.com/. [Accessed 03 March 2024].
[127] SeaVolt. Offshore floating solar technology. 2023, https://www.seavolt.be/. [Accessed 03 March 2024].
[128] Ewoud H, Olaf De S, Cornelis Frans DH. Floating structure having ellipsoid buoyant members. 2022.
[129] Ewoud H, Olaf de S, Cornelis Frans Donald H. Articulated floating structure. 2023, European Patent Office EP4267455A1.
[130] Ewoud H, Olaf de S, Cornelis Frans Donald H. Floating structure having ellipsoid buoyant members. 2023, European Patent Office EP4267454A1.
[131] Ewoud H, Hendrik H, Cornelis Frans Donald H, Olaf de S. A floating structure and a method of manufacturing a floating structure. 2024, European Patent Office EP4324732A1.
[132] Ewoud H, Olaf de S, Cornelis Frans Donald H. A floating structure. 2024, European Patent Office EP4324735A1.
[133] Ewoud H, Cornelis Frans Donald H. A floating structure. 2023, European Patent Office EP4230515A1.
[134] Ewoud H, Cornelis Frans Donald H, Carel Alexander M. An articulated structure. 2023, European Patent Office EP4190681A1.
[135] Oceans of Energy. North sea 1: Offshore solar. 2024, https://oceansofenergy.blue/. [Accessed 03 March 2024].
[136] Allard Pieter Van H. Array of pontoons for solar panel and connection modules therefor. 2020, United States Patent and Trademark Office US11332223B2.
[137] Allard Pieter Van H, Fabian Jeroen K. A pontoon with flotation members for supporting an energy conversion installation on a body of water. 2023, WIPO (PCT) WO2023239235A1.
[138] Fabian Jeroen K, Hendricus Johannes Van Poppelen M, Pieter Van Hoeken A. Pontoon with removable hydrodynamic element. 2022, Netherlands Patent Office NL2032416B1.
[139] Smadja L, Smadja PI. Floating solar panel systems. 2018, United States Patent US 10, 141, 885 B2.
[140] OceanSun. A bold solution to our global energy needs. 2018, https://oceansun.no/. [Accessed 03 March 2024].
[141] Børge B. Solar power plant. 2020, United States Patent and Trademark Office US10644645B2.
[142] Børge B. Photovoltaic solar power plant. 2023, Chile Patent Office CL2023000488A1.
[143] Børge B. Photovoltaic system for offshore deployment. 2019, Norwegian Patent Office NO343405B1.
[144] Børge B, Petter Kristensen G, Farhan A. Mooring of floating photovoltaic power plants. 2023, WIPO (PCT) WO2023158316A1.
[145] SolarisFloat. Tracking floating PV solutions. 2018, https://www.solarisfloat.com/. [Accessed 03 March 2024].
[146] Nuno C, Carla G, Ricardo P, Luis P, Nuno M, Jorge Teixeira da S. Rotating floating platform. 2022, European Patent Office EP3515801B1.
[147] Nuno C, Carla G, Ricardo P, Luis P, Nuno M, Jorge Teixeira da S. Floating module for modular solar panel platforms. 2019, United States Patent and Trademark Office US10480828B2.
[148] Nuno C, Carla G, Ricardo P, Luis P, Nuno M, Jorge Teixeira da S. Solar panel tracking system. 2019, Colombia Patent Office CO2019002375A2.
[149] Fred Olsen 1848 AS. The floating PV technology - BRIZO. 2024, https://www.fredolsen1848.com/. [Accessed 03 March 2024].
[150] Sunlit Sea AS. Produce electricity with floating solar. 2019, https://sunlitsea.no/. [Accessed 03 March 2024].
[151] Per Filip L. Floating solar panels. 2021, WIPO (PCT) WO2021130283A1.
[152] Sunfloat B. Floating solar cells. 2013, https://www.climate-kic.org/start-ups/sunfloat/. [Accessed 03 March 2024].
[153] Scotra. Floating solar power. 2022, http://scotra.co.kr/. [Accessed 03 March 2024].
[154] Moss Maritime. Floating offshore structures. 2024, https://www.mossww.com/. [Accessed 03 March 2024].
[155] Alexander Minge T, Audun Arnesen N, Ingrid L, Ole Petter L. Floating solar power plant. 2021, Norwegian Patent Office NO347181B1.
[156] Novar. Solar panels on water. 2023, https://www.novar.nl/. [Accessed 03 March 2024].
[157] SolarinBlue. The future of solar is at sea. 2013, https://solarinblue.com/. [Accessed 03 March 2024].
[158] Antoine R, Jean-Christophe D, Naman B, Friedrich N. Assembly for a floating power generation system. 2023, WIPO (PCT) WO2023180674A1.
[159] Antoine R, Jean-Christophe D, Naman B, Friedrich N. Floating power system package. 2023, French Patent and Trademark Office (INPI) FR3133830A1.
[160] SINN power. Floating PV. 2023, https://www.sinnpower.com/en. [Accessed 03 March 2024].
[161] Sunrise. Solar floating system. 2010, https://www.srise.com.tw/index.php. [Accessed 03 March 2024].
[162] Systems UF. Floating solar solution PV. 2017, https://floatingupsolar.com/. [Accessed 03 March 2024].
[163] Cazzaniga R. Apparatus for the generation of electrical energy by photovoltaic panels. 2021, European Patent Office EP3771090A1.
[164] Ciel et Terre. Floating solar: A bold and innovative solution. 2006, https://ciel-et-terre.net/. [Accessed 03 March 2024].
[165] Prouvost S, Le Blan B. Floating assembly for generating solar power. 2024, European Patent Office EP4143080B1.
[166] Ciel et Terre International SAS. Panel support device. 2017, Japan Patent Office JP6833781B2.
[167] Gaveau A. Floating support device for a photovoltaic panel. 2014, European Patent Office EP3083392B1.
[168] Emmanuel F, Papon G, Veloso M, Colin B. Anchoring of floating solar power plants. 2012, WIPO (PCT) WO2014016508A1.
[169] CIMC Raffles. Renewable energy. 2023, http://www.cimc-raffles.com/en/. [Accessed 03 March 2024].
[170] CIMC Offshore Engineering Institute Co ltd. Single-column photovoltaic power generation array platform. 2022, China National Intellectual Property Administration CN115180082A.
[171] CIMC Offshore Engineering Institute Co ltd. Inter-multi-body multi-step motion compensation connection method for offshore floating photovoltaic system. 2023, WIPO (PCT) WO2023155355A1.
[172] CIMC Offshore Engineering Institute Co ltd. Semi-submersible offshore photovoltaic power generation platform and offshore photovoltaic power generation array. 2022, China National Intellectual Property Administration CN114802627B.
[173] CIMC Offshore Engineering Institute Co ltd. Offshore wind and solar complementary power generation system and offshore floating bearing platform. 2022, China National Intellectual Property Administration CN114644089B.
[174] CIMC Offshore Engineering Institute Co ltd. Floating body module and offshore floating photovoltaic system. 2022, China National Intellectual Property Administration CN217554145U.
[175] Kim SH, Yoon SJ, Choi W. Design and construction of 1 MW class floating PV generation structural system using FRP members. Energies 2017;10:1142, https://doi.org/10.3390/en10081142.
[176] Cazzaniga R. Floating PV structures. In: Rosa-Clot M, Marco Tina G, editors. Floating PV plants. Academic Press; 2020, p. 33–45.
[177] Tina GM, Ventura C, Scavo FB. Technological and design solutions for enhancement of photovoltaic producibility. In: Jeguirim M, editor. Recent advances in renewable energy technologies. Academic Press; 2021, p. 91–148.

[178] Pringle AM, Handler RM, Pearce JM. Aquavoltaics: Synergies for dual use of water area for solar photovoltaic electricity generation and aquaculture. Renew Sustain Energy Rev 2017;80:572–84, https://doi.org/10.1016/j.rser.2017.05.191.
[179] Wim S, Aldo K. Challenges and potential for offshore solar. 2022, https://zonopwater.nl/home. [Accessed 03 March 2024].
[180] Claus R, Lopez M. Key issues in the design of floating photovoltaic structures for the marine environment. Renew Sustain Energy Rev 2022;164:112502, https://doi.org/10.1016/j.rser.2022.112502.
[181] Hu J, Teng K, Li C, Li X, Wang J, Lund PD. Review of recent water photovoltaics development. Oxf Open Energy 2023;2:oiad005, https://doi.org/10.1093/ooenergy/oiad005.
[182] Rijksdienst voor Ondernemend Nederland. Technology readiness levels (TRL). 2022, https://www.rvo.nl/onderwerpen/trl. [Accessed 03 March 2024].
[183] Whittaker T, Folley M, Hancock J. Environmental loads, motions, and mooring systems. In: Rosa-Clot M, Marco Tina G, editors. Floating PV plants. Academic Press; 2020, p. 47–66.
[184] Chakrabarti SK. Chapter 4 - loads and responses. In: Chakrabarti SK, editor. Handbook of offshore engineering. London: Elsevier; 2005, p. 133–96.
[185] Gubesch E, Abdussamie N, Penesis I, Chin C. Effects of mooring configurations on the hydrodynamic performance of a floating offshore oscillating water column wave energy converter. Renew Sustain Energy Rev 2022;166:112643, https://doi.org/10.1016/j.rser.2022.112643.
[186] Smets A, Jäger K, Isabella O, van Swaaij R, Zeman M. Solar energy: The physics and engineering of photovoltaic conversion, technologies and systems. UIT Cambridge Limited; 2016.
[187] Jiro D. GRABIT. 2024, https://nl.mathworks.com/. [Accessed 03 March 2024].
[188] Yongkang S, Yanji W, Zhi Yung T, Zuogang C. Hydroelastic analysis of offshore floating photovoltaic based on frequency-domain model. Ocean Eng 2023;289:116213, https://doi.org/10.1016/j.oceaneng.2023.116213.
[189] Ohkusu M, Namba Y. Hydroelastic analysis of a large floating structure. J Fluids Struct 2004;19(4):543–55, https://doi.org/10.1016/j.jfluidstructs.2004.02.002.
[190] Yong C, Chunyan J, Gangjun Z, Oleg G. Hydroelastic analysis of oblique irregular waves with a pontoon-type VLFS edged with dual inclined perforated plates. Mar Struct 2016;49:31–57, https://doi.org/10.1016/j.marstruc.2016.05.008.
[191] Maeda H, Ikoma T, Masuda K, Rheem C-K. Time-domain analyses of elastic response and second-order mooring force on a very large floating structure in irregular waves. Mar Struct 2000;13(4):279–99, https://doi.org/10.1016/S0951-8339(00)00032-0.
[192] Colomés O, Verdugo F, Akkerman I. A monolithic finite element formulation for the hydroelastic analysis of very large floating structures. Internat J Numer Methods Engrg 2023;124(3):714–51, https://doi.org/10.1002/nme.7140.
[193] Li Z, Chen D, Feng X. Hydroelastic and expansibility analysis of a modular floating photovoltaic system with multi-directional hinge connections. Ocean Eng 2023;289:116218, https://doi.org/10.1016/j.oceaneng.2023.116218.
[194] Yago K, Endo H. On the hydoroelastic response of box-shaped floating structure with shallow draft. J Soc Nav Archit Jpn 1996;1996(180):341–52, https://doi.org/10.2534/jjasnaoe1968.1996.180_341.
[195] Yago K, Endo H. On the hydoroelastic response of box-shaped floating structure with shallow draft (tank test with large scale model). J Soc Nav Archit Jpn 1996;1996(180):341–52, https://doi.org/10.2534/jjasnaoe1968.1996.180_341.
[196] Hiroshi K, Masataka F, Motohiko M. Theoretical and experimental predictions of the hydroelastic response of a very large floating structure in waves. Appl Ocean Res 1998;20(3):135–44, https://doi.org/10.1016/S0141-1187(98)00017-0.
[197] Yoon J-S, Cho S-P, Jiwinangun RG, Lee P-S. Hydroelastic analysis of floating plates with multiple hinge connections in regular waves. Mar Struct 2014;36:65–87, https://doi.org/10.1016/j.marstruc.2014.02.002.
[198] Shi Y, Wei Y, Tay ZY, Chen Z. Hydroelastic analysis of offshore floating photovoltaic based on frequency-domain model. Ocean Eng 2023;289:116213, https://doi.org/10.1016/j.oceaneng.2023.116213.
[199] Fu S, Moan T, Chen X, Cui W. Hydroelastic analysis of flexible floating interconnected structures. Ocean Eng 2007;34(11):1516–31, https://doi.org/10.1016/j.oceaneng.2007.01.003.
[200] Huang H, jun Chen X, yi Liu J, ji Miao Y, Ji S. A method to estimate dynamic responses of VLFS based on multi-floating-module model connected by elastic hinges. China Ocean Eng 2021;35:687–99, https://doi.org/10.1007/s13344-021-0061-9.
[201] Huang H, jun Chen X, yi Liu J, Ji S. A method to predict hydroelastic responses of VLFS under waves and moving loads. Ocean Eng 2022;247:110399, https://doi.org/10.1016/j.oceaneng.2021.110399.
[202] Xu P, Zhang Z, Li S, Song Q, Liu W. Numerical investigation into the dynamic responses of floating photovoltaic platform and mooring line structures under freak waves. J Mar Sci Eng 2024;12. https://doi.org/10.3390/jmse12010096.
[203] Wei Y, Ou B, Wang J, Yang L, Luo Z, Jain S, et al. Simulation of a floating solar farm in waves with a novel sun-tracking system. IOP Conf Series: Mater Sci Eng 2023;1288(1):012041.
[204] Zhang F, Shi W, Wang Q. A study on the hydrodynamics and coupling effects of the multibody floating photovoltaic (FPV) concept. J Mar Sci Eng 2023;11:1491, https://doi.org/10.3390/jmse11081491.
[205] Zhang D, Du J, Yuan Z, Yu S, Li H. Motion characteristics of large arrays of modularized floating bodies with hinge connections. Phys Fluids 2023;35(7):077107, https://doi.org/10.1063/5.0153317.
[206] Daniel HH, Haryo DA, Fandy RA. Geometric analysis of pontoon and mooring line towards hydrodynamic response. E3S Web Conf 2024;499:01015, https://doi.org/10.1051/e3sconf/202449901015.
[207] van der Zanden J, Bunnik T, Cortés A, Delhaye V, Kegelart G, Pehlke T, et al. Wave basin tests of a multi-body floating PV system sheltered by a floating breakwater. Energies 2024;17:9, https://doi.org/10.3390/en17092059.
[208] Ikhennicheu M, Blanc A, Danglade B, Gilloteaux J-C. OrcaFlex modelling of a multi-body floating solar Island subjected to waves. Energies 2022;15:23, https://doi.org/10.3390/en15239260.
[209] Zhang C, Santo H, Magee AR. Review and comparative study of methodologies for hydrodynamic analysis of nearshore floating solar farms. Offshore Technol Conf Asia 2022;Day 2 Wed, March 23, 2022. D021S003R001. https://doi.org/10.4043/31673-MS.
[210] Chen M, Ouyang M, Guo H, Zou M, Zhang C. A coupled hydrodynamic–structural model for flexible interconnected multiple floating bodies. J Mar Sci Eng 2023;11:4, https://doi.org/10.3390/jmse11040813.
[211] Al-Yacouby AM, Halim ERBA, Liew MS. Hydrodynamic analysis of floating offshore folar farms subjected to regular waves. In: Emamian SS, Yusof F, Awang M, editors. Aadvances in manufacturing engineering. Springer Science and Business Media Deutschland GmbH; 2020, p. 375–90, https://doi.org/10.1007/978-981-15-5753-8_35.
[212] Baruah G, Karimirad M, Friel D, Mackinnon P, Abbasnia A, Sarmah N. Development of a CFD model for simulating a floating solar platform in irregular wave regimes. Trends in Renewable Energies Offshore; 2022, p. 717–25, https://doi.org/10.1201/9781003360773-80.
[213] Dallán F. Dynamic responses of floating photovoltaic arrays under wave loads [Doctoral thesis], Queen's University Belfast; 2024, p. 274.
[214] Friel D, Doran J, Karimirad M, Whittaker T. Hydrodynamic investigation of design parameters for a cylindrical type floating solar system. In: Proceedings of the 4th international conference on renewable energies offshore. 12, 2020, p. 15, https://doi.org/10.1201/9781003134572.
[215] Claus R, Lópes M. A methodology to assess the dynamic response and the structural performance of floating photovoltaic systems. Sol Energy 2023;262:111826, https://doi.org/10.1016/j.solener.2023.111826.
[216] Abbasnia A, Karimirad M, Friel D, Whittaker T. Fully nonlinear dynamics of floating solar platform with twin hull by tubular floaters in ocean waves. Ocean Eng 2022;257:111320, https://doi.org/10.1016/j.oceaneng.2022.111320.
[217] Joo H-J, Heo S-J, Kim S-H, Choi W. Wind load distribution in float photovoltaic system. Appl Sci 2023;13:22, https://doi.org/10.3390/app132212144.
[218] Yang RY, Yu SH. A study on a floating solar energy system applied in an intertidal zone. Energies 2021;14. https://doi.org/10.3390/en14227789.
[219] Delacroix S, Bourdier S, Soulard T, Elzaabalawy H, Vasilenko P. Experimental modelling of a floating solar power plant array under wave forcing. Energies 2023;16. https://doi.org/10.3390/en16135198.
[220] Cheng B, Adrian Wing-Keung L. Co-locating offshore wind and floating solar farms – effect of high wind and wave conditions on solar power performance. Energy 2023;266:126437, https://doi.org/10.1016/j.energy.2022.126437.
[221] Chen K, Li D, Wang W, Fu Q, Zhang J, Xu Y, et al. Wave induced losses simulation of floating solar photovoltaic systems at open waters. In: The 33rd international ocean and polar engineering conference all days. International ocean and polar engineering conference, vol. All Days, 2023, ISOPE–I–23–097.
[222] Rubén C, Fernando S, Alejandro C, Mario L, Daniel C, Gianmaria G, et al. Experimental proof-of-concept of HelioSea: A novel marine floating photovoltaic device. Ocean Eng 2024;299:117184, https://doi.org/10.1016/j.oceaneng.2024.117184.
[223] Mario L, Rubén C, Fernando S, Zenaida A H-G, Alejandro C-R, Orlando S. Advancing offshore solar energy generation: The HelioSea concept. Appl Energy 2024;359. https://doi.org/10.1016/j.apenergy.2024.122710.
[224] Song J, Kim J, Chung WC, Jung D, Kang YJ, Kim S. Wave-induced structural response analysis of the supporting frames for multiconnected offshore floating photovoltaic units installed in the inner harbor. Ocean Eng 2023;271:113812, https://doi.org/10.1016/j.oceaneng.2023.113812.
[225] Zhiyu J, Jian D, Simone S, Glenn T, Zhao H, Musa B, et al. Design and model test of a soft-connected lattice-structured floating solar photovoltaic concept for harsh offshore conditions. Mar Struct 2023;90:103426, https://doi.org/10.1016/j.marstruc.2023.103426.
[226] Song J, Kim J, Lee J, Kim S, Chung W. Dynamic response of multiconnected floating solar panel systems with vertical cylinders. J Mar Sci Eng 2022;10. https://doi.org/10.3390/jmse10020189.
[227] Yan C, Shi W, Han X, Li X, Verma AS. Assessing the dynamic behavior of multiconnected offshore floating photovoltaic systems under combined wave-wind loads: A comprehensive numerical analysis. Sustain Horiz 2023;8:100072, https://doi.org/10.1016/j.horiz.2023.100072.
[228] Wenhui K, Zixiang L, Yue H. Design and hydrodynamic performance analysis of a two-module wave-resistant floating photovoltaic device. J Phys 2023;2565:111408, https://doi.org/10.1088/1742-6596/2565/1/012014.

[229] Wang C, Song X, Fu Q, Cui L, Chen P. Design and optimization of PV power supply system for marine buoys. J Mar Sci Eng 2023;11:1808, https://doi.org/10.3390/jmse11091808.
[230] Bugeja R, Mule' Stagno L, Branche N. The effect of wave response motion on the insolation on offshore photovoltaic installations. Sol Energy Adv 2021;1:100008, https://doi.org/10.1016/j.seja.2021.100008.
[231] Abu K, Mahedi H, Md Tasnim R, Nawshad H, Md Hasan F, Saifuddin A, et al. Optimization and techno-economic assessment of 50 MW floating solar power plant on hakaluki marsh land in Bangladesh. Renew Energy 2023;216:119077, https://doi.org/10.1016/j.renene.2023.119077.
[232] Alcañiz A, Monaco N, Isabella O, Ziar H. Offshore floating PV–DC and AC yield analysis considering wave effects. Energy Convers Manage 2024;300:117897, https://doi.org/10.1016/j.enconman.2023.117897.
[233] Magkouris A, Rusu E, Rusu L, Belibassakis K. Floating solar systems with application to nearshore sites in the Greek Sea Region. J Mar Sci Eng 2023;11:722, https://doi.org/10.3390/jmse11040722.
[234] Cengel YAa. Heat and mass transfer : Fundamentals & applications. New York: McGraw-Hill Education; 2020.
[235] Faiman D. Assessing the outdoor operating temperature of photovoltaic modules. Prog Photovolt Res Appl 2008;16(4):307–15, https://doi.org/10.1002/pip.813.
[236] Chowdhury G, Haggag M, Poortmans J. How cool is floating PV? A state-of-the-art review of floating PV's potential gain and computational fluid dynamics modeling to find its root cause. EPJ Photovolt 2023;14:24, https://doi.org/10.1051/epjpv/2023015.
[237] Kjeldstad T, Lindholm D, Marstein E, Selj J. Cooling of floating photovoltaics and the importance of water temperature. Sol Energy 2021;218:544–51, https://doi.org/10.1016/j.solener.2021.03.022.
[238] Elminshawy NA, Osama A, Naeim N, Elbaksawi O, Marco Tina G. Thermal regulation of partially floating photovoltaics for enhanced electricity production: A modeling and experimental analysis. Sustain Energy Technol Assess 2022;53:102582, https://doi.org/10.1016/j.seta.2022.102582.
[239] Elminshawy NA, El-Damhogi D, Ibrahim I, Elminshawy A, Osama A. Assessment of floating photovoltaic productivity with fins-assisted passive cooling. Appl Energy 2022;325:119810, https://doi.org/10.1016/j.apenergy.2022.119810.
[240] Elminshawy NA, Osama A, El-Damhogi D, Oterkus E, Mohamed A. Simulation and experimental performance analysis of partially floating PV system in windy conditions. Sol Energy 2021;230:1106–21, https://doi.org/10.1016/j.solener.2021.11.020.
[241] Amiot B, Le Berre R, Giroux-Julien S. Evaluation of thermal boundary conditions in floating photovoltaic systems. Prog Photovolt Res Appl 2023;31(3):251–68, https://doi.org/10.1002/pip.3631.
[242] Tina GM, Bontempo Scavo F, Merlo L, Bizzarri F. Comparative analysis of monofacial and bifacial photovoltaic modules for floating power plants. Appl Energy 2021;281:116084, https://doi.org/10.1016/j.apenergy.2020.116084.
[243] Tina GM, Bontempo Scavo F, Merlo L, Bizzarri F. Analysis of water environment on the performances of floating photovoltaic plants. Renew Energy 2021;175:281–95, https://doi.org/10.1016/j.renene.2021.04.082.
[244] Dörenkämper M, Wahed A, Kumar A, de Jong M, Kroon J, Reindl T. The cooling effect of floating PV in two different climate zones: A comparison of field test data from the netherlands and Singapore. Sol Energy 2021;214:239–47, https://doi.org/10.1016/j.solener.2020.11.029.
[245] Liu H, Krishna V, Lun Leung J, Reindl T, Zhao L. Field experience and performance analysis of floating PV technologies in the tropics. Prog Photovolt Res Appl 2018;26:957–67, https://doi.org/10.1002/pip.3039.
[246] Amiot B, Pabiou H, Le Berre R, Giroux-Julien S. An innovative method for measuring the convective cooling of photovoltaic modules. Sol Energy 2024;274:112531, https://doi.org/10.1016/j.solener.2024.112531.
[247] Willemse B, Nielsen S, Pretorius J, Owen M, Rix A. A comparative evaluation of heat dissipation factors for open-rack and floating solar photovoltaic installations. SSRN Electron J 2023. https://doi.org/10.2139/ssrn.4547936.
[248] Rahaman MA, Chambers TL, Fekih A, Wiecheteck G, Carranza G, Possetti GRC. Floating photovoltaic module temperature estimation: Modeling and comparison. Renew Energy 2023;208:162–80, https://doi.org/10.1016/j.renene.2023.03.076.
[249] Nisar H, Kashif Janjua A, Hafeez H, shakir S, Shahzad N, Waqas A. Thermal and electrical performance of solar floating PV system compared to on-ground PV system-an experimental investigation. Sol Energy 2022;241:231–47, https://doi.org/10.1016/j.solener.2022.05.062.
[250] Manoj Kumar N, Chakraborty S, Kumar Yadav S, Singh J, Chopra SS. Advancing simulation tools specific to floating solar photovoltaic systems – comparative analysis of field-measured and simulated energy performance. Sustain Energy Technol Assess 2022;52:102168, https://doi.org/10.1016/j.seta.2022.102168.
[251] Radhiansyah, Rachmilda TD, Hamdani D. Performance analysis of offshore floating PV systems in isolated area. In: 3rd international conference on high voltage engineering and power systems. 2021, p. 651–5, https://doi.org/10.1109/ICHVEPS53178.2021.9600926.
[252] Karatas Y, Yilmaz D. Experimental investigation of the microclimate effects on floating solar power plant energy efficiency. Clean Techn Env Policy 2021;23:2157–70, https://doi.org/10.1007/s10098-021-02122-y.
[253] Peters IM, Nobre AM. On module temperature in floating PV systems. In: 47th IEEE photovoltaic specialists conference. 2020, p. 0238–41, https://doi.org/10.1109/PVSC45281.2020.9300426.
[254] Waithiru C L, Chang-sub W, Dong-chan K, Kwang-Wook K, Boram K, GunHyun L, et al. Floating photovoltaic module temperature operation characteristics. In: 33rd european photovoltaic solar energy conference and exhibition. 2017, p. 2304–10, https://doi.org/10.4229/EUPVSEC20172017-6BV.1.40.
[255] Charles Lawrence Kamuyu W, Lim JR, Won CS, Ahn HK. Prediction model of photovoltaic module temperature for power performance of floating PVs. Energies 2018;11. https://doi.org/10.3390/en11020447.
[256] Tryakin D, Shurkalov P. Investigation of temperature effect on photovoltaic modules of the nizhne-bureyskaya floating solar power plant. In: International conference on industrial engineering, applications and manufacturing. 2023, p. 239–44, https://doi.org/10.1109/ICIEAM57311.2023.10138984.
[257] Fuentes MK. A simplified thermal model for Flat-Plate photovoltaic arrays. Albuquerque, NM (USA): Sandia National Labs.; 1987.
[258] Golroodbari SZ, Ayyad AW, van Sark W. Offshore floating photovoltaics system assessment in worldwide perspective. Prog Photovolt Res Appl 2023;31:1061–77, https://doi.org/10.1002/pip.3723.
[259] Golroodbari SZ, van Sark W. Simulation of performance differences between offshore and land-based photovoltaic systems. Prog Photovolt 2020;28:873–86, https://doi.org/10.1002/pip.3276.
[260] Dzamesi SKA, Ahiataku-Togobo W, Yakubu S, Acheampong P, Kwarteng M, Samikannu R, et al. Comparative performance evaluation of ground-mounted and floating solar PV systems. Energy Sustain Dev 2024;80:101421, https://doi.org/10.1016/j.esd.2024.101421.
[261] Dragon A. Study case: The water-cooling effect on floating photovoltaic plants performance. KTH, Energy Technol 2024;86.
[262] Kaplanis S, Kaplani E, Kaldellis JK. PV temperature prediction incorporating the effect of humidity and cooling due to seawater flow and evaporation on modules simulating floating PV conditions. Energies 2023;16:4756, https://doi.org/10.3390/en16124756.
[263] Dörenkämper M, de Jong MM, Kroon J, Nysted VS, Selj J, Kjeldstad T. Modeled and measured operating temperatures of floating PV modules: A comparison. Energies 2023;16:7153, https://doi.org/10.3390/en16207153.
[264] Refaai MRA, Dhanesh L, Ganthia B, Mohanty M, Subbiah R, Anbese E. Design and implementation of a floating PV model to analyse the power generation. Int J Photoenergy 2022;2022:1–13, https://doi.org/10.1155/2022/3891881.
[265] Kjeldstad T, Nysted VS, Kumar M, Oliveira-Pinto S, Otnes G, Lindholm D, et al. The performance and amphibious operation potential of a new floating photovoltaic technology. Sol Energy 2022;239:242–51, https://doi.org/10.1016/j.solener.2022.04.065.
[266] Elminshawy NA, Osama A, Saif AM, Tina GM. Thermo-electrical performance assessment of a partially submerged floating photovoltaic system. Energy 2022;246:123444, https://doi.org/10.1016/j.energy.2022.123444.
[267] Patel SS. The influence of albedo and cooling on the yield of floating PV systems [Master's thesis], Stellenbosch University; 2021, p. 185, http://hdl.handle.net/10019.1/110547.
[268] Majumder A, Innamorati R, Frattolillo A, Kumar A, Gatto G. Performance analysis of a floating photovoltaic system and estimation of the evaporation losses reduction. Energies 2021;14. https://doi.org/10.3390/en14248336.
[269] Biniyam Zemene Taye AHN, Workineh TG. Design of floating solar PV system for typical household on debre mariam Island. Cogent Eng 2020;7(1):1829275, https://doi.org/10.1080/23311916.2020.1829275.
[270] Sheikh YA, Butt AD, Paracha KN, Awan AB, Bhatti AR, Zubair M. An improved cooling system design to enhance energy efficiency of floating photovoltaic systems. J Renew Sustain Energy 2020;12:053502, https://doi.org/10.1063/5.0014181.
[271] Junianto B, Dewi T, Sitompul CR. Development and feasibility analysis of floating solar panel application in palembang, South sumatra. J Phys Conf Ser 2020;1500:012016, https://doi.org/10.1088/1742-6596/1500/1/012016.
[272] Dörenkämper M, Villa S, Kroon J, de Jong MM. The impact of system sizing and water temperature on the thermal characteristics of floating photovoltaic systems. Energies 2024;17. https://doi.org/10.3390/en17092027.
[273] Oliveira-Pinto S, Stokkermans J. Assessment of the potential of different floating solar technologies – overview and analysis of different case studies. Energy Convers Manage 2020;211:112747, https://doi.org/10.1016/j.enconman.2020.112747.
[274] Ayyad A, Golroodbari S, van Sark W. Floating offshore photovoltaics across geographies: An enhanced model of water cooling. Energies 2024;17. https://doi.org/10.3390/en17051131.
[275] Ravichandran N, Ravichandran N, Panneerselvam B. Comparative assessment of offshore floating photovoltaic systems using thin film modules for Maldives Islands. Sustain Energy Technol Assess 2022;53:102490, https://doi.org/10.1016/j.seta.2022.102490.
[276] Lindholm D, Selj J, Kjeldstad T, Fjær H, Nysted V. CFD modelling to derive U-values for floating PV technologies with large water footprint. Sol Energy 2022;238:238–47, https://doi.org/10.1016/j.solener.2022.04.028.
[277] Lindholm D, Kjeldstad T, Selj J, Marstein ES, Fjær HG. Heat loss coefficients computed for floating PV modules. Prog Photovolt Res Appl 2021;29(12):1262–73, https://doi.org/10.1002/pip.3451.

[278] Lereng IH. Study on the cooling effect for floating PV modules in thermal contact with water and the potential for modeling floating PV. Nor Univ Life Sci 2018;90, http://hdl.handle.net/11250/2561972.
[279] Maia CB, Diniz ASA, Bonfim SA, Kazmerski LL. Evaluation of the electrical parameters and performance of floating PV generators. Renew Energy Env Sustain 2024;9:5, https://doi.org/10.1051/rees/2024003.
[280] Grisanti M, Mannino G, Tina G, Ortis A, Cacciato M, Battiato S, et al. Thermal models of monofacial and bifacial PV modules: Machine learning and physical estimation models comparison. In: 2023 IEEE 50th photovoltaic specialists conference. 2023, p. 1–3, https://doi.org/10.1109/PVSC48320.2023.10360013.
[281] Niyaz HM, Kumar M, Gupta R. Estimation of module temperature for water-based photovoltaic systems. J Renew Sustain Energy 2021;13:053705, https://doi.org/10.1063/5.0059794.
[282] Micheli L, Talavera DL, Marco Tina G, Almonacid F, Fernández EF. Techno-economic potential and perspectives of floating photovoltaics in Europe. Sol Energy 2022;243:203–14, https://doi.org/10.1016/j.solener.2022.07.042.
[283] C J R, Lim K, Kurnia J, Roy S, Bora B, Medhi B. Design study on the parameters influencing the performance of floating solar PV. Renew Energy 2024;223:120064, https://doi.org/10.1016/j.renene.2024.120064.
[284] Getie E, Jember Y. Potential assessment and performance evaluation of a floating solar photovoltaic on the great ethiopian renaissance dam. Int J Photoenergy 2022;2022:12, https://doi.org/10.1155/2022/6964984.
[285] Liu L, Wang Q, Lin H, Li H, Sun Q, wennersten R. Power generation efficiency and prospects of floating photovoltaic systems. Energy Procedia 2017;105:1136–42, https://doi.org/10.1016/j.egypro.2017.03.483.
[286] Prilliman M, Stein JS, Riley D, Tamizhmani G. Transient weighted moving-average model of photovoltaic module back-surface temperature. IEEE J Photovolt 2020;10:1053–60, https://doi.org/10.1109/JPHOTOV.2020.2992351.
[287] Simpson JJ, Paulson CA. Mid-ocean observations of atmospheric radiation. Q J R Meteorol Soc 1979;105(444):487–502, https://doi.org/10.1002/qj.49710544412.
[288] Sellers WD. Physical climatology. Chicago: University of Chicago Press; 1965.
[289] Willis J. Some high values for the albedo of the sea. J Appl Meteorol Clim 1971;10(6):1296–302, https://doi.org/10.1175/1520-0450(1971)010<1296:SHVFTA>2.0.CO;2.
[290] Payne RE. Albedo of the sea surface. J Atmos Sci 1972;29(5):959–70, https://doi.org/10.1175/1520-0469(1972)029<0959:AOTSS>2.0.CO;2.
[291] Gordon HR, Jacobs MM. Albedo of the ocean-atmosphere system: Influence of sea foam. Appl Opt 1977;16:2257–60, https://doi.org/10.1364/AO.16.002257.
[292] Katsaros KB, McMurdie LA, Lind RJ, DeVault JE. Albedo of a water surface, spectral variation, effects of atmospheric transmittance, sun angle and wind speed. J Geophys Res: Ocean 1985;90:7313–21, https://doi.org/10.1029/JC090iC04p07313.
[293] Bryon B H. Estimating albedo for evapotranspiration models. Grad Fac Tex Tech Univ 1989.
[294] Winckler JR, Anderson K. Geomagnetic and albedo studies with geomagnetic latitude. Phys Rev 1954;93:596–605, https://doi.org/10.1103/PhysRev.93.596.
[295] Jin Z, Charlock TP, Smith Jr WL, Rutledge K. A parameterization of ocean surface albedo. Geophys Res Lett 2004;31(22). https://doi.org/10.1029/2004GL021180.
[296] Fogarty MC, Fewings MR, Paget AC, Dierssen HM. The influence of a sandy substrate, seagrass, or highly turbid water on albedo and surface heat flux. J Geophys Res: Ocean 2018;123(1):53–73, https://doi.org/10.1002/2017JC013378.
[297] Huang CJ, Qiao F, Chen S, Xue Y, Guo J. Observation and parameterization of broadband sea surface albedo. J Geophys Res: Ocean 2019;124(7):4480–91, https://doi.org/10.1029/2018JC014444.
[298] Huang CJ, Wang G, Chen S, Guo J, Qiao F. An effective parameterization of broadband ocean surface albedo applicable to all skies. Ocean Model 2024;190:102394, https://doi.org/10.1016/j.ocemod.2024.102394.
[299] Du J, Jacinthe P-A, Song K, Zhou H. Water surface albedo and its driving factors on the turbid lakes of Northeast China. Ecol Indic 2023;146:109905, https://doi.org/10.1016/j.ecolind.2023.109905.
[300] Golroodbari S, van Sark W. On the effect of dynamic albedo on performance modelling of offshore floating photovoltaic systems. Sol Energy Adv 2022;2:100016, https://doi.org/10.1016/j.seja.2022.100016.
[301] Jin Z, Qiao Y, Wang Y, Fang Y, Yi W. A new parameterization of spectral and broadband ocean surface albedo. Opt Express 2011;19(27):26429–43, https://doi.org/10.1364/OE.19.026429.
[302] Patel S, Rix A. The impact of water surface albedo on incident solar insolation of a collector surface. In: 2020 international SAUPEC/RobMech/PRASA conference. 2020, p. 1–6, https://doi.org/10.1109/SAUPEC/RobMech/PRASA48453.2020.9041116.
[303] Patel S, Rix A. Water surface albedo modelling for floating PV plants. In: 6th Southern African Solar Energy Conference (SASEC), vol. 19, 2019, p. 9.
[304] Cosgun AE, Demir H. Investigating the effect of albedo in simulation-based floating photovoltaic system: 1 MW bifacial floating photovoltaic system design. Energies 2024;17. https://doi.org/10.3390/en17040959.
[305] Ziar H, Sönmez FF, Isabella O, Zeman M. A comprehensive albedo model for solar energy applications: Geometric spectral albedo. Appl Energy 2019;255:113867, https://doi.org/10.1016/j.apenergy.2019.113867.
[306] Ziar H, Prudon B, Lin F-YV, Roeffen B, Heijkoop D, Stark T, et al. Innovative floating bifacial photovoltaic solutions for Inland Water Areas. Prog Photovolt Res Appl 2021;29:725–43, https://doi.org/10.1002/pip.3367.
[307] Yakubu RO, Quansah DA, Mensah LD, Ahiataku-Togobo W, Acheampong P, Adaramola MS. Comparison of ground-based and floating solar photovoltaic systems performance based on monofacial and bifacial modules in Ghana. Energy Nexus 2023;12:100245, https://doi.org/10.1016/j.nexus.2023.100245.
[308] Rimon GR, Ahmed MS, Khan MR. Albedo and temperature aware analysis of bifacial vs monofacial floating photovoltaics in Bangladesh. In: 12th international conference on electrical and computer engineering. 2022, p. 13–5, https://doi.org/10.1109/ICECE57408.2022.10088821.
[309] Ates A, Yilmaz O, Gülgen F. Investigating the effect of shading on the capacity factor of floating photovoltaic systems. Celal Bayar Univ Fen Bilim Derg 2022;18. https://doi.org/10.18466/cbayarfbe.1020070.
[310] Setiawan F, Dewi T, Yusi S. Sea salt deposition effect on output and efficiency losses of the photovoltaic system; a case study in palembang, Indonesia. J Phys Conf Ser 2019;1167:012028, https://doi.org/10.1088/1742-6596/1167/1/012028.
[311] Gao X, Wang T, Liu M, Lian J, Yao Y, Yu L, et al. A framework to identify guano on photovoltaic modules in offshore floating photovoltaic power plants. Sol Energy 2024;274:112598, https://doi.org/10.1016/j.solener.2024.112598.
[312] Ahn S-H, Kim GG, Choi JH, Kang Y-B, Hyun JH, Ahn H-K. Power prediction of PV modules contaminated by bird droppings via an image thresholding process. IEEE J Photovolt 2024;14:557–68, https://doi.org/10.1109/JPHOTOV.2024.3364811.
[313] Hegazy AA. Effect of dust accumulation on solar transmittance through glass covers of plate-type collectors. Renew Energy 2001;22(4):525–40, https://doi.org/10.1016/S0960-1481(00)00093-8.
[314] Jiang Y, Lu L, Lu H. A novel model to estimate the cleaning frequency for dirty solar photovoltaic (PV) modules in desert environment. Sol Energy 2016;140:236–40, https://doi.org/10.1016/j.solener.2016.11.016.
[315] Jones RK, Baras A, Saeeri AA, Al Qahtani A, Al Amoudi AO, Al Shaya Y, et al. Optimized cleaning cost and schedule based on observed soiling conditions for photovoltaic plants in central Saudi Arabia. IEEE J Photovolt 2016;6(3):730–8. http://dx.doi.org/10.1109/JPHOTOV.2016.2535308.
[316] Hammad B, Al-Abed M, Al-Ghandoor A, Al-Sardeah A, Al-Bashir A. Modeling and analysis of dust and temperature effects on photovoltaic systems' performance and optimal cleaning frequency: Jordan case study. Renew Sustain Energy Rev 2018;82:2218–34, https://doi.org/10.1016/j.rser.2017.08.070.
[317] Al-Kouz W, Al-Dahidi S, Hammad B, Al-Abed M. Modeling and analysis framework for investigating the impact of dust and temperature on PV systems' performance and optimum cleaning frequency. Appl Sci 2019;9(7). http://dx.doi.org/10.3390/app9071397.
[318] Sotoudeh F, Mousavi SM, Karimi N, Lee BJ, Abolfazli-Esfahani J, Manshadi MK. Natural and synthetic superhydrophobic surfaces: A review of the fundamentals, structures, and applications. Alex Eng J 2023;68:587–609, https://doi.org/10.1016/j.aej.2023.01.058.
[319] Zahedi R, Ranjbaran P, Gharehpetian GB, Mohammadi F, Ahmadiahangar R. Cleaning of floating photovoltaic systems: A critical review on approaches from technical and economic perspectives. Energies 2021;14(7). http://dx.doi.org/10.3390/en14072018.
[320] REGlobal. Cleaning techniques for floating solar systems. 2021, https://reglobal.org/cleaning-techniques-for-floating-solar-systems/. [Accessed 03 March 2024].
[321] Golroodbari S, Vaartjes D, Meit J, van Hoeken A, Eberveld M, Jonker H, et al. Pooling the cable: A techno-economic feasibility study of integrating offshore floating photovoltaic solar technology within an offshore wind park. Sol Energy 2021;219:65–74, https://doi.org/10.1016/j.solener.2020.12.062.
[322] Mannino G, Tina GM, Cacciato M, Merlo L, Cucuzza AV, Bizzarri F, et al. Photovoltaic module degradation forecast models for onshore and offshore floating systems. Energies 2023;16. https://doi.org/10.3390/en16052117.
[323] Luo W, Isukapalli SN, Vinayagam L, Ting SA, Pravettoni M, Reindl T, et al. Performance loss rates of floating photovoltaic installations in the tropics. Sol Energy 2021;219:58–64, https://doi.org/10.1016/j.solener.2020.12.019.
[324] Kumar M, Kumar A. Experimental validation of performance and degradation study of canal-top photovoltaic system. Appl Energy 2019;243:102–18, https://doi.org/10.1016/j.apenergy.2019.03.168.
[325] Goswami A, Sadhu PK. Degradation analysis and the impacts on feasibility study of floating solar photovoltaic systems. Sustain Energy Grids Netw 2021;26:100425, https://doi.org/10.1016/j.segan.2020.100425.
[326] Li Z, Ma M, Han T, Ma J. A PV module life prediction method with flexible consideration of environmental stress coupling weights. In: IEEE 2nd international power electronics and application symposium. 2, 2023, p. 1868–73, https://doi.org/10.1109/PEAS58692.2023.10395120.
[327] Kaaya I, Ascencio-Vásquez J, Weiss K-A, Topič M. Assessment of uncertainties and variations in PV modules degradation rates and lifetime predictions using physical models. Sol Energy 2021;218:354–67, https://doi.org/10.1016/j.solener.2021.01.071.
[328] Bala Subramaniyan A, Pan R, Kuitche J, TamizhMani G. Quantification of environmental effects on PV module degradation: A physics-based data-driven modeling method. IEEE J Photovolt 2018;8(5):1289–96, https://doi.org/10.1109/JPHOTOV.2018.2850527.

[329] Trapani K, Millar D. Hydrodynamic overview of flexible floating thin film PV arrays. Offshore Energy Storage Symp 2016.
[330] Lee G-H, Choi J-W, Seo J-H, Ha H. Comparative study of effect of wind and wave load on floating PV: Computational simulation and design method. J Korean Soc Manuf Process Eng 2019;18:9–17, https://note.org/10.14775/ksmpe.2019.18.11.009.
[331] Maarten D, Daan van der W, Kostas S, Minne M. de J, Folkerts W. Influence of wave induced movements on the performance of floating PV systems. In: European photovoltaic solar energy conference and exhibition. 6DO.9.1, 2019, p. 1759–62, https://doi.org/10.4229/EUPVSEC20192019-6DO.9.1.
[332] I C, L I, A M, D S. Seakeeping assessment of a floating object with installed photovoltaic system. In: Selma E, C. Guedes S, editors. Sustainable development and innovations in marine technologies. Taylor and Francis Group; 2022, p. 12.
[333] Tay ZY. Three-dimensional hydroelasticity of multi-connected modular offshore floating solar photovoltaic farm. J Mar Sci Eng 2023;11:10, https://doi.org/10.3390/jmse11101968.
[334] Song J, Imani H, Yue J, Yang S. Hydrodynamic characteristics of floating photovoltaic systems under ocean loads. J Mar Sci Eng 2023;11:9, https://doi.org/10.3390/jmse11091813.
[335] Dallan F, Madjid K, Trevor W, Doran J. Experimental hydrodynamic assessment of a cylindrical-type floating solar system exposed to waves. J Ocean Eng Sci 2023;8:461–73, https://doi.org/10.1016/j.joes.2023.08.004.
[336] Choi SM, Park C-D, Cho S-H, Lim B-J. Effects of various inlet angle of wind and wave loads on floating photovoltaic system considering stress distributions. J Clean Prod 2023;387:135876, https://doi.org/10.1016/j.jclepro.2023.135876.
[337] Ameen M B, Islam A, Ayman M, Nabil A.S. E, Heba Y.M. S, Yasser E, et al. Conceptual design of a novel partially floating photovoltaic integrated with smart energy storage and management system for Egyptian North lakes. Ocean Eng 2023;279:114416, https://doi.org/10.1016/j.oceaneng.2023.114416.
[338] Chi Z, Jian D, Kok Keng A, Han Vincent L. Development of compliant modular floating photovoltaic farm for coastal conditions. Renew Sustain Energy Rev 2024;190:114084, https://doi.org/10.1016/j.rser.2023.114084.
[339] Zhang Y, Zhang X, Chen Y, Tian X, Li X. A frequency-domain hydroelastic analysis of a membrane-based offshore floating photovoltaic platform in regular waves. J Fluids Struct 2024;127:104125, https://doi.org/10.1016/j.jfluidstructs.2024.104125.
[340] Kristiansen T, Grøn P, Faltinsen O. A floating membrane solar Island study. In: 9th international conference on hydroelasticity in marine technology. 2022.
[341] Yang Y, Ren K, Zhou B, Sun SY, Huang L. Wave interaction with multiple adjacent floating solar panels with arbitrary constraints. Phys Fluids 2024;36:037121, https://doi.org/10.1063/5.0198106.
[342] Wei Y, Zou D, Zhang D, Zhang C, Ou B, Riyadi S, et al. Motion characteristics of a modularized floating solar farm in waves. Phys Fluids 2024;36(3):033320, https://doi.org/10.1063/5.0199248.
[343] Bin W, Yan L, Lei H, Ye Y, Yao Q. Dynamic analysis of a novel star-type floating photovoltaic system with flexible connectors. Ocean Eng 2024;304:117854, https://doi.org/10.1016/j.oceaneng.2024.117854.
[344] Mosciatti Urzua EA. Experimental study of scale effects of a multi-body floating solar photovoltaic power plant [Master thesis], Universidad Politécnica de Madrid; 2023-2024, https://matheo.uliege.be/handle/2268.2/19550.
[345] Junfeng D, Deqing Z, Yanfeng Z, Kun X, Anteng C, Shujie Z. Design and comparative analysis of alternative mooring systems for offshore floating photovoltaics arrays in ultra-shallow water with significant tidal range. Ocean Eng 2024;302:117649, https://doi.org/10.1016/j.oceaneng.2024.117649.
[346] Xu P, Wellens PR. Theoretical analysis of nonlinear fluid–structure interaction between large-scale polymer offshore floating photovoltaics and waves. Ocean Eng 2022;249:110829, https://doi.org/10.1016/j.oceaneng.2022.110829.
[347] Xu P, Wellens PR. Fully nonlinear hydroelastic modeling and analytic solution of large-scale floating photovoltaics in waves. J Fluids Struct 2022;109:103446, https://doi.org/10.1016/j.jfluidstructs.2021.103446.
[348] Ohmatsu S. Numerical calculation of hydroelastic responses of pontoon type VLFS. J Soc Nav Archit Jpn 1997;1997(182):329–40, https://doi.org/10.2534/jjasnaoe1968.1997.182_329.
[349] Ertekin R, Kim JW. A parametric study of the hydroelastic response of a floating, mat-type runway in regular waves. In: IEEE oceanic engineering society. OCEANS'98. conference proceedings (Cat. No. 98CH36259). 2, 1998, p. 988–92 vol.2, https://doi.org/10.1109/OCEANS.1998.724385.
[350] Watanabe E, Utsunomiya T, Wang C, Hang LTT. Benchmark hydroelastic responses of a circular VLFS under wave action. Eng Struct 2006;28(3):423–30, https://doi.org/10.1016/j.engstruct.2005.08.014.
[351] Meylan MH. Time-dependent motion of a floating circular elastic plate. Fluids 2021;6:1–13, https://doi.org/10.3390/fluids6010029.
[352] Hiroshi K, Masataka F, Motohiko M. Theoretical and experimental predictions of the hydroelastic response of a very large floating structure in waves. Appl Ocean Res 1998;20(3):135–44, https://doi.org/10.1016/S0141-1187(98)00017-0.
[353] Liu X, Sakai S. Time domain analysis on the dynamic response of a flexible floating structure to waves. J Eng Mech 2002;128(1):48–56, https://doi.org/10.1061/(ASCE)0733-9399(2002)128:1(48).
[354] Schreier S, Jacobi G. Experimental investigation of wave interaction with a thin floating sheet. Int J Offshore Polar Eng 2021;31(04):435–44, https://doi.org/10.17736/ijope.2021.mk76.
[355] Tina GM, Bontempo Scavo F. Energy performance analysis of tracking floating photovoltaic systems. Heliyon 2022;8(8):e10088, https://doi.org/10.1016/j.heliyon.2022.e10088.
[356] Yang P, Chua LH, Irvine K, Imberger J. Radiation and energy budget dynamics associated with a floating photovoltaic system. Water Res 2021;206:117745, https://doi.org/10.1016/j.watres.2021.117745.
[357] Widayat AA, Ma'arif S, Syahindra KD, Fauzi AF, Setiawan EA. Comparison and optimization of floating bifacial and monofacial solar PV system in a Tropical region. In: 2020 9th international conference on power science and engineering. 2020, p. 66–70, https://doi.org/10.1109/ICPSE51196.2020.9354374.
[358] Haohui L, Luo W, Kumar A, Reindl T, Hacke P. Evaluation of risk for potential-induced degradation in floating PV systems. In: 36th european photovoltaic solar energy conference and exhibition. 2019, p. 1324–30, https://doi.org/10.4229/EUPVSEC20192019-5BO.7.4.